DILUTION REFRIGERATION AND A CALORIMETRIC MEASUREMENT OF THE QUADRUPOLE COUPLING CONSTANT IN RHENIUM METAL

Thesis by

Stephen Dell Rockwood

In Partial Fulfillment of the Requirements

For the Degree of

Doctor of Philosophy

California Institute of Technology

Pasadena, California

1970

(Submitted November 6, 1969)

TABLE OF CONTENTS

ACKNOWLEDGMENTS

I wish to express my sincere gratitude to Dr. E. H. Gregory for both suggesting this program of research and his professional guidance throughout its development. I also wish to thank Dr. D. L. Goodstein for many fruitful suggestions as well as for his expert supervision during the final phases of this work.

My thanks to Dr. J. E. Mercereau and the Low Temperature Physics group for their interest in the completion of this project. My gratitude also to Mr. Edward Boud and Mr. Fred Wild for their able technical assistance and to a fellow graduate student, Mr. John Wallace for constructing portions of the electronic equipment.

Financial support was provided by the National Science Foundation in the form of a graduate traineeship. I am also indebted to the Air Force Institute of Technology for granting me an educational delay from active duty service thus allowing me to complete this program.

Finally, my sincere gratitude to my wife, Jane, for it is to her patience and understanding that I owe the ultimate completion of this work.

ABSTRACT

A dilution refrigerator has been constructed capable of producing steady state temperatures less than .075°K. The first part of this work is concerned with the design and construction of this machine. Enough theory is presented to allow one to understand the operation and critical design factors of a dilution refrigerator. The performance of our refrigerator is compared with the operating characteristics of three other dilution refrigerators appearing in the present literature.

The dilution refrigerator constructed was used to measure the nuclear contribution to the low temperature specific heat of a pure, single-crystalline sample of rhenium metal. Measurements were made in magnetic fields from 0 to 12.5 kOe for the temperature range .13°K – .52°K. The second part of this work discusses the results of these experiments. The expected nuclear contribution is not found when the sample is in the superconducting state. This is believed to be due to the long spin-lattice relaxation times in superconductors. In the normal state, for the temperature range studied, the nuclear contribution is given by A/T^2 where A = .061 ± .002 millijoules-K/mole. The value of A is found to increase to A = .077 ± .004 millijoules-K/mole when the sample is located in a magnetic field of 12.5 kOe.

From the measured value of A the splitting of the energy levels of the nuclear spin system due to the interaction of the internal crystalline electric field gradients with the nuclear quadrupole

moments is calculated. A comparison is made between the predicted and measured magnetic dependence of the specific heat. Finally, predictions are made of future nuclear magnetic resonance experiments which may be performed to check the results obtained by calorimetery here and further, to investigate existing theories concerning the sources of electric field gradients in metals.

INTRODUCTION

The problem chosen for consideration was the splitting of the nuclear energy levels in a single crystal of pure metallic rhenium due to the interaction of the crystalline electric field gradient and the nuclear quadrupole moment. The first observation of this effect was reported by Keesom[44] in making measurements of the specific heat on a polycrystalline sample of rhenium at temperatures down to .37°K. The effect manifests itself in the form of a rise in the specific heat at low temperature due to thermal excitations of the nuclear spin system. This rise in the specific heat will have a $1/T^2$ dependence in the limit that kT is much greater than the separation of the levels and the coefficient of this term will give a measure of the quadrupole coupling constant.

At ~ .4°K the effect in rhenium is just becoming visible with the nuclear contribution representing about 25% of the total specific heat of the metal in the normal state. Therefore, in order to determine accurately the coefficient of this $1/T^2$ term the obvious approach is to take the sample to lower temperatures.

The method of refrigeration chosen was a dilution refrigerator. This device was in the very early stages of development at the time this project was being considered and research on it was actively being conducted by several experimenters.[3,4,6]

This paper will consist of two parts:

I. A sufficiently detailed description of the dilution refrigerator will be presented to allow one to appreciate the problems to be considered in designing the components of this machine.

II. The theory and experimental details of the measurement of the low temperature specific heat of rhenium will be discussed.

PART I

DILUTION REFRIGERATION

Chapter I. Introduction

A. Dilution Refrigeration

Following the discovery by Walters and Fairbank[1] of the phase separation phenomena of liquid He^3-He^4 solutions, a powerful method of cooling to temperatures previously reached only by adiabatic demagnetization was proposed by London, Clarke, and Mendoza.[2] The phase separation phenomena in He^3-He^4 solutions is characterized by the fact that for certain temperatures and He^3 concentrations, the solution separates into two immiscible fluids. The upper phase is a He^3 rich solution which floats on top of a He^4 rich superfluid. Refrigeration is produced by the "evaporation" of He^3 from the upper phase into the He^4 rich lower phase. An important feature is that the He^3 is recirculated, thereby producing continuous refrigeration. This is a distinct advantage of the dilution process in comparison to adiabatic demagnetization. Another inherent advantage of the dilution refrigerator is that it can be used in conjunction with high or low magnetic fields.

The first successful refrigerator operating on the "evaporation" process was built by Hall, Ford, and Thompson[3] in 1966 and reached a sustained temperature of 65 m^oK ($1m^oK = 10^{-3}\ ^oK$). Neganov, Borisov, and Liburg[4] working independently and at about the same time built a high capacity device that reached $25m^oK$.

Vilches and Wheatley have modified the original design and produced a device that cools to about 10m^{o}K in continuous operation.[5] With another apparatus, operating non-continuously and precooled by a continuously operating refrigerator, they have reached a temperature of 4.5m^{o}K.[6] The purpose of this part will be to discuss the general principle and critical design considerations of the continuously operating dilution refrigerator. Specific examples of characteristics will be given in reference to the refrigerator built by the author.

Chapter II. Theory

A. Dilution Refrigeration

The critical components of the dilution refrigerator are shown schematically in Figure 1. The phase boundary between the two liquids, He^3 and He^4, exists in the component called the mixing chamber. The fluid on top is nearly pure He^3 and the fluid below is He^4 superfluid with about 6% He^3. The He^3 atoms are preferentially pumped across the phase boundary by the action of the still. At the still one ideally pumps away pure He^3 from the He^3-He^4 mixture. This is possible, even though the percentage of He^3 is very small (~ 1%), because of the large difference in the vapor pressure of the two liquids. For example, at .5^{o}K the vapor pressure of He^3 is about 180μ (1μ = 10^{-3} mmHg), whereas the vapor pressure of the He^4 is about .01μ. Thus, by applying a small amount of heat at the still almost pure He^3 is evaporated and pumped away. The still and the mixing chamber are connected by a continuous column of superfluid He^4. As He^3 is removed at the still the constancy of the chemical potential of He^4 in the

superfluid requires He^3 to "evaporate" from the condensed region into the dilute region across the phase boundary. In analogy to the evaporation of a liquid, there is a latent heat, and cooling takes place at the phase boundary in the mixing chamber. This He^3 is circulated and recondensed in the condenser. The condenser is located in a He^4 bath that is cooled by pumping its vapor through a separate line to about 1^oK.

Just below the condenser is a large impedance to the flow of He^3. The purpose of the impedance is, for a normal He^3 circulation rate, to force the gas pressure in the condenser to be high enough to condense He^3 at the temperature of this He^4 bath.

The heat exchangers are very vital to the operation of the refrigerator and will be discussed in greater detail later in Chapter III, as will all the other components. Their purpose is to use the cold fluid flowing out of the mixing chamber to remove heat from the incoming warmer fluid leaving the condenser.

B. He^3-He^4 Solutions

In order to calculate the properties of He^3-He^4 solutions, one must first select some model. Since He^4 is a superfluid, it will offer no resistance to the movement of He^3 atoms so one might expect *a priori* the He^3 atoms in a solution of He^4 to behave as a dilute Fermi gas. This indeed appears to be true from the specific heat data of Edwards et al.[7] In the temperature range below 0.5^oK, these data are fit well by the specific heat of an ideal Fermi-Dirac gas[11] with an effective He^3 mass $m^* = 2.5m_3$ (m_3 = mass of He^3 atom). The

specific heat measurements were extended by Anderson et al.,[8] well into the degenerate region and the ratio of m^*/m_3 was found to vary slightly with concentration. Some of the low temperature data are shown in Figure 2. The variation of m^* with the concentration of He^3 is attributed to the weak interaction between He^3 atoms. Calculations based on the model of a weakly interacting Fermi-Dirac gas have been done by Bardeen, Baym, and Pines[9] (BBP) and by Ebner.[10]

For the dilution refrigerator, it is sufficient to know the properties of pure He^3 and solutions with less than 10% He^3 atoms. This can be seen by examining the phase separation curve, Figure 3. Region 1 is normal fluid, region 2 is superfluid; region 3 is inaccessible to mixtures of He^3 and He^4 and is the region of interest here. For concentrations and temperatures falling inside region 3 a He^3 rich phase will separate out on top and a He^4 rich phase will settle to the bottom. The He^3 concentration of the upper and lower phases may be read off the right and left hand branches, respectively, of the phase separation curve. Since the dilution refrigerator generally runs below $0.2^{\circ}K$, it can be seen immediately that the He^3 concentration in the dilute phase is less than 10%, while the upper concentrated phase is essentially pure He^3. A remarkable, and very important, feature of He^3-He^4 solutions is that the He^3 concentration in the dilute phase does not go to zero as the temperature approaches zero. The limiting value of the concentration has been carefully studied[6,13] and is about 6.3%. There is thus no intrinsic limit to temperatures at which one can employ the dilution process.

This finite solubility of He^3 in He^4 is discussed in Reference 14. The basic fact is that a single He^3 quasiparticle is more strongly bound to liquid He^4 than it is to liquid He^3.

Since the specific heat of He^3-He^4 solutions shows a He^3 concentration dependence as discussed above, to calculate the thermodynamic properties of the solution one must assume some form for the He^3-He^3 interaction. In their work, BBP[9] assume the interparticle interaction to be weak and independent of spin, velocity, and concentration. The interaction potential between two particles separated by a distance $\vec{r}$ is given in terms of its Fourier transform by

$$V(\vec{r}) = \int V(k)\ e^{i\vec{k}\cdot\vec{r}}\ d\vec{k}/(2\pi)^3 \qquad (1)$$

For isotropic systems $V(\vec{k}) = V(k)$. The effective mass is then given by[9]

$$m^*/m_o = 1 - (N(0)/2k_f^2) \int_0^{2k_f} V(k)\ k\ [1 - \frac{k^2}{2k_f^2}]\ dk \qquad (2)$$

where m_o is the value of m^* at zero concentration. (The He^3 concentration will be denoted by x from here on.)

$$N(0) = m^*\ k_f/2\pi\hbar^2 \qquad (3)$$

is the density of energy states at the Fermi surface. The wave vector at the Fermi surface, k_f, depends on the concentration in the following manner;

$$k_f = (3\pi^2\ n_3)^{1/3} = (3\pi^2\ N_A/v)^{1/3} \qquad (4)$$

where n_3 = the number density of He^3 atoms, N_A is Avagadro's number and v is the volume containing one mole of He^3. v is given by[15]

$$v = V_m/x = 27.58/x + 7.60 + 1.65\ x^2 \text{ cc/mole } He^3 \qquad (5)$$

where V_m is the molar volume of the solution.

To then calculate m^* from Equation (2) BBP took a two parameter form for V(k) given by

$$V(k) = V_o \cos(\beta k) \qquad (6)$$

A best fit to the experimental data could be achieved by taking $\beta = 3.16$ Å and $V_o = -.0754\ m_4 s^2/n_4 = -1.303 \times 10^{-38}$ ergs cm^3 where m_4 is the mass of a He^4 atom, s is the velocity of first sound in He^4 at T = 0, and n_4 is the number density of pure He^4 at T = 0.

This form is limited to He^3 concentrations less than 5%. Ebner[10] has extended the calculations to concentration of 30% using a more complicated form for V(k). Using both these forms in Equation (2) Radebaugh[15] has computed m^*/m_o. He finds that the concentration dependence agrees with the four experimental points of the specific heat data (see Figure 4). Knowing k_f from Equation (4) the Fermi temperature can then be computed from

$$T_f = \hbar^2 k_f^2/2k_B m^* \qquad (7)$$

where k_B is Boltzmann's constant.

Stoner[11] has evaluated the specific heat C_f of a Fermi-Dirac gas as a function of T/T_f. Recently the temperature range of

these calculations has been extended by Radebaugh.[15] Thus, knowing T_f from Equation (7) above, it is possible to calculate the specific heat and entropy of a dilute solution with an accuracy of a few percent. The input data are the effective mass and the He^3 number density. The former is given by Equation (2), and the latter can be obtained from the He^3 concentration and Equation (5).

However, to go further and calculate the enthalpy, chemical potential, and other related thermodynamic properties, one needs the deviations of He^3 in solutions from that of an ideal Fermi-Dirac gas. This deviation will be considerable because of the He^3 interaction and binding energy.

For He^3 in solution the chemical potential can be written as

$$\mu_3 (x,T) = \mu_f (x,T) + \mu_3' (x,T) \tag{8}$$

where μ_f is the molar chemical potential of an ideal Fermi-Dirac gas with an effective particle mass m^*. μ_f is given by

$$\begin{aligned} \mu_f &= H_f - TS_f = \frac{5}{3} U_f - TS_f \\ &= RT_f + \frac{5}{3} \int_0^T C_f \, dT - T \int_0^T \left(\frac{C_f}{T} \right) dT \end{aligned} \tag{9}$$

where H_f is the molar enthalpy of an ideal Fermi gas, S_f the molar entropy, U_f the internal energy of an ideal Fermi-Dirac gas and R the gas constant. Since C_f is known in the form of a power series in T[11,15] the above integrals can be done numerically.

The second term (in Equation (8)), μ_3' (x,T), the degree

to which the He^3 in solution deviates from an ideal Fermi-Dirac gas, can be evaluated from the experimental data along the dilute solubility curve. In the phase separated solution the chemical potential of He^3 must be the same in both the dilute and concentrated regions. Considering the concentrated phase as pure He^3 then

$$\mu_f (x_d,T) + \mu_3' (x_d,T) = \mu_3^{\circ} (T) \qquad (10)$$

where x_d denotes the concentration of the dilute phase on the solubility curve (Figure 2) and μ_3° denotes the chemical potential of pure He^3. This is given by

$$\mu_3^{\circ}(T) = -L_3^{\circ} + \int_o^T C_3^{\circ}\, dT - T \int_o^T (C_3^{\circ}/T)\, dT \qquad (11)$$

where L_3° is the molar heat of vaporization of pure He^3 at $T = 0$. The expression $\mu_3^{\circ} + L_3^{\circ}$ can be calculated from the properties of pure He^3[15] and the μ_f term in Equation (10) can be computed from Equation (9) for each point on the solubility curve. Thus, one can calculate the μ_3' term of Equation (10).

Using their assumed form for V(k) BBP have made theoretical calculations of $\mu_3'(x)$ in Reference 9. Radebaugh has also compiled values of $\mu_3'(x)$ in Reference 15 where he used Ebner's form for V(k) in computing m^*. Thus, one has available expressions for $\mu_{3d}(x,T) \equiv \mu_f(x,T) + \mu_3'(x,T)$, the partial chemical potential for He^3 in the dilute phase.

Also present in the dilute phase is superfluid He^4. If μ_{4d} is the partial potential for He^4 in the dilute phase then this

will be related to μ_{3d} found above by

$$x \left(\frac{\partial \mu_{3d}}{\partial x}\right)_{T,P} + (1-x) \left(\frac{\partial \mu_{4d}}{\partial x}\right)_{T,P} = 0 \qquad (12)$$

In the steady state condition the superfluid is not accelerating thus

$$\vec{\nabla} \mu_{4d}(x,T) = 0 \qquad (13)$$

Equation (13) is directly related to the setting up of the osmotic pressure gradient which drives the He^3 through the superfluid He^4 in the dilute phase. If π is the osmotic pressure of He^3 in He^4, then

$$\pi V_4 = - [\mu_4(x,T) - \mu_4(0,T)] \qquad (14)$$

where V_4 is the molar volume of He^4 in solution equal to $27.58 - 3.30x^3$ cc/mole[13,17]. Writing Equation (12) in integral form yields

$$\mu_4(x,T) - \mu_4(0,T) = - \int_0^x \left(\frac{x}{1-x}\right) \left.\frac{\partial[\mu_{3d}(x,T)]}{\partial x}\right|_T dx \qquad (15)$$

and substituting this into Equation (14) gives the osmotic pressure

$$\pi V_4 = \int_0^x \frac{x}{1-x} \left[\frac{\partial \mu_{3d}(x,T)}{\partial x}\right]_T dx \qquad (16)$$

The integral can be evaluated because μ_{3d} is known as a function of x as explained above. This osmotic pressure is of the order of 1-2 cm Hg for temperatures below $.2^{\circ}K$ and at concentrations of 6.3%. This is a relatively small driving pressure for any kind of viscous

fluid flow. This presents a design problem in minimizing the flow impedance throughout the device.

In order to understand the design and operation characteristics of the dilution refrigerator better, one needs to investigate the viscosity and thermal conductivity for both pure and dilute solutions of He^3. For pure He^3 the limiting low temperature viscosity deduced from ultrasonic attentuation experiments[18] is

$$\eta_c T^2 = 2 \times 10^{-6} \text{ dynes-sec-}^{\circ}K^2/cm^2 \qquad (17)$$

η_c denoting the viscosity in the concentrated phase. Higher temperature data can be found in Reference 19.

The thermal conductivity is given in the limit of low temperatures by[5]

$$K_c T = 33 \text{ erg/sec-cm } [1-T/.54^{\circ}K]^{-1} \qquad (18)$$

On the dilute side one needs the limiting low temperature viscosity of nearly saturated (x = .0635) dilute solutions. Such measurements have never been made directly but the viscosity can be deduced from the ultrasonic attenuation measurements. Roach has calculated the viscosity using the BBP potential.[20,5] The result for x = .063 is

$$\eta_d T^2 = 5 \times 10^{-7} \text{ dynes-sec } {}^{\circ}K^2/cm^2 \qquad (19)$$

The thermal conductivity of dilute solutions is given in Reference 16. At low temperatures $K_d T$ is approximately constant. For design purposes setting x = .063 one can take the value

$$K_d T = 30 \text{ erg/sec-cm} \qquad (20)$$

At higher temperatures ($.1^{\circ}K < T < .8^{\circ}K$) K_d rises due to the He^4 phonon conduction. There are few measurements available in this temperature range. However, Baym and Ebner have computed values over the range of interest.[21] Within a factor of two it is adequate to take

$$K_d \approx 2 \times 10^4 \ (.01/x) \text{ erg/sec-cm } ^{\circ}K \qquad (21)$$

C. Applications to the Dilution Refrigerator

To recall the refrigeration process as described briefly in Section A refer to Figure 1. Essentially pure He^3 enters the mixing chamber where it floats on top of, and is in equilibrium with the dilute solution of He^3 in He^4. At very low temperatures this He^3 concentration is about 6.3%. The dilute phase communicates with the still via the return line. Owing to the superfluidity of the He^4, the He^3 moves through it behaving essentially as a dilute Fermi gas as described in the last section. Since the temperature of the still is higher than that of the mixing chamber the He^3 concentration is lower. This variation of concentration with temperature can be obtained from the condition that μ_{4d}, the chemical potential of He^4 in the dilute phase, is a constant. This follows directly from Equation (14). μ_{4d} is a function of x and T so the equation, μ_{4d} = constant, determines x(T) if its value is known somewhere. If one assumes the mixing chamber to be less than $.1^{\circ}K$, then the zero temperature value,

$x = .064$ can be taken:

$$\mu_{4d}(x,T) = \mu_{4d}(.064,0) \tag{22}$$

Equation (22) can be solved as follows: In Equation (15) take $1 - x \tilde{=} 1$ and as before let μ_4^o denote the chemical potential of pure He^4. Then,

$$\mu_{4d}(x,T) = \mu_4^o(T) - \int_o^x x \left[\frac{\partial \mu_{3d}}{\partial x}\right]_T dx \tag{23}$$

since $\mu_{3d}(x,T)$ is known the integral can be evaluated numerically with the initial condition imposed by Equation (22). The concentration as a function of T can then be displayed by plotting profiles of $\mu_{4d} = \text{const.}$ The results are shown in Figure 6. In the temperature range of ~ 75 m$\mathring{K}$ to 175 m$\mathring{K}$ the function is linear with $xT = 4.7 \times 10^{-3}\ \mathring{K}$. At the very low temperatures $x(T) - x(0) \approx -3.3T^2\ \mathring{K}^2$. Reading off the left hand branch one can see that for mixing chamber temperatures less than .1 ^oK and a typical still temperature of .75 ^oK the concentration of He^3 in the still will be on the order of 1%. With the material now developed it is possible to analyse the operation of the dilution refrigerator.

(1) Refrigeration Capacity

The quantity that is of primary interest is the heat absorption rate. Consider first the case where only pure He^3 circulates. (The effects of He^4 circulation will be discussed later.) Under steady state conditions the heat absorption rate $\dot{Q}$ can be written as the enthalpy difference across the phase boundary

$$\dot{Q}/\dot{n}_3 = H_3\ (x_d, T) - H_3^{C}\ (T_i) \tag{24}$$

where $\dot{n}_3$ is the He^3 molar circulation rate, $H_3(x_d, T)$ is the enthalpy of He^3 in the He^4 along the dilute solubility curve, and $H_3^{C}\ (T_i)$ is the enthalpy of He^3 in the incoming concentrated phase at an inlet temperature of T_i. Under the assumption above, that only pure He^3 circulates $H_3^{C}\ (T_i) = H_3^{o}\ (T_i)$, the enthalpy of pure He^3 at T_i, which is given by

$$H_3^{o}\ (T_i) = \int_o^{T_i} C_3^{o}\, dT + L_3^{o} \tag{25}$$

L_3^{o} is the latent heat of vaporization for pure He^3 and is added here to be consistent with Equation (11). The quantity $H_3\ (x_d, T)$ is given by

$$H = H_o + \int_o^{T} C\, dT \tag{26}$$

where $C = xC_f + (1-x)\ C_4^{o}$ is the specific heat of the total solution; C_f being the specific heat of the weakly interacting Fermi gas derived in Section B and C_4^{o} is the specific heat of pure He^4. The zero point enthalpy is given by

$$H_o = x\mu_3\ (T=0) + (1-x)\ \mu_4\ (T=0) \tag{27}$$

In Figure 7 a plot is given of $H_3(x_d, T)$, $H_3^{o}(T)$, and $\dot{Q}/\dot{n}_3$. From this graph it is obvious that the incoming He^3 can be at a much higher temperature than the outgoing dilute He^3. It is also apparent that the ultimate temperature of the mixing chamber is determined

solely by the temperature of the incoming He^3 (assuming heat leaks are small). For example, reading horizontally on Figure 7, if the last heat exchanger runs at $.3^{\circ}K$, then the mixing chamber will run at ~ $85m^{\circ}K$, which represents the nominal operating temperatures of the machine here at Caltech operating with no load. If one were heating the mixing chamber at a rate of say .2 joules/mole He^3, then with the last heat exchanger at $.3^{\circ}K$ as above, the mixing chamber will run at ~ $.1^{\circ}K$. Normal circulation rates are 2×10^{-5} moles He^3/sec, so the above power input of .2 joules/mole He^3 corresponds to a permissible load on the order of 4μ watt (1μw = 10^{-6} watts) while holding the mixing chamber at $.1^{\circ}K$. For temperatures less than $40m^{\circ}K$ the expressions for $H_3(x_d,T)$ and $H_3^{\circ}(T_i)$ may be fit to within 1% by $94T^2$ j/mole He^3 and $12T_i^2$ j/mole He^3, respectively. Equation (24) then may be written as

$$\dot{Q}(T,T_i)/\dot{n}_3 = 94T^2-12T_i^2 \text{ j/mole-He}^3 \tag{28}$$

If there is ideal heat exchange so that the fluid flowing into the mixing chamber is at the same temperature as the mixing chamber, then $T_i = T$ and one gets the maximum cooling capacity of

$$\dot{Q}(T,T)/\dot{n}_3 = 82T^2 \text{ j/mole He}^3 \tag{29}$$

(2) Heat Exchange

From the discussion above, it is obvious that efficient heat exchange is of vital importance. However, heat exchange between liquid helium and a solid at low temperature is difficult due to the so-called

Kapitza boundary resistance.[22] This is thought to be essentially an acoustical impedance mismatch between the phonons in the liquid and those in the solid. This thermal resistance, at low temperatures, varies roughly as $1/AT^3$ where A is the area of the He-solid interface. Thus for efficient heat exchange it is necessary to have large areas of contact. It is possible to obtain large surface areas in a small volume using sintered copper powder. For this reason sintered copper in a block copper body is used as the heat exchange medium. The heat exchangers were the object of considerable study. The results of this study and the final exchanger configuration chosen will be discussed in Chapter III.

Within a heat exchanger the thermal conduction path from the dilute side to the condensed side involves the following resistances in series: intrinsic He^3 resistance, boundary resistance of pure He^3 to copper sponge, thermal resistance of the copper structure, and boundary resistance to dilute He^3.

The intrinsic He^3 resistance is known[16] and is not a problem. The pure He^3 to copper and pure He^4 to copper boundary resistance has been investigated by Anderson, Connolly, and Wheatley.[22] They find that below $.1^oK$ the thermal boundary resistance is given by

$$R_{He^3\text{-}Cu} = 2 \times 10^{-5}/T^3 \text{ sec-cm}^2\text{-K}^{o4}/\text{erg} \qquad (30)$$

while the resistance for pure He^4 is smaller but has the same T dependence.

The thermal resistance of sponge to copper body can be

estimated by measuring the electrical resistance and using the Wiedemann-Franz relation. With properly made sponges where the contact between the sponge and the body is good this resistance is not a problem.

The thermal resistance between copper and dilute solutions has not been measured to any great extent. Some preliminary work has been done by Wheatley et al., and is reported in Reference 5. The model developed there assumes a transfer of energy into He^4 phonons which then give up energy to the He^3 quasiparticle by the He^3-He^4 phonon interaction. If energy were to be transmitted directly from the walls into collective density modes of the He^3 quasiparticles (which have all the heat capacity) the mismatch would be much worse than the numbers found. The He^3 quasiparticle – He^4 phonon interaction has been studied by Baym and Ebner[21] and they find that at low temperatures the mean-free path becomes very long. The result is that He^4 phonons emitted by the wall are simply reabsorbed without ever transferring energy to the He^3. This will result in a temperature difference between the He^4 phonon system, which will become warmer, and the He^3 system. The He^3 system maintains a thermal equilibrium at a lower temperature due to the frequent quasiparticle interactions. There is thus developed a He^4 phonon-He^3 quasiparticle thermal resistance.

This problem has been considered quantitatively in Reference 5. Following the arguments developed there, imagine two sets of phonons, one at a temperature T_1 in equilibrium with the walls and a second at a temperature T_2 in equilibrium with the He^3. Assuming no driving heat

flows, an initial energy difference ΔU_o between the two sets of phonons will be assumed to relax according to

$$\Delta U(t) = \Delta U_o \, e^{-t/\tau} \tag{31}$$

where τ is some relaxation time. At any instant the rate of heat transfer between the two sets of phonons is given by

$$\dot{Q} = \frac{-d(\Delta U)}{dt} = \frac{1}{\tau} \Delta U(t) \tag{32}$$

With this heat flow the energy difference between the two baths will stabilize at temperatures T_1 and T_2, such that

$$\dot{Q} = \frac{1}{\tau} [U(T_1) - U(T_2)] \tag{33}$$

The quantity U is the internal energy of the He^4 phonons with velocity c_1 in a volume V and at a temperature T given by

$$U(T) = \frac{\pi^2}{30} \frac{V}{\hbar^3 c_1^3} (kT)^4 \tag{34}$$

Then using Equation (33) this leads to a thermal resistance which is given by

$$R(T)_{\text{phonon-He}^3} \equiv \frac{\Delta T}{\dot{Q}} = \frac{15}{2\pi^2} \left(\frac{\hbar^3 c_1^3}{V k^4} \right) \left(\frac{\tau}{T^3} \right) \tag{35}$$

Numerically this is

$$R(T)_{\text{phonon-He}^3} = \frac{3.3 \times 10^{-5} \, \tau}{VT^3} \quad (\text{cm}^4 \, {}^{\circ}\text{K}^4/\text{erg}) \tag{36}$$

Notice this is inversely proportional to the volume of the dilute

solution which is what one would expect for such a thermal resistance between two "phonon baths." The relaxation time τ may be estimated by $\tau = \lambda/c_1$ where λ is the mean free path found by Baym and Ebner.[21] At low temperatures they give $\tau \sim T^{-2}$ so that the thermal resistance given by Equation (36) varies as T^{-5} for low T.

Thus the total thermal resistance between copper and dilute He^3 is the sum of the Kapitza boundary resistance, inversely proportional to the area, and the He^4 phonon -He^3 resistance, inversely proportional to the volume. This geometric dependence has been checked in Reference 5 and the agreement is reasonable. Considering the above, one can see a possible design problem if the He volumes in the heat exchangers are too small. If the dimensions involved are substantially less than the phonon mean free path at low temperatures, then there will be little heat exchange between the cold He^3 system and the rest of the material.

The approximate size of a heat exchanger may be estimated using the above results. Consider a sponge as being made up of a volume of small spheres of diameter d. The ratio of area to volume is then $6d^{-1}$. The copper powder in the present work has an average diameter of $d \sim 5\mu$, in which case the surface to volume ratio is $\sim 1.2 \times 10^4$ cm^{-1}. This is actually an underestimate because the powder is quite irregularly shaped thus having a higher area to volume ratio than a sphere. However, using the estimate of spheres above as a lower limit and substituting into Equation (30) the boundary resistance R may be expressed in terms of the volume of the copper.

$$R \approx 2 \times 10^{-9}/V_{cu}T^3 \quad (\text{sec } {}^{o}K^4 cm^3/\text{erg}) \tag{37}$$

Then from Equation (36)

$$R_{total} \approx 2 \times 10^{-9}/V_{cu}T^3 \quad (\text{sec-cm}^3 {}^{o}K^4/\text{erg}) + 3.3 \times 10^{-5} \frac{\tau}{V_{H\ell}T^3} \left(\frac{cm^3 - {}^{o}K^4}{erg}\right) \tag{38}$$

Using values of τ computed by Baym and Ebner[21] the second term above coming from the He^3-phonon resistance is small for temperatures above 15 to 20 $m^{o}K$ if the volume of copper and the free volume for He are roughly the same. In practice, all heat exchangers run well above 20 $m^{o}K$.

For good heat exchange one wants the time t that a He^3 atom spends in the heat exchanger to be much greater than τ, the thermal relaxation time. If n_3 is the number of He^3 atoms in the exchanger and $\dot{n}_3$ is their rate of circulation, then $t = n_3/\dot{n}_3$. Now $\tau = RC$ where R is given by Equation (37) and $C = n_3 c$ with c being the effective specific heat per He^3 atom. For pure He^3 at low temperatures, the specific heat per particle is

$$c_{He^3} = \Gamma kT \quad \Gamma = 3.0 \ {}^{o}K^{-1} \text{ (Reference 15)}$$

and for dilute solutions, it is

$$c_{dilute} = \gamma kT \quad \gamma = 13.0 \ {}^{o}K^{-1} \text{ (Reference 5)}$$

Now, as stated one wants $(\tau/t) \ll 1$ and

$$\tau/t = R\dot{n}_3\, c = \frac{\dot{n}_3}{T^2}\,(RT^3)\,(\frac{c}{T}) \qquad (39)$$

It is a sufficient approximation for design purposes to use the same value for RT^3 (as given by Equation (37)) on both the dilute and concentrated sides. The ratio of the specific heats c_c/c_d is 4.3, thus the dilute side exchanger will require roughly four times the volume of copper as the concentrated side. Taking roughly appropriate numbers of $\dot{n}_3/N_A = 3 \times 10^{-5}$ moles/sec and $V_{cu} = 1$cc then $(\tau/t)_c \approx (1\ m^oK/T)^2$ for the concentrated phase and $(\tau/t)_d \approx (\frac{2m^oK}{T})^2$ for the dilute phase. Recalling that the criterion for adequate heat exchange was $(\tau/t) \ll 1$ it is obvious that this will be the case since the lowest heat exchanger will be on the order of 20 to 30 m^oK for a mixer temperature of 10 m^oK as achieved by Wheatley.

(3) Still Design; He^3 and He^4 Circulation

The continuously-operating refrigerator moves He^3 from the mixing chamber to the still by the osmotic pressure given by Equation (16). He^3 is evaporated at the still, brought to room temperature, compressed to about 30 mm Hg and recondensed. Any He^4 that is circulated with the He^3 is harmful. This can be seen most easily by referring to the phase separation curve (Figure 3). Assume that the circulating gas contains only 80% He^3. Upon condensation, this gas will be normal fluid (Region 1). Its temperature will be lowered as it moves down the heat exchanger section. Below $.7^oK$ phase separation will begin to occur. Now to continue cooling the two-phase mixture it is necessary to remove the "heat of separation" as well as thermal energy from the two phases. In accord with the

absorption of heat upon dilution at constant T, heat is given off by separation of He^3 from He^4. This effect will be greatest where the slope of the phase separation curve is least.

A quantitative analysis of the effects of He^4 circulation is very complex and has not been attempted for temperatures above $.2^oK$. Below $.2^oK$ Radebaugh[15] has shown that Equation (28) becomes altered to

$$\dot{Q}(T,T_i)/\dot{n} = x\, H_3(x_d, T) - \left[\left(\frac{x-x_d}{1-x_d}\right) H_3^{\,o}(T_i) + x_d \left(\frac{1-x}{1-x_d}\right) H_3(x_d, T_i)\right] \quad (40)$$

where x is the He^3 concentration in the circulating gas, $\dot{n}$ is the number of moles of gas circulated, and x_d is the He^3 concentration of the dilute phase evaluated at T_i, the inlet temperature to the mixing chamber.

The modification of Equation (28) to the form of Equation (40) is due to the fact that the amount of pure He^3 available for refrigeration has been reduced to $n_3 = n\left(\frac{x-x_d}{1-x_d}\right)$ and the dilute solution already separated out at T_i contains $n_{3d} = n\, x_d\left(\frac{1-x}{1-x_d}\right)$ moles of He^3.

Notice that if the He^3 ratio becomes lower than 70% the incoming fluid will be superfluid at temperatures corresponding to the temperature of the main impedance. The refrigerator will fail to operate under such conditions.

It is the primary function of the still to provide a large He^3 circulation rate. To do this one must minimize the He^4 circulation and at the same time maintain an adequate He^3 flow rate. As has been explained before, the vapor pressure of He^4 at a normal still temperature

of ~ .75°K is very low. However, it is the nature of superfluid He^4 to form a thin film of liquid which covers all surfaces at temperatures below the superfluid transition temperature. The He^4 that escapes from the still comes almost entirely from this film creeping up the pump lines until reaching temperatures at which it may evaporate. The film flow rate is directly proportional to the smallest perimeter it encounters and is largely temperature independent below 1°K [23] so the He^3 vapor pressure dominates the He^3:He^4 ratio if the film flow can be restricted. This is done by pumping the still through a flow limiting orifice. The size of the orifice is determined by the criterion that, for the gas flow desired, the pressure drop across the orifice should be a substantial portion of the He^3 vapor pressure. If the orifice is too large, there will be too much He^4 circulation due to the film flow. If the orifice is too small, the pumping speed will be too low and the still will run relatively hot. This will allow more He^4 to evaporate from the bulk liquid and again the ratio will decrease.

The vapor pressure of He^3 in solution as a function of concentration and temperature is shown in Figure 8. The data shown there were calculated in Reference 15. It has also been measured experimentally[24] and the agreement is good. Using these results and knowing the concentration as a function of temperature (Figure 6), it is possible to deduce the vapor pressure of the liquid in the still as a function of still and mixer temperatures. Radebaugh[15] has also computed the heat of vaporization of dilute solutions as a function of concentration and temperature; combining these data with the vapor pressure data one can find the optimum still temperature. This

temperature is somewhere between .6 and .7°K for mixer temperatures below about .1°K. If the still temperature were higher, too much He^4 would be vaporized and if it were lower the pumping speed will be reduced because of the lowered vapor pressure.

(4) Flow Impedance and Viscous Heating

For laminar flow the volume flow rate $\dot{V}$ is related to the pressure head ΔP by

$$\dot{V} = \Delta P/\eta Z \tag{41}$$

where η is the coefficient of viscosity of the fluid and Z is an impedance factor depending only on geometry. The viscous heating rate $\dot{Q}$ is $\dot{V}\Delta P$ so,

$$\dot{Q} = Z\eta\dot{V}^2 \tag{42}$$

Assuming pure He^3 is circulating, then the volume flow rate is 36.8 $\dot{n}_3/N_A$ cc/sec where $\dot{n}_3/N_A$ is the molar flow rate. For dilute solutions at low temperatures where x = .063, the volume flow rate is 433 $\dot{n}_3/N_A$ cc/sec. The viscous heating will produce an increase in temperature ΔT of the flowing He^3. This may be computed from the effective specific heats per atom given earlier as

$$\begin{aligned} &\text{a.}\quad C_c = \Gamma kT \qquad \Gamma = 3.0^{\circ}K^{-1} \qquad \text{(concentrated)} \\ &\text{b.}\quad C_d = \gamma kT \qquad \gamma = 13.0^{\circ}K^{-1} \qquad \text{(dilute)} \end{aligned} \tag{43}$$

Then one has for $\Delta T/T \ll 1$

$$\frac{\Delta T}{T} = \frac{\dot{Q}}{CT} = \frac{Z\eta\dot{V}^2}{CT} = (\eta T^2)\,\frac{(V_4 N_A/\dot{n}_3)^2}{(N_A C/T)}\,\frac{(Z\dot{n}_3/N_A)}{T^4} \tag{44}$$

using Equation (41)a. and b., the ratio of volume flow rate to molar flow rate given above, and the values for viscosity from Equations (17) and (19), this may be written in the form

$$a.\ \left(\frac{\Delta T}{T}\right)_c = .07 \left(\frac{Z}{10^8\ cm^{-3}}\right) \left(\frac{\dot{n}_3/N_A}{10^{-5}\ moles/sec}\right) \left(\frac{20m^oK}{T}\right)^4$$

$$b.\ \left(\frac{\Delta T}{T}\right)_d = .54 \left(\frac{Z}{10^8\ cm^{-3}}\right) \left(\frac{\dot{n}_3/N_A}{10^{-5}\ moles/sec}\right) \left(\frac{20m^oK}{T}\right)^4 \qquad (45)$$

From these equations one can see the viscous heating is about eight times greater on the dilute side. Therefore, one wants as small as possible flow impedance between mixing chamber and still. Recall that this is also desired in order to minimize the drop in He^3 concentration between the mixer and still on the dilute side as pointed out previously. However, this is technically difficult and is in opposition to having large volumes of copper in the heat exchangers. Moreover, $(\Delta T/T)$ varies as T^{-4} and thus the viscous heating will rapidly become a major problem at temperatures below $20m^oK$. Compounding this is the fact that the dilute side is colder than the incoming concentrated phase.

D. Intrinsic Limits

As discussed in the previous section the viscous heating is proportional to $\dot{n}_3^2$, whereas the refrigeration capacity available at a given temperature is linear in $\dot{n}_3$. Clearly, there will be some intrinsic limiting low temperature. This will occur when the heat created by the viscous heating and conducted into the mixing chamber is equal to the refrigeration available.

Assume the dilute He^3 is flowing through a tube of diameter d. The geometeric impedance of the tube is then given by $Z = 128L/\pi d^4$ where L is the length of the tube. Assume also that the temperature depends only on the distance ℓ along the tube.

Neglecting the residual heat leak from surrounding materials there will be three major heat sources in a continuously-operating dilution refrigerator. They are: viscous heating, the enthalpy of the incoming He^3, and heat conducted along the column of dilute fluid. The viscous heating is given by Equation (42) and using Z for the cicular tube given above,

$$\dot{Q} = \left\{ \frac{128\ \Delta\ell}{\pi d^4} \right\} \frac{(\eta T^2)}{T^2} \left(\frac{V_4}{X_o} \right)^2 \dot{n}_3^{\,2} \tag{46}$$

where $V_4 = 27.5\ cc/N_A$ is the average volume per He^4 atom, $X_o = .063$, and $\dot{n}_3$ is the circulation rate in atoms/sec.

The heating rate from cooling the incoming fluid is

$$\dot{n}_3 \int_{T_1}^{T_2} C_c\, dT$$

T_2 = temp of last heat exchanger

T_1 = temp of M.C.

and the heat brought in by conduction is

$$\frac{\pi d^2}{4} (KT) \left[\frac{-1}{T^2} \left(\frac{dT}{d\ell} \right)^2 + \frac{1}{T} \frac{d^2T}{d\ell^2} \right] \Delta\ell$$

The results to be derived are intended to be applied at low temperatures ($T < 10$ to $20 m^oK$) so one can use Equations (19) and (20)

for ηT^2 and KT, respectively and C_c is given by Equation (43)a. These heating sources must be balanced by the refrigeration rate, $\dot{n}_3\ [H(T_2)-H(T_1)]$ (Equation (28)), which at low temperatures may be approximated by $\dot{n}_3\ C_d\ \Delta T$; which is, using Equation (43)b, $\dot{n}_3\ kT\ \gamma \frac{dT}{d\ell}\ \Delta\ell$ where $\gamma = 13^{o}K^{-1}$. The energy balance equation is

$$\left(\frac{128}{\pi d^4}\right)\left(\frac{\eta T^2}{T^2}\right)\left(\frac{V_4}{X_o}\right)^2 \dot{n}_3^2 + \dot{n}_3\,\frac{\Gamma k T^2}{2} + \frac{\pi d^2}{4}\,(KT)\left[\frac{-1}{T^2}\left(\frac{dT}{d\ell}\right)^2 + \frac{1}{T}\,\frac{d^2T}{d\ell^2}\right] \tag{47}$$

$$= \dot{n}_3\ \gamma kT\ dT/d\ell$$

The KT term is smallest so for simplicity one may neglect it and write immediately

$$T\,\frac{dT}{d\ell} = \left(\frac{1}{\gamma k}\right)\left[\frac{A\dot{n}_3}{T^2} + \left(\frac{\Gamma k}{2}\right)T_2^2\right] \tag{48}$$

where

$$A = \left(\frac{128}{\pi d^4}\right)(\eta T^2)\left(\frac{V_4}{X_o}\right)^2$$

Equating the two sources of heat (viscous heating and heat extracted from the incoming fluid) to the cooling capacity given by equation (29) and using values for ηT^2, V_4, and X_o mentioned previously, one gets the equation

$$T_{limit} = (.72 \times 10^{-2})\ \frac{1\ mm}{d}\ {}^{o}k \quad \text{(continuous operation)} \tag{49}$$

as the temperature at which the two terms become equal. Using a typical value for d of .8mm this yields a temperature of $T = 9m^{o}K$. Notice that

this compares very nicely with the $10m^{o}K$ limit achieved by Vilches and Wheatley.[5] It indicates that adding additional heat exchanges to operate at temperatures below about $20m^{o}K$ will not be too helpful. The viscous induced heating will be comparable to the amount of heat you are extracting from the incoming fluid. Wheatley has noticed this effect experimentally. He found that increasing the number of heat exchangers beyond five has little effect on the final mixing chamber temperature. The limiting low temperature derived above should also be somewhat larger due to the KT term which was neglected for simplicity. The obvious approach of lowering T_{limit} by greatly increasing d is not possible because of a gravitational instability problem in the dilute solution. The instability arises because the fluid in the dilute phase becomes heavier as the temperature is increased. This is in turn due to the concentration of He^3 in the dilute phase which is decreasing with increasing temperature (Figure 6). Hence the fluid in the second heat exchanger is heavier than the fluid in the mixing chamber. Convective instabilities may develop which will destroy the thermal isolation of the various components. The instability is damped by the viscosity of the fluid and the tubing impedance. Since for viscous flow the impedance varies as d^{-4} the diameter of the tube exiting from the mixing chamber must be kept small. Hall encountered problems of convective mixing in his first refrigerator.[3]

If one is running a single-cycle refrigerator where the He^3 is not recondensed then the second term is not present. One has only

$$\frac{dT}{d\ell} = \left(\frac{1}{\gamma k}\right) \frac{A\dot{n}_3}{T^3}$$

This case (with the thermal conduction included) has been considered by Wheatley et al.[5] To take into account the conduction term they substituted

$$\frac{dT}{d\ell} = \left(\frac{1}{\gamma k}\right) \frac{A\dot{n}_3}{T^3} (1-f) \tag{50}$$

into Equation (47), (minus the second term) and arrive at a differential equation for f given by

$$t \frac{df}{dt} = \frac{f}{1-f} \; t^6 - 4(1-f) \tag{51}$$

where $t = T/T_o$, and the characteristic temperature T_o is given by

$$T_o = \left[\frac{32}{d^2} \frac{(\eta T^2)(KT)(V_4/X_o)^2}{k^2 \gamma^2} \right]^{1/6} \tag{52}$$

Notice that T_o does not involve $\dot{n}_3$, hence f will not, and the temperature gradient (Equation (50)) is linear in $\dot{n}_3$. The dependence of f on t from Equation (46) is determined by numerical integration. They find the intrinsic limit of the single-cycle device to be given by

$$T_{limit} = 4 \left(\frac{1mm}{d}\right)^{1/3} m^oK \quad \text{(single-cycle)} \tag{53}$$

Using their value of d = .6mm this gives an intrinsic limited temperature of $4.7m^oK$. They have reached a limit of $4.5m^oK$ with such a device.[6] The $d^{-1/3}$ dependence makes it difficult to decrease this further by using a larger pumping tube (on the mixing chamber). Notice that Equation (49) where the conduction term was neglected goes as d^{-1}. The inclusion of the conduction term will

undoubtedly make the temperature T_ℓ given there a much slower function of d such as the $d^{-1/3}$ found in Equation (53).

At sufficiently low temperatures the transport equations will become limited by boundary scattering. Then η will be independent of T and depend linearly on d, while K will depend linearly, both on T and d. The above analysis will not apply in this case.

Chapter III. Details of the Refrigerator Construction

A. General Characteristics

The actual appearance of the refrigerator is shown in Figure 9. The dilution refrigerator section and the pumped He^4 pot used to condense the circulated gas are located within a vacuum space. The vacuum space is surrounded by liquid He^4 boiling at atmospheric pressure. This outer bath of liquid He^4 is contained in a conventional glass dewar system which can fit between the pole pieces of Varian 15" magnet. This places a maximum allowable outer diameter of 2-1/4" on the glass dewar system. This, in turn, determines the diameter of all the interior components.

The outer bath of He^4 is left unpumped because this allows one to transfer more liquid into it at any time without disturbing the operation of the refrigerator. The inner He^4 pot is filled from the outer bath through a needle valve. It holds about 35cc of liquid and must be refilled about every five or six hours during operation. The pot is pumped through a flow limiting orifice and runs at a nominal temperature of $1.1^\circ K$ during operation. This pumping system is entirely separate from the circulation system of the dilution refrigerator.

While being refilled the temperature of the pot will rise to 1.7 - 2.0°K. The refilling operation takes only two to three minutes and the operation of the dilution refrigerator is disturbed very little.

B. Condenser and Flow Limiting Impedance

The condenser consists of 4.5gm of -325 mesh copper powder sintered into a copper body. This copper body is made to be a "slip-fit" into a copper sleeve which passes through the He^4 pot as shown in Figure 10. In this way there is no possibility of an internal leak of He^3 out of the condenser and into the He^4 pot system. Thermal contact between the condenser and the sleeve is improved by coating their surfaces with silicone vacuum grease.

By observing the decrease in pressure from tanks of a known volume, the condensing rate of the condenser was found to be 4×10^{-5} moles/sec at a pressure of 30mm-Hg. 30mm-Hg was chosen as the condensing pressure because this corresponds to the vapor pressure of He^3 at 1.3°K. Now the main impedance must be made large enough that a pressure of 30mm-Hg will not force more than 4×10^{-5} moles/sec through it. If more than this amount of liquid can pass through the impedance the condenser will operate empty. This will allow vapor to pass to the lower portions of the refrigerator and hinder its operation by causing an extreme load on the heat exchangers. In order to assure that this does not happen the main impedance is designed to require a pressure greater than 30mm-Hg to force 4×10^{-5} moles/sec of liquid through it. To calculate this value of impedance the viscosity of He^3 was taken to be 30×10^{-6} c.g.s. units at 1°K.[25]. The molar volume is 37cc/mole thus,

$$Z = \Delta P/\eta\dot{V} = 9 \times 10^{11}\ \text{cm}^{-3}$$

when ΔP = 30mm-Hg and $\dot{V} = 4 \times 10^{-5}$ moles/sec.

The impedance actually used had a measured value of $Z = 1.5 \times 10^{12}\ \text{cm}^{-3}$, the factor of two being added for safety. As long as the value is large enough to satisfy the conditions outlined above the operation will be self-regulating in that if the circulation increases or decreases the pressure will rise or fall accordingly in order to drive the flow. The flow rate does not depend on this impedance but rather is determined by the pumping speed of the diffusion pump and pumping lines running to the still.

The impedance was made by passing a 7.3" piece of No. 31 manganin wire inside of a .010" I.D. bore tube (No. 31 gauge = .00893"). The tube O.D. was then drawn down from .0160" to .0157". The impedance was measured by flowing dry nitrogen gas through it at a known pressure head. The viscosity was taken from the handbook of physics and the volume rate of flow determined by collecting the gas by water displacement in a graduated cylinder while timing with a stopwatch.

C. Heat Exchangers

As described in the last chapter, the heat exchangers are very vital to the efficient operation of the dilution refrigerator. They also present design problems in that one desires a small flow impedance, but a large heat exchange surface and good thermal contact between sides. In this light a systematic study was made in an attempt to maximize the ratio of surface area to flow impedance. Sintered

copper sponges of various densities were made and their respective areas and flow impedances measured. The ratio of area to impedance as a function of sponge density was thus obtained. This was done using both 5μ and 40μ diameter, 99.9% pure copper powder. (Copper powder was purchased from Alcan Metal Powders, Inc., Berkeley, California.)

The body into which the powder was packed and sintered was OFHC copper. ETP copper was tried but it tended to blister and become porous during sintering with the result being a sponge which was not vacuum tight.

The sintering was done in a hydrogen atmosphere at about 625° C. In all cases the sponge appeared to sinter well to the copper body. No swaging of the body after sintering, as reported necessary by other authors,[5] was ever needed. It is believed that good adhesion of the sponge to the body wall can be achieved by sintering at these lower temperatures. When a sponge was heated above about 700°C, it tended to contract and pull away from the body. The powder particles, when viewed under a microscope before sintering, are very jagged and irregular in shape. It is believed that overheating tends to cause all of them to become rather spherical in shape, thereby reducing their total volume. The result is that the sponge cracks away from the walls.

A poor sponge will result if the powder is not packed firmly enough. The smallest sponge density possible seemed to be about .5 gm/cc with the 5μ powder just packed tight enough to keep from falling out.

The flow impedance for turbulent flow was taken to be

$$Z = (P_2^2 - P_1^2)/2\eta\dot{V}P_1$$

where P_2 is the driving pressure, P_1 the terminal pressure, $\dot{V}$ the volume rate of flow, and η is the viscosity. The impedance was measured experimentally by the same method used for the main impedance described in Section 1 above. The typical unit of impedance for these sponges was 10^8 cm^{-3}.

A plot of a quantity called the flow conductance defined as K = volume/impedance is shown in Figure 11. A summary of all the data from the sponges is given in Table 1.

The area of three sponges was determined by running adsorption isotherms with nitrogen gas.[26] Measurements of this type are tedious and the areas obtained are not extremely accurate. However, the results as shown in Figure 11 do give the general trend of the area as a function of density.

It was desired to find a maximum in the product of the area per unit volume times the conductance as defined above. This product is displayed in Figure 12. Notice that the very fast decrease in conductance with density entirely dominates the product. From this graph one can see that the desired maximum occurs at the lowest densities. In looking for a maximum in the product KA an implicit assumption has been that there is an equal weighting between area and impedance as far as the efficiency of the refrigerator is concerned. This may not be the case but the behavior of the conductance with respect to density so dominates that the results obtained here are probably correct outside of some unforeseen extreme dependence of the efficiency upon area.

Faced with the problem of making sponges of very small density a new type of sponge was developed. The process consisted of grinding

up one of the medium density sponges made of the 5μ powder into small pieces about 1mm in diameter. These "pebble sponges" were then used as stock from which another sponge was made. The resulting sponge had a very small flow impedance with the volume resistivity being a factor of 10 less than the best we had made previously or that had been reported by other authors[5] (see Table 1). On the other hand, the measured surface area of this sponge was as large as the conventional type. The new sponge had also sintered to the body wall, as well as the conventional sponges. This fact was determined by measuring the electrical resistance between the sponge and the body. The resistance was measured by passing currents of 1 to 5 amps through the sponge-body interface and measuring the voltage developed with a microvoltmeter. The connections to the sponge were made as shown in Figure 13a. The resulting values at room temperature were 6.0μΩ for one of the best conventional sponges and 6.7μΩ for the new reground type.

If one makes the assumption that the geometry for heat flow is the same as for electrical current flow, then the resistance measured above gives a measure of the thermal contact between the sponge and the copper body. For heat flow $\dot{Q} = K(A/\ell)\,\Delta T$ and for electrical resistance $R = \rho(\ell/A)$. Then multiplying the two relations $\dot{Q}R = \rho K\,T$. Now the Wiedemann-Franz relations is

$$\rho K = L_o T \tag{54}$$

where

$$L_o = 2.445 \times 10^{-8}\ V^2/{}^oK$$

inserting this value for ρK above gives

$$\dot{Q}R = L_o T\Delta T = L_o T^2 \left(\frac{\Delta T}{T}\right)$$

Now, imposing the condition that the temperature drop should be less than .1 of the overall temperature of the piece, i.e., that $\Delta T/T \leq .1$, then

$$R \leq .1\ L_o T^2/\dot{Q} \tag{55}$$

Now for low temperatures ($T \leq .030^oK$) the specific heat of He^3 as given by Equation (43a) is $C_3 = 3n_3 R_G T$ and decreasing as T increases. R_G is the gas constant. The enthalpy is then $H = 3/2\ n_3 R_G T^2$ so an approximation to $\dot{Q}$ which is conservatively large is $\dot{Q} = (3/2)\ \dot{n}_3 R_G T^2$. Using this in Equation (55) gives the condition on R.

$$R \leq \frac{.1\ L_o}{(3/2)\dot{n}_3 R_G}$$

Notice this is independent of temperature and valid for all heat exchangers. Using a typical value of $\dot{n}_3 = 2 \times 10^{-5}$ moles/sec one gets

$$R \leq 9.8\mu\ \Omega \tag{56}$$

as the limiting condition on the electrical resistance. Notice that both sponges measured are well within this range.

The final design chosen for the heat exchangers is shown in Figure 13b. Both sponges are in the same body so there is a minimum thermal impedance between sides. Both halves are sponges made from the reground stock described above.

There is a question as to the flow pattern through the reground type sponges. That is, will there be channeling of the fluid through the larger holes between the "pebble sponge" so that the total area of the sponge will not be utilized? This may be true on the condensed side where one has pure He^3 but on the dilute side where one needs the best heat exchange and the least flow impedance, the superfluid He^4 will readily penetrate all of the sponge. Furthermore, if the mean free path of He^4 excitations is much less than the pore size of the pebble sponge the He^4 will act as an exchange medium between the He^3 and the entire sponge area. The pebble sponges are made from low density conventional sponges, hence, if the pore size is unaffected by sintering the ratio of mean free path to pore size will be just as good in one case as in the other. On the condensed side one may want to use a conventional sponge if the "flow-channeling" seems to be a problem.

Experiments with our present refrigerator indicate that the heat exchangers are operating at least as efficiently as the conventional type. However, it must be realized that they are not operating at as low a temperature as will be necessary in a larger refrigerator. These problems will be discussed in detail in the coming section on operation characteristics.

Connection of lines to the sponge is made as shown in the enlargement in 13b. In order to avoid the possibility of plugging the lines with the soft solder used the copper capillary tube is threaded and screwed into the tapped hole in the body. These joints, as well as the brass caps, are soldered in place using a small torch,

soft solder and a non-corrosive flux. The interconnecting cupronickel tubing is soft soldered in place using an iron and at the same time, air is forced through the tubing to alleviate further the problem of plugging the capillary tubes.

D. Interconnecting Tubing and Mechanical Supports

The interconnecting tubing is cupronickel (70% Cu — 30% Ni) obtained from Superior Tube Company, Norristown, Pennsylvania. This alloy was chosen for several reasons. At low temperatures its coefficient of thermal conductivity is equal to or less than that of stainless steel.[27] It can easily be soldered with soft solder without resorting to strong acid fluxes and because of this, it is more resistant to corrosion than stainless steel once soldered in place. It also is quite ductile; draws easily without leaving weak spots that can occur with stainless steel, and bends easily during assembly.

The tubing on the condensed side has an I.D. of .010" and a .003" wall. On the dilute side the bore is .030" and again a .003" wall. The sizes and lengths of these tubes are determined by the problems of thermal conduction and convection on the dilute side, and the necessity of suppressing vapor formation on the condensed side.

Consider the problem of the condensed side first. If at some point the hydrostatic pressure of the fluid becomes less than the vapor pressure of the liqud corresponding to the temperature of this point, then a vapor bubble will form. This "vapor-lock" can disrupt the liquid flow. The vapor must also be recondensed somewhere, most likely in the heat exchangers, which will produce undesired

heating of these components. This problem is present only in the high temperature components near the still. For at a temperature of .8°K the vapor pressure of He^3 is about 3mm-Hg. Unless the pressure rise from the still on the dilute side is greater than this pressure, vapor will be formed in the still heat exchanger and passed on to the first heat exchanger. This problem was noted in the first refrigerator. In this machine the first heat exchanger tended to run very hot, equal to the still temperature or even above, and was more closely linked to changes in the He^4 pot temperature than those of the still. The problem was solved by running a 2" piece of No. 31 manganin wire down the .010" bore tube between the still and the first heat exchanger. This gave an impedance of $2 \times 10^{11} cm^{-3}$ between the still and first heat exchanger, the value desired having been calculated as described before for the main impedance.

For a temperature of .5°K the vapor pressure of He^3 is equivalent to the hydrostatic pressure of a column of liquid He^3 3cm high. Thus the problem of vapor formation is absent in the lower portions of the refrigerator. The problem in the lower temperature portions can, in principle, be viscous heating. However, there is nothing to be gained by making the impedance of the tubing much less that of the heat exchangers. Table 2 gives all the values selected for the interconnecting tubing on both the condensed and dilute sides.

On the dilute side the major problem is caused by the fact that the He^3 concentration decreases as the temperature increases. (Refer to Figure 6), creating the gravitational instability discussed in Chapter II, Section D. This problem was noted by Hall in his first

refrigerator[3] when pumping with a coaxial line having a .325" I.D. on the outer tube and a .205" O.D. on the inner tube. The problem may be lessened by decreasing the tube diameters. As the viscosity increases with decreasing temperature the tube diameters may be increased. No problems of convective instability have been observed with the tube sizes given in Table 2.

The thermal conduction in the dilute solution is limited by the collision of phonons with the He^3 quasiparticles. This is not altered by the flowing He^3 because the He^3 flow velocity is so much less than the phonon velocity. To obtain the variation of temperature with length one must solve the conduction equation $\dot{Q} = K_d A \, dT/d\ell$ together with the enthalpy conservation equation $d\dot{Q}/d\ell = 5/2 \, R\dot{n}_3 \, dT/d\ell$. This leads to the energy balance equation

$$\frac{5}{2} R\dot{n}_3 \frac{dT}{d\ell} = \frac{\pi}{4} d^2 K_d \frac{d^2T}{d\ell^2} \tag{57}$$

where d is the diameter of the tube, ℓ the distance along the tube, and K_d is given by Equation (21). The solution of Equation (57) will give an exponential variation of temperature with length. The characteristic length is

$$\ell' = \frac{\pi/4 \, d^2 K_d}{5/2 \, \dot{n}_3 R} \tag{58}$$

If one takes x = .01 as the concentration in the still and substitutes this into Equation (21) to get K_d, then Equation (58) is numerically

$$\ell' = \frac{1}{3} \left(\frac{d}{1mm}\right)^2 \tag{59}$$

where a value of 2×10^{-5} moles/sec has been taken for $\dot{n}_3$. This distance is very small in comparison to the lengths of tubing between the various components. There is thus essentially no thermal conduction along the interconnecting tubes.

Pitch-bonded graphite is used for the mechanical connections between the various components. It was chosen because of its rather unusual thermal conduction properties reported by Shore et al.,[28] and more recently Edwards et al.[29] For temperatures in the range of 2-4°K the thermal conductivity is reasonably large thus facilitating the pre-cooling of the various components. On the other hand, at 0.3°K the thermal conductivity is some four times less than that of teflon and seven times less than that of nylon. The graphite thus behaves rather like a heat switch. It is strong, easily machined and as an added bonus, aids in pumping out the He^4 exchange gas which is used in the vacuum jacket during cooling of the entire device from 77°K to 4°K.

The connecting links are of modular form and thread onto the brass end caps of the heat exchangers as shown in Figure 13b. The heat exchangers are located in line with the graphite supports in order to use all available radial space at the expense of some increase in the overall length of the device.

E. Still Design

The still is shown in Figure 14. The design of the still is dictated by the need to suppress He^4 film flow. The upper portion is made from a single piece of copper. This is done to assure

uniformity of temperature up to the flow limiting orifice thereby minimizing the possibility of He^4 vaporizing from the film.

The design of the upper portion of the still has been the subject of an extensive investigation by Wheatley et al.,[5] the final result of which has been a total new design concept.[30]

The placement of the heater in the still is quite important. It must be located in a position from which all the heat flows directly into the bulk liquid and does not heat any of the regions near the flow limiting orifice. The heater consists of approximately 150Ω of No. 39 Evanohm wire coiled upon a piece of masking tape. This flat coil is then epoxied onto a piece of nylon as shown in Figure 14. The nylon provides thermal isolation between the heater and the copper walls of the still. The electrical connections to the heater are made with No. 38 copper wire. The two copper wires are fed through a .020" I.D. cupronickel tube which is soldered into the wall of the still as shown. After the upper and lower portions of the still have been soft soldered together this tube is filled with Stycast 2850GT epoxy (Emerson-Cumming Corporation, Los Angeles, California). This particular epoxy has a thermal coefficient of expansion which is quite close to that of copper. This feedthrough for the wires is quite dependable and has always been helium leak tight.

An added feature of this still was the addition of a liquid level sensor fashioned after the design by Boghosian et al.[31] This level sensor was added because in the first model there was always a question as to where the liquid level was in the still.

The level sensor consists of a piece of thin brass inserted inside the copper body of the still to form a coaxial capacitor. The spacing between the brass and the copper is .002" on the radius. Insulation from the sides is provided by wrapping the brass sleeve with one layer of .001" mylar and at the upper and lower ends a disc of ~ .001" mica is placed. The measured value of this capacitor at room temperature is 180 pf. The capacitor is then connected into the tank circuit of a tunnel diode oscillator, the total circuit being shown in the insert of Figure 14.

The dielectric constant of liquid He is approximately 5% larger than that of He vapor. Thus as the liquid level in the still rises there will be an increase in the capacitance of the coaxial capacitor. This increase in capacitance will produce a decrease in the natural frequency of the oscillator. Since the frequency can be monitored with extreme precision one has a very sensitive level detector. For our purpose it was not necessary to know the liquid level to any high degree of accuracy, therefore, to simplify the electronics a 1100pf capacitor was added in parallel with the level sensing capacitor in order to lower the resonant frequency. This obviously decreases the sensitivity for one is now looking for a 5% change in roughly 10% of the total capacitance. Since the frequency varies as $1/\sqrt{c}$ this will correspond to approximately .2% change in the frequency from entirely empty to entirely full.

For the values of the inductor and the capacitor chosen the resonant frequency was roughly 300 K Hz with the still empty.

This frequency decreased by about 600 Hz when the still was full. The signal was amplified with a transistor amplifier (Model TA-4B, Infrared Instruments, Santa Barbara, California) and the frequency counted with a Hewlett-Packard Model 5245L electronic counter (Hewlett-Packard Co., Palo Alto, California).

The tunnel diode and tank circuit were located on the bottom of the still as shown in Figure 14. At these temperatures the oscillator was very stable with the frequency not varying more than ± 1 Hz over periods of time on the order of one hour. Since the total change in frequency from empty to full is ~ 600 Hz it was quite easy to monitor the liquid level in the still with considerably more precision than was ever necessary. In fact, since the total height is .80" one could monitor the level down to changes approaching ± (.8/600)" or about .002".

The bottom of the still is also made from a single piece of copper. Located in this piece is a sintered copper sponge which serves as a heat exchanger for the incoming liquid, cooling it to the temperature of the still. This sponge is sintered inside a copper sleeve which is then "greased" into the hole in the bottom of the still just as was done with the condenser at the He^4 pot. The sponge consists of 2.4 gm. of -325 mesh copper powder and has a free volume of .47 cc. The connecting tubes to the still heat exchanger are Cu 1/16" O.D., tubing available on campus. A 1-1/2" length of this tube is hard-soldered to either end of the heat exchanger and during this process the copper tubing is annealed. After annealing, the tubing

is quite soft, and can easily be bent in the direction necessary to connect onto the other components. The connections to the cupronickel tubing are made with small brass sleeves. The sleeve is bored half way through with a 1/16" drill to accommodate the copper tube. It is then bored the rest of the way with a No. 73 drill to fit over the .013" O.D. cupronickel tubing used on the dilute side. The end into which the cupronickel fits is counter-bored with a No. 60 drill to create a pocket for making a soft solder fillet. The soldering is done with an iron and air is passed through the tubing to prevent plugging.

The return line to the still on the dilute side enters through the bottom as shown in Figure 14. The problem of convective instability is most important in this line for the temperature is high and the viscosity small. To avoid a possible breakdown of the flow pattern in this length of tubing due to this gravitational instability the tubing is bent into the shape of a double hairpin as shown. Since the temperature gradient is quite steep along these tubes, as shown in the last section; Equation (59), the temperature at point A is essentially the same as that of the first heat exchanger. Thus the gravitationally unstable fluid between the still and point B is counterbalanced by the stable fluid between points B and A.

F. Mixing Chamber

Since the dilution refrigerator was intended to be used primarily as an experimental tool, rather than itself being the object of study, the mixing chamber was constructed of copper. The design is shown in Figure 15. If the refrigerator is being used to cool other

experimental apparatus the advantages of the copper mixing chamber, as opposed to one of a nonconducting material such as cast epoxy, are several. It is much easier to make thermal contact with the cold liquid through a copper mixing chamber which can easily be provided with numerous mechanical fixtures and thermal grounds. The disadvantage is that an accurate determination of the ultimate temperature of the refrigerator is no longer possible.

With a nonconducting chamber one can place a paramagnetic salt such as Cerium Magnesium Nitrate (CMN) directly in the helium liquid and do magnetic thermometery on it. With a copper chamber the eddy currents prevent such measurements. All of the details of this thermometery will be discussed in Chapter VI.

Thermal contact between the liquid and the copper is improved by the addition of the thin vanes of copper. The vanes are made by passing a .002" thick strip of copper shim stock through the loose fitting gear train on the lathe. This produces a corrugated strip with the steps being about 1/4" high. The strip is then fitted inside the mixing chamber and soft soldered at all points of contact. After soldering the open ends of the corrugation are cut and folded away from one another into a radial alignment as shown in Figure 15. They are cut open in this manner to avoid the possibility of forming stagnant pockets of liquid inside the mixing chamber.

The inlet and outlet tubes pass through 1/16" O.D. copper nipples made from the same tubing used on the still heat exchanger. The ends of the tubes are threaded with No. 2-56 thread and tapped

into the upper portion of the mixing chamber. These joints are then hard soldered. The outbored ends of the tubing are counter-bored in the same manner described previously for the brass coupling sleeves to allow for a good soft solder fillet.

The inlet tube of .010" I.D. Cupronickel terminates just below the top of the inner wall of the mixing chamber. The outlet tube is .030" I.D., again of cupronickel and terminates approximately .050" above the bottom surface. Both are soft soldered into place using an iron and non-corrosive flux.

The thermometer on the mixing chamber is a calibrated Speer 100Ω, 1/2 watt carbon resistor (grade 1002) (Speer Carbon Co., Bradford, Pa.). The calibration of this resistor is described in detail in Chapter VI on temperature measurement. The outer insulating coating has been thinned down by using a grinding wheel to reduce the O.D. from .140" to .110". This leaves about .005" insulation on the radius. The resistor is then greased into a hole drilled in the lug on the bottom of the mixing chamber. There is also a tapped No. 4-40 hole in this lug which serves as the connection point for the sample. Equally spaced around the perimeter of the mixer bottom are three No. 2-56 screws which are used as thermal grounds for electrical leads running to and from the sample.

G. Testing

The major problem in assembling the dilution refrigerator is vacuum leaks. During construction the device was leak checked by sections using a mass spectrometer leak detector. The still, He^4 pot, and

other components are easily checked in this manner because the pumping impedance to them is small. However, with the heat exchanger system the pumping impedance is higher and the response of the leak detector much slower. Still one detects large leaks quite readily this way. After the entire device is assembled and the isolation vacuum can is put in place this chamber is then pumped with the mass spectrometer leak detector. Helium gas is now circulated through the refrigerator. This test is performed both at room temperature and liquid N_2 temperature. Any leak in the system is quickly discovered by this test but it is not localized. Great difficulty was experienced with leaks that appeared only at liquid N_2 temperature. For this reason, it was necessary to develop a method of leak detection that would allow the localization of leaks while the entire device was at liquid nitrogen temperatures. This was done by placing the assembled refrigerator into a clear dewar filled with liquid N_2. The mounting cap is sealed onto the nitrogen dewar with an o-ring and clamp screws so that the dewar may be pressurized. Helium gas at about 5 PSI over atmospheric pressure is then forced into the nitrogen dewar causing the liquid N_2 to stop boiling. The nitrogen is now very quiet and free of any apparent disturbances. High pressure helium gas (about 2 atm) is then forced into the refrigerator. The experiment is performed in a darkened room with the refrigerator lighted from behind. The bubbles of gas escaping from a leak are quite easily seen and the leak is thus localized. This method is surprisingly sensitive with leaks as small as $\sim 5 \times 10^{-6}$ cc/sec, as measured with the calibrated leak detector, having been found in this

manner.

A second test which must be performed during assembly is that of flow impedance testing. This must be done to check against the possibility of partial or total plugging of the interconnecting lines during assembly. The impedances of all the heat exchangers are known so that any spurious impedance is quickly detected. Values for the impedance of the assembled refrigerator are given in Table 3.

In practice the still was assembled and then connected to the pumping system to be leak-checked. The heat exchangers and mixing chamber, assembled as one unit, are then connected. The return line to the still on the dilute side is soldered in place and the inlet line to the heat exchanger on the condensed side is plugged with a small ball of solder. This portion of the refrigerator is then leak tested. Next the end of the tubing which was plugged is cut off and the flow impedance of the entire refrigerator measured. The main impedance is not connected at this point because its very large impedance would hide any problems in the rest of the refrigerator. Finally the main impedance is soldered in place.

H. Room Temperature Components

The arrangements of components as shown in Figure 16 provides a flexible and efficient gas handling system. An effort was made to minimize the number of valves and all those shown have been found to be essential. The size of the storage tanks is determined by the size of the refrigerator and the gas charge needed to fill it. The volume of our storage tanks is such that the He^3-He^4 gas mixture is stored

at less than atmospheric pressure. This is necessary since the mechanical pump can not safely stand a back pressure greater than one atmosphere. Another advantage is that leaks in the storage system are quickly detected by an increase in the pressure while at the same time little He^3 gas is lost. The air that may have leaked into the helium mixture is easily removed by circulating the gas through tubing immersed in liquid He^4.

The mechanical pump is a Welch, Model 1402KGB, rotary pump with an oil sealed shaft designed principally for use in closed systems (Welch Scientific Co., Skokie, Ill.). A word of caution might be added here in that this pump was found to leak around the fiber gasket oil seal of the pump body allowing air to leak into the system when the exhaust side of the pump was running at less than 1 atm. This leak was sealed by painting around the gasket seal with glyptal varnish.

After the system had been assembled and made helium leak tight all air was removed from the back side of the mechanical pump by pumping through valve No. 14 with another pump. This valve was then closed and the system has not been opened to air since this time. When the mechanical pump is not running, Valve No. 13 is opened so that both input and exhaust are at the same pressure.

The diffusion pump is an NRC Model B-2 booster pump. It was chosen because of its relatively fast pumping speed for pressures in the range of 10 to 20 microns.

All the valves, with the exception of No. 3, are Hoke model

4151M2B bellows-sealed valves with a Kel-F tip. Valve No. 3 is a Veeco bellows-sealed valve with a 1-1/2" bore. (Valves were obtained from Castle Controls, Inc., Pasadena, Calif.)

All the lines from Valve No. 5 to the input of the dewar are 1/4" I.D. soft copper tubing. From the dewar cap down into the refrigerator the input line is 1/8" stainless steel with a .010" wall. Just before the input line enters the isolation vacuum chamber there is a spiral of 18" of .050" bore copper tubing which is in the outer He^4 bath. This aids in precooling the incoming gas to helium temperatures and also acts to block room temperature radiation.

The tubing running from the booster pump to the still is graduated in length and diameter as shown in Figure 9 in order to to maximize the pumping speed. For the pressures involved the gas flow is always viscous. Since the viscosity increases with temperature it is necessary to use larger bore tubing in the high temperature sections. The size of tubing required was calculated using Poseville's law for the gas flow,

$$\Delta P = \frac{128}{\pi} \eta(T) \left(\frac{L}{D^4}\right) \dot{V}$$

where $\eta(T)$ is the viscosity of helium gas as a function of temperature,[27] L is the length of tubing, D the diameter, and $\dot{V}$ is the volume rate of flow at the mean pressure. $\dot{V}$ was calculated from a molar circulation rate of 3×10^{-5} moles/sec which is about the maximum pumping speed of the booster pump. With the sizes of tubes shown the pressure drop across the pin hole is roughly twice the pressure drop in the lines and the calculated pressure of $\sim 250\mu$ in the still compares quite well

with the known vapor pressure of the liquid at a typical still temperature of ~ .75°K. (See Figure 8).

While the refrigerator is not in use it is pumped through valve No. 15 with No. 1 and No. 2 also open. The system to the right of valves No. 3, 4 and 7 is filled with the helium gas charge. The external port at valve No. 15 also allows one to sample a small quantity of gas coming from the still during operation (needle valve No. 2 slightly opened) in order to measure the ratio of He^3 to He^4. This measurement is made using a calibrated mass spectrometer leak detector (G.E. Model M-60).

There are two liquid nitrogen traps in the system. Trap I is a conventional glass cold finger and catches mostly pump oil from the mechanical pump. The glass is joined into the metal system using standard Kovar metal to glass seals. Trap II has a finger of 1" diameter filled to a height of 4" with Linde 13x molecular sieve pellets through which all the circulated gas must flow. These molecular sieve pellets are wrapped in nylon mesh to catch the powder which is always present with them. The molecular sieve trap will catch any residual air and water vapor which might be in the system. Between runs the trap is degassed by heating it with a heat lamp while pumping through valve No. 15 as explained above.

Pressures are read on the input side with a conventional mercury manometer system. A small amount of low vapor pressure oil (such as used in oil manometers) was added to cover the mercury surface to a depth of roughly 3mm. This was done to prevent the diffusion

of Hg vapor into the gas handling system where it would have a very harmful affect on the thin bellows contained in the Hoke valves.

The thermocouple gauge on the "high" vacuum side is used to monitor the pressure in the still line. It reads from 0 to 1000μ, with an expanded scale from 0 to 100μ, which is the region of greatest interest. This gauge is also used to check for blockage of the refrigerator during start-up. This is done simultaneously with the leak detection procedure as described in the last section. After the refrigerator has been pre-cooled to LN_2 temperature helium gas is admitted to the input side only through valve No. 15 and No. 1. Prior to this the refrigerator has been under vacuum and the T.C. gauge on the still side will be reading ~ 0μ. If the refrigerator is not blocked one will observe a rapid rise in the pressure on the T.C. gauge roughly thirty seconds after the helium gas has been admitted through valve No. 15.

(I) Auxiliary Cryostat Components

(1) Needle Valve

The needle valve used to fill the He^4 pot is shown in Figure 17a. The barrel and bottom are made of brass. The valve stem is stainless steel and is threaded with a micrometer screw thread. The valve seat is monel alloy No. 400 (Pacific Metals, Inc., Los Angeles, Calif.) and is designed so that it is easily replaced. This is necessary only after many months of use. Hard soldered to the stainless steel valve stem is a piece of thin walled (.010") stainless tube which runs to the top of the dewar and passes out through an o-ring seal as shown in Figure 9. This tube is capped off at the top and

used for opening and closing the valve. The fill line running from the valve to the pot is .010" bore cupronickel tubing.

(2) Isolation Vacuum Chamber Connection

The isolation vacuum can must be designed to be readily removed in order to give easy access to the refrigerator. One also needs a joint that will be dependably leak-tight in liquid He^4. The design of this joint using a crushed indium seal as shown in Figure 17b has proven very satisfactory. The upper and lower flanges are made of brass. Care was taken to see that the surfaces in the region of the indium seal were turned flat and free of any radial scratches. The protruding portion of the upper flange is a tight slip-fit (~ .001" clearance on the diameter) into the lower mating flange. This assures good alignment of the can. The indium seal is made from .030" diameter pure indium wire. The wire is wrapped once around the upper flange and cut on the bias with a razor blade so that the ends join smoothly. The two flanges are joined using eight No. 8-32 bolts with spring loaded washers. The bolts are tightened down until the two brass faces are flush at the outer edge. Differences in thermal contractions between the indium, brass, and the bolts is countered by the use of the spring washers.

The indium forms a very good cold weld between the surfaces. To break the joint later, two No. 4-40 screws are threaded into the lower flange. The retaining bolts are loosened and the two "jack" screws are then tightened, pushing the two faces apart.

No special care is taken in cleaning the two surfaces before

making a new seal other than to remove bits of the indium remaining from the last time.

(3) Radiation Baffles

The amount of power generated by room temperature blackbody radiation which is conducted down the pumping lines into the refrigerator and isolation vacuum chamber can be quite large. To prevent this, baffles, shaped as shown in the insert of Figure 9, are placed in all of the lines. The baffles in the still and He^4 pot pumping lines are made from a single piece of brass whose surface has been roughened with a piece of coarse sandpaper and then chemically blackened. These baffles slip into the pumping lines and rest where the tubing diameter is decreased upon entering the isolation can. They are kept cool by the pumped gas which is flowing past them.

The baffle in the isolation vacuum pumping line is made of copper. Since there is very little gas flowing past it, this baffle must be thermally grounded by another means. This is done by soldering its lowest face to the large brass flange through which the tubing passes. This brass flange is always at $\sim 4^{\circ}K$ due to the outer bath of liquid He^4.

There is also a 1/8" diameter line that exits into the vacuum can to provide a conduit for the electrical leads. This is also baffled with a copper piece having the same design as the others.

(4) Electrical Leads

There are ten electrical leads coming into the present apparatus. They begin from a hermetic seal at room temperature and are

fed down a thin walled stainless tube as mentioned above. Screwed into the brass flange near the exit point for the wires is a 1/8" diameter copper lug. The wires are wrapped around this lug for several turns (~ 4" of their length) to provide thermal grounding. They then are attached to a terminal board consisting of ten small gold plated jacks and receptacles which are mounted in a piece of lucite. This terminal board allows one to easily disconnect the wiring of the lower portions of the refrigerator in case it is necessary to remove sections of it.

Of the wires coming from room temperature to the terminal board five are No. 38 gauge Evanohm (Wilbur B. Driver Co., Newark, N.J.) and five are No. 40 gauge copper. The choice of which type to use for a given purpose should be based upon whether the relatively high (81 ohm/ft), temperature independent, resistance of the Evanohm wire is important. Certainly, it would be leads carrying much current; such as heaters, but would not be in the thermometer leads.

A summary of all the important parameters of construction for each of the components has been prepared in Table 3.

Chapter IV. Operation

A. Starting Up

Following the tests on the system at LN_2 temperatures He^4 exchange gas is admitted to the isolation vacuum chamber. Liquid He^4 is then transferred into the outer bath. When the refrigerator has reached $4.2^{\circ}K$ the exchange gas is pumped out. At the same time the

He^4 pot is filled. While the refrigerator is held at ~ 4^oK the pressure in the isolation vacuum is reduced to ~ 1×10^{-5}mm Hg in a period of roughly forty-five minutes. At this time pumping on the He^4 pot is begun and its temperature is reduced to ~ $1.^oK$ in a few minutes. Condensation of the He^3-He^4 gas charge into the system is then started.

The amount of gas needed to fill the refrigerator is computed from the known volumes of the system and the molar volumes for He^3 and He^4 taken at 0^oK. These are 36.8cc/mole and 27.6cc/mole, respectively.

There must be enough He^3 liquid to fill all the volumes on the input side from the condenser to the mixing chamber. The amount of liquid He^4 must be enough to fill the dilute heat exchangers and a substantial portion of the still. Our tanks contain 13.4 STP liters of a He^3-He^4 gas mixture 37% of which is He^3. During start up 11.5 STP liters of this gas are condensed into the refrigerator. This produces more He^3 liquid than is necessary but aids in a rapid start up of the refrigerator for reasons to be explained. The gas is condensed into the refrigerator through the condenser only. The time required to condense the entire charge of gas desired is taking around forty minutes. The condensing rate is proportional to the input pressure so it is advantageous to have more than the needed amount of gas, within reason, considering the cost of He^3 gas. During the time the gas is being condensed all components of the refrigerator cool to approximately 1.7^oK. For a temperature profile of the device during

a typical startup see Figure 18.

As soon as condensation has been completed valve No. 3 is opened as quickly as is possible without letting the pressure on the back side of the pump go above 1 atm. Gas is now being circulated with the mechanical pump and within a time span of less than five minutes all components will have cooled to approximately .6°K. At this point every effort is being made to circulate the gas as fast as possible. The He^4 pot is refilled for safety, since the major load on it has been during the condensation process, and the power to the booster pump is turned on.

During the cool down to .6°K phase separation of the liquid occurs. Now, in essence, one has a "U" tube with He^4 at the bottom and He^3 floating on the top of either side. In order to get the phase boundary into the mixing chamber all of the He^3 from the still side must be pumped around to the input side. To have a rapid startup this must be done as soon as possible. This is the reason for condensing in an amount of He^3 that is larger than will be needed during steady state operation and also the motive for pumping as fast as possible during the startup.

Within about ten minutes after the power to the booster pump has been turned on the pump will begin to function. The pressure as read on T.C. gauge No. 2 will drop quickly to about 10μ. During this time the refrigerator will have cooled to about .5°K. With the booster pump now working, the desired amount of heat is applied to the still. For this refrigerator about .42 m watts ($.42 \times 10^{-3}$ watts)

seems to work best. The still will warm sharply to ~ .65°K as shown in Figure 18 and all the other components will continue to cool. The power is applied to the still in order to increase the He^3 circulation as explained previously.

The refrigerator will now continue to cool at a very steady (and reproducible) rate without any further attention. In fact the starting procedure outlined above has become so routine that it is possible to predict the temperatures of all the components knowing only the elapsed time since the beginning of He^4 transfer several hours earlier. The typical time required for reaching the lowest temperature is ~ four and one-half hours from the start of He^4 transfer.

The most important points of this start up routine are: (1) the addition of extra He^3 and (2) a circulation rate that is as large as possible. On earlier runs where this routine was not followed the refrigerator would stall at a temperature of ~ .5°K for periods of one to two hours. This was apparently just the time required to move enough He^3 around to the input side to move the phase boundary into the mixing chamber.

It is a characteristic of He^3 liquid to expand as its temperature is lowered.[50] This results in a movement of the phase boundary towards the still as the refrigerator cools. If the amount of He^3 in the system is large enough it is possible for the phase boundary to pass out of the mixing chamber and into the dilute side of the lowest heat exchanger. This phenomenon does occur in our refrigerator at about .2°K and is a consequence of the extra amount

of He^3 condensed in at the beginning. Evidence of this occurrence is a sudden increase of cooling in the lowest heat exchanger and a cessation of cooling in the mixing chamber as can be seen by referring to Figure 18. To correct the situation valve No. 4 is shut, thus stopping the circulation. Gas is stored in the storage tanks until enough He^3 has been stored to move the phase boundary back into the mixing chamber. Once cooling has resumed in the mixing chamber circulation is begun again and the refrigerator will cool to its ultimate temperature without further attention.

Since the amount of gas condensed in is always the same the temperature at which the phase boundary will pass out of the mixing chamber is quite predictable. The corrective action outlined above can be taken in advance with no resulting stalls of the refrigerator in its cool-down process.

B. Steady State Operation

The most important design aspect in determining the ultimate temperature of a dilution refrigerator is the number of heat exchanger stages. Our machine is comparatively small, having only two heat exchangers below the still as compared to the five employed by Wheatley et al.,[5] in reaching $10m^{o}K$. The ultimate temperature of our machine has not been accurately determined because a copper mixing chamber was used. This problem was discussed in the section on mixing chamber design. A steady state temperature of $78m^{o}K$ has been recorded by measuring the paramagnetic susceptibility of a sample of CMN attached to the mixing chamber. The details of all the thermometry are to be discussed in the next chapter.

This temperature of $78m^{o}K$ is only an upper limit to the temperature of the fluid in the mixing chamber. Every effort has been made to assure good thermal contact between the CMN and the mixing chamber; however, it is still quite possible that the liquid is on the order of several millidegrees less than the temperature recorded.

In a single-cycle process where the He^3 is pumped out, but not recirculated, a temperature of $59m^{o}K$ has been recorded. The fact that this temperature is significantly lower than that recorded under steady state conditions is a good indication that more heat exchangers would be quite beneficial. In continuous operation the major heat leak is obviously the incoming fluid. The addition of two more stages of heat exchange to this refrigerator should undoubtedly move its ultimate temperature down into the region of 20 to $30m^{o}K$. The addition of many more than 4 stages will probably have little affect since the final heat exchangers must work at such a low temperature. With the assumption of ideal heat exchange, no viscous heating, no He^4 circulation, and no external heat leaks, one can calculate the minimum temperature possible with a two stage device. Conservation of energy in the mixing chamber yields the equation

$$U_{3c}\ (T_n) - U_{3c}\ (T_{m.c.}) = T_{m.c.}\ \Delta S\ (T_{m.c.}) \qquad (54)$$

where U_{3c} is the molar internal energy of the concentrated solution (assumed here to be pure He^3), and ΔS is the change in entropy between

the concentrated and dilute solutions. The subscripts on the temperature, T, are m.c. for mixing chamber and n for the n^{th} heat exchanger. At low temperatures $U_{3c}(T)$ is given by[5]

$$U_{3c}(T) = 12.5\ T^2\ \text{j/mole-}^{o}\text{K}^2 \tag{55}$$

This quantity and $T\Delta S(T)$ are plotted in Figure 19. Applying conservation of energy to the n^{th} exchanger, under the assumptions above, the change in internal energy on the concentrated side must equal the heat input to the fluid flowing out of the mixing chamber, that is

$$U_{3c}(T_{n-1}) - U_{3c}(T_n) = H(T_n) - H(T_{m.c.}) \tag{56}$$

$H[T, x(T)]$ is given in Figure 7. Thus given $T_{m.c.}$ the right side of Equation (54) is given in Figure 19 as is $U_{3c}(T_{m.c.})$. Thus $U_{3c}(T_2)$ and hence T_2 is determined. Then inserting T_2 and $T_{m.c.}$ into Equation (56) and using Figures 7 and 19 for H and U respectively one finds T_1, or in general T_{n-1}.

For the case $T_{m.c.} = 28\text{m}^{o}\text{K}$ the above calculation yields $T_2 = 70\text{m}^{o}\text{K}$, $T_1 = 190\text{m}^{o}\text{K}$ and $T_o = 750\text{m}^{o}\text{K}$. The last value here is quite typical of the still temperature. Thus, in principle, one should be able to reach $28\text{m}^{o}\text{K}$ with only two heat exchangers.

During single-cycle operation when the load due to the incoming fluid has been eliminated the temperature of the various components may be used to estimate the residual heat leak. The temperature recorded on the last heat exchanger was $190\text{m}^{o}\text{K}$ when the CMN was reading $60\text{m}^{o}\text{K}$. It should be pointed out immediately that the

following calculation will not be very accurate because the resistance thermometer used on the heat exchanger is not calibrated with great precision, surely no better than ~ 15%. Also recall that 60m°K is only an upper limit for the mixing chamber temperature. However, taking 190m°K as T_2, 60m°K as $T_{m.c.}$ and reading from Figure 7 gives a heat leak ~ 2×10^{-2} j/mole He^3. The He^3 circulation rate is 2×10^{-5} moles/sec, thus the heat leak is on the order of a few ergs/sec. This is not an unreasonable number and is certainly good as an order of magnitude estimate.

The cooling capacity of the machine was measured by recording the equilibrium temperature of the mixing chamber for a known amount of heat applied to it. The heater consisted of 170Ω of Evanohm wire wrapped around the outside of the mixing chamber and glued into place with collodion. The heating power was determined by measuring, at room temperature, the voltage across the heater and the voltage across a 100Ω precision resistor in series with the heater. The later measurement gives the current. The voltage measurements were made using a Leeds & Northrup potentiometer (Model 8686, Leeds & Northrup Co., Philadelphia, Pa.). The cooling capacity of our refrigerator, along with that of others from the literature, is shown in Figure 20. These data have been corrected for temperature differences due to the Kapitza boundary resistance using the data of Anderson et al.[22] At most this correction was 5m°K. The quantity to consider among these curves is the He^3 circulation rate. Notice especially the very high circulation rate reported by Neganov et al.[4] For our refrigerator

the He^3 circulation was measured to be 2.0×10^{-5} moles/sec while the cooling capacity data were being taken. At .1°K the heat extraction rate is 6.4μ watts so that

$$\dot{Q}/\dot{n}_3 = .32 \text{ joules/mole } -He^3 \text{ (at .1°K)}$$

This is to be compared with the .82j/moles-He^3 at .1°K predicted by Equation (29) under conditions of perfect heat exchange. The ratio of these two numbers can then be used as a measure of efficiency for the refrigeration process. By this definition our refrigerator has an efficiency of 39% at .1°K.

A similar analysis of the data of Wheatley et al.,[5] yields an efficiency of 75% at .1°K. This is further evidence of the need for several stages of heat exchange. Notice, however, that the average efficiency per exchanger is decreasing, being 15% for five exchangers and 20% for our two. He^4 circulation will also tend to lower the efficiency of the heat exchangers.

During operation the ratio of He^3 to He^4 in the gas being pumped from the still is measured with a calibrated mass spectrometer leak detector (G.E. Model M-60). The ion accelerating voltage of this machine is readily adjustable. To tune the spectrometer tube to He^3 the accelerating voltage is simply increased by a factor of 4/3 from its value at the He^4 resonance peak. The leak detector was calibrated by sampling gas from a prepared source containing a known ratio of He^3 to He^4. The He^3 to He^4 ratio measured during operation was always very close to 6.0 under steady state conditions. The He^4 circulation in the system is evident from the high temperature of the first

heat exchanger.

The temperature of the still is weakly linked to the mixing chamber temperature. The trend is for the still to become warmer as the mixing chamber cools. This effect can be seen in Figure 18. The concentration of He^3 in the still is determined by the concentration of He^3 in the dilute phase at the mixing chamber temperature. This dependence is given in Figure 6 (Equation (23)). As the temperature of the mixing chamber decreases the He^3 concentration in the still decreases. With a fixed pumping speed the result is that the temperature of the still increases as the mixing chamber cools. From the measured still and mixing chamber temperatures it is possible to plot the vapor pressure of the liquid in the still as the refrigerator cools down. This line is shown in Figure 8 (line A) and gives a measure of the pumping efficiency at the still. Ideally, one would like to maintain a constant still temperature for all mixing chamber temperatures. This, however, implies an infinitely fast pumping speed.

Line B in Figure 8 shows the pumping characteristic of the refrigerator before the room temperature lines were increased from 1-1/2" I.D. to the present 2-1/8" I.D. The ultimate temperature of this earlier machine was ~ 100m$^\circ$K and its cooling capacity was very poor. The fact that its ultimate temperature is close to that of the present model only indicates that the heat leaks are small. Another limiting factor with the first machine, due to its slow pumping speed, was that the still became quite warm (~ .9°K) as the mixing chamber reached its limit of .1°K. With the still running at this

temperature the He^4 circulation became a problem. The lowered ratio of He^3 to He^4 then caused further deterioration of the cooling capacity.

In searching for optimum operating conditions, still powers varying from .1 milliwatts to .6 milliwatts have been tried with the present machine. Ideally, $T_{m.c.}$ should be independent of the circulation rate. In actual operation $T_{m.c.}$ tends to increase slowly as T_{still}, and the circulation rate, are increased at the highest heater powers. This is due to inadequate heat exchange, a decreasing He^3:He^4 ratio, and possibly, viscous heating. If the still is allowed to run at a very low temperature, with a resulting low circulation, the He^3:He^4 ratio becomes so small that the refrigerator will not operate. A still power of .42 milliwatts seems to be optimum in achieving a minimum temperature while maintaining adequate cooling capacity.

In concluding this chapter the utility of the dilution refrigerator as an experimental tool should be emphasized. It provides a very steady temperature base for conducting experiments with the working temperature being readily adjusted by the application of small amounts of heat to the mixing chamber. The useful working temperature range varies between the lower limit of the machine and about .4°K. This upper limit overlaps nicely with the lower limit of temperatures possible in conventional He^3 refrigerators. As for stability, temperature fluctuations on the order of a few millidegrees are normal for this machine for times on the order of one hour. This stability could undoubtedly be improved by the addition of a feedback

network between the mixing chamber heater and the mixing chamber thermometer. Regulation would be best where the cooling rate (the slope of Figure 18) is large, at temperatures somewhat above the lower limit. This slope and the specific heat of the experimental addenda will determine the time constant for temperature variation.

Chapter V. Suggested Improvements

The most obvious start toward improving the existing machine is to add extra heat exchangers. Two more exchangers could be fitted on a piece of nylon rod which would be attached to the bottom of the still. These would serve as the two high temperature exchangers leaving the existing two exchangers in place. The new exchangers would flank the still in the wide portion of the dewar where there is extra space on the radius (see Figure 9). These two exchangers should be lower than the still in order to avoid problems with the liquid level. The high temperature exchangers do not need to be as large as the present two but the concentrated side of exchanger No. 1 should be large enough to handle the He^4 circulation. Volumes of copper powder of about .5 cc and .25 cc for the concentrated side of exchangers one and two, respectively, should be adequate. The He liquid volumes should be roughly the same as the copper volumes. On the dilute side the copper volumes should be about .5cc in each exchanger.

Another possible improvement which should be tried is to increase the diameter of the line connecting the mixing chamber and the last heat exchanger of the dilute side. This is based on the

observation of an increase in cooling rate just prior to having the phase boundary pass out of the mixing chamber and into the dilute side of the last heat exchanger. There is also an increase in the circulation rate as this happens so it is possible that the impedance of the line in question is too high.

If the number of heat exchangers is increased as discussed above it would probably be worthwhile to build a new mixing chamber. This should be done to assure the best possible thermal contact between the sample and the mixer at the lowest temperatures. The copper vanes used in the present chamber should be replaced by a copper sponge sintered into the bottom of the new mixing chamber. This will place it in the cold, dilute solution. There should be an opening drilled in the sponge through which the He^3 is pumped out of the dilute phase in order to avoid increasing the pumping impedance on the dilute side. The bottom should be made from a single piece of copper with good mechanical connections to which samples may be attached. It has been our experience that threaded, gold plated copper connections give very good thermal contact.

A final change which might be considered, but requires considerably more construction, is the addition of a new still fashioned after the design of Reference 30. This would greatly improve the He^3:He^4 ratio and hence the cooling capacity. A possible problem with this type of still could be keeping the liquid level from rising into the pumping line. The use of a level sensor as in our still could be helpful if this problem occurred.

Chapter VI. Thermometry

A. Thermometry

1. Resistance Thermometers

Speer 100Ω, 1/2 watt, (grade 1002) carbon resistors (Speer Carbon Co., Bradford, Pa.) are used as thermometers on all the components of the refrigerator. The resistors used on the He^4 pot, heat exchangers, and the still were calibrated against the vapor pressure of He^4 in the temperature range $1.1^\circ K - 4.2^\circ K$. The resistors used on the mixing chamber and the sample were calibrated further against the vapor pressure of He^3 to a temperature of $.41^\circ K$. The resistor used on the sample was then calibrated against the magnetic susceptibility of a cerium-magnesium-nitrate (CMN) standard. The resistance as a function of temperature over the range $.13^\circ K - 4.2^\circ K$ could be fit to within 3% by the equation

$$T = \frac{a \log_{10} R}{(\log_{10} R - b)^2} - c \qquad (57)$$

where $a = .053^\circ K$, $b = 2.064$, and $c = .033^\circ K$ for the resistor used on the sample. The functional form of Equation (57) is taken from Reference 34. The values for these constants were nearly identical for resistors taken from the same batch. For example, the two resistors calibrated in the He^3 refrigerator had values of 100.3Ω and 99.2Ω, 162Ω and 161Ω, and 434Ω and 430Ω for temperatures of $295^\circ K$, $4.2^\circ K$, and $.416^\circ K$, respectively. In contrast the resistors used on the heat exchangers, although of the same make and grade,

were purchased about one year earlier. These two agreed quite well with each other but differed greatly from those of the new batch, having constants of a = .114°K, b = 2.005, c = .033°K. The constant c is probably a correction for the self-heating of the resistor during the resistance measurement and may be different for a different power setting of the measuring bridge or if the thermal contact of the resistor is altered. On each experimental run the resistance of the thermometers was checked at three fixed temperature points; room temperature, liquid nitrogen boiling point, and liquid He^4 boiling point. The resistance at these temperatures never varied by a measurable amount from one run to the next.

To establish good thermal contact between the resistor and the component whose temperature is to be measured the outer insulating coating of the resistor is thinned down. The O.D. of the resistor is reduced from .140" to .110". This leaves about .005" of insulating material on the radius. The diameter is reduced by using a fine file while the resistor is being turned in a lathe. A final cut is made by turning the resistor by hand on a fine grinding wheel. Care is taken to assure that the resistor remains as round as possible. The resistor is then greased into a hole drilled into the component of interest.

The resistance is measured using a low power input AC bridge. A block diagram of the bridge components is shown in Figure 21. The power input to the resistor is variable but with decreasing power, sensitivity is lost. The power setting used for most measure-

ments was $\sim 4 \times 10^{-10}$ watts into a 1000Ω resistor. The oscillator puts out a constant voltage to the sensing resistor, hence the power decreases as R^{-1}. The value of 1000Ω corresponds to a temperature of .150°K. If one desires to estimate the temperature difference between the resistor and its surroundings a measure of the thermal boundary resistance is needed. This is a difficult quantity to obtain; however, in measuring the thermal conductivity of insulators Harrison[32] finds a conductance between a metal and an insulator of

$$C \sim (10^{-3} \text{ watts/cm}^2\text{-K}^4)\ AT^3$$

which should apply to within an order of magnitude in the present case. Taking $A = 1\ \text{cm}^2$, $T = .15°\text{K}$, then $C = 3 \times 10^{-6}$ watts/K and with a power input of 10^{-10} watts the temperature drop is on the order of a few tenths of a millidegree across the boundary. However, I have observed in my temperature calibration the need for a much larger correction. (Constant c of Eq. (57).) Hence the main problem may be that the internal self-heating of the carbon coupled with its poor thermal conductivity keeps the heat inside. At any rate if the power input to the resistor is kept constant the resistance as a function of temperature is reproducible and once calibrated serves as a good thermometer.

2. Magnetic Thermometry

To calibrate the resistor that was to be used for thermometry during the specific heat measurements a paramagnetic salt pill of CMN (chemical formula $Ce_2Mg_3(NO_3)_{12} \cdot 24H_2O$) was prepared. Temperature measurements are made by measuring the magnetic susceptibility χ, and

assuming the substance obeys Curie's law $\chi \sim 1/T$. CMN is known to obey Curie's law to temperatures at least as low as 10 mK.[35] The susceptibility is obtained by measuring the mutual inductance between two coils in which the CMN is located. This mutual inductance is directly proportional to the susceptibility and the constant of proportionality is independent of temperature. Thus the mutual inductance, once calibrated as a function of temperature over some convenient temperature range, can be extrapolated with some confidence assuming that $M \sim 1/T$.

The mutual inductance measurements were made using a 17-cps mutual inductance bridge built by Cryotronics, Inc. (Cryotronics, Inc., W. Main Street, High Bridge, N.J.). This bridge has a range of 200μh ($1\mu h = 10^{-6}$h) with a quoted resolution of 8×10^{-4} μh. In operation an inductive unbalance is nulled by a voltage derived from a resistive network. There are three front panel controls designated range, coarse, and fine which are a part of this resistive network. When the bridge is nulled the unknown inductance is proportional to the product of these three controls. It is also necessary to null any resistive unbalance in the leads. This is done with two other front panel controls designated A and B. Once the resistive unbalance has been cancelled initially it is not necessary to change controls A and B by any significant amount. The output of the bridge was displayed on the y-axis of an oscilloscope with a sensitivity of 20 mvolts/cm. A signal taken off the primary oscillator tap on the back panel is fed into the x-axis input of the scope. The display on the scope is an ellipse where a resistive unbalance

is indicated by an increase in length of the minor axis and an inductive unbalance is indicated by a tilting of the major axis with respect to the x-axis of the scope. A null is indicated by a horizontal line. The sensitivity of our bridge was roughly 5×10^{-3} μh, thisnumber being determined by the signal to noise ratio of the coil set. All readings were taken with the range switch in the X1 position.

The measuring coils are shown in Figure 22a. The basic design of the coils follows that of Abel et al.,[36] with the specific dimensions being determined by many factors inherent to our apparatus. The coils fit on the outside of the brass tail of the isolation vacuum can and are immersed in the liquid He^4 outer bath. The radial dimensions of the coils are determined by the space available. The length is limited primarily by the need to reduce: (1) the influence of nearby magnetic materials; such as the end cap, soft soldered onto the vacuum jacket; (2) the eddy current heating of the copper mixing chamber. The sensitivity of the coil set will be determined by the length and placement of the secondary windings. Finally, the secondaries must also be placed on the primaries in such a way as to keep the variation of the field over the volume of the CMN at a minimum. A suitable compromise of these factors led to the dimensions shown in Figure 22. Yet to be determined is the number of turns per unit length for the secondary and the primary, n_p and n_s. The sensitivity is proportional to the product $n_p n_s$. n_p should be kept small to reduce the source of eddy current heating. The ratio of $n_s/n_p = 6$ was chosen.

The construction of the coils proceeded as follows: Two

sheets of .001" mylar was wrapped around a split brass mandrel of the appropriate diameter. On top of the mylar two sheets of onion skin paper were wrapped and painted with epoxy (Stycast 2850 GT diluted with tolulene). The coils were wound with No. 42 formvar coated copper wire. The winding was done on a lathe with a feed of 80 turns/inch for both the primary and the two secondaries. The primary consisted of six layers with 224 turns/layer thus, n_p = 192 turns/cm. During winding the coil was painted with the epoxy mentioned above after about every third layer. After the primary was finished one sheet of .001" mylar was placed over it and then the winding of the secondaries began. In winding the first secondary a record was kept of the number of turns on each layer. When the second secondary was wound the number of turns in each layer was reproduced to ± one turn and the total number of turns was reproduced exactly. The two secondaries were wound in the same direction and then wired together such that the induced current in one opposed the current in the other.

In spite of the precautions taken during the winding of the secondaries the net mutual inductance of the set was outside the 200μh range of the bridge. It is also necessary to be able to adjust the inductance so that as the CMN cools the total inductance always stays within the range of the bridge. For these reasons a second coil set was wound with dimensions as shown in Figure 22b. This set is located at room temperature and its mutual inductance is adjustable. The coils are wound on bakelite forms with the secondary being a slip fit inside of the primary. As the secondary is pushed from one extreme of the

of the primary to the other the net mutual inductance changes by roughly ± 100mh. The adjustment is controlled by using a micrometer feed on the movable secondary. The compensating coils are enclosed in a grounded copper box to reduce electronic noise. All the leads running from the bridge to the dewar and the compensating coil set are shielded cable. There is one ground point for the entire system of the bridge, oscilloscope, and coil sets. As the liquid He^4 level in the outer bath falls there can be problems with the resistive balance due to the change in resistance of the leads with the change in temperature. This problem is eliminated by using No. 25 Evanohm wire for the electrical leads from room temperature into the dewar. The large gauge wire is used to reduce the total impedance of the leads and hence maintain a high sensitivity for the coil set.

Three grams of powdered CMN were used and contained in a nylon chamber having the shape of a right circular cylinder. The diameter was .615" and the height was .410". This cylinder was attached to a nylon rod 3" in length. At the top of the rod was a gold plated copper cap and a No. 4-40 screw which attached to the mixing chamber. Silver soldered to the copper cap were 300 No. 39 Cu wires which extended down through the center of the nylon rod and into the CMN chamber. These Cu wires have an A/ℓ of 2×10^{-3} cm. The hole in the nylon rod through which the wires pass is filled with Resiweld epoxy to increase the rigidity of the assembly. To improve thermal contact with the Cu wire mesh the CMN powder is mixed into Apiezon-N

vacuum grease which has been warmed slightly to increase its fluidity. The resistor to be calibrated is also inserted into the middle of this mixture with the axis of the resistor running parallel to the axis of the measuring coils.

Prior to the calibration of the resistor against the CMN it had been calibrated in the temperature range .41°K – 4.2°K as discussed in Section A-1 of this chapter. When calibrated against the CMN the resistance as a function of temperature agreed very well with an extrapolation of the previous calibration down to about .11°K. Below this temperature dR/dT became increasingly smaller and it was apparent that the resistor was no longer in thermal equilibrium with the CMN. This was further substantiated by observing an increase in the temperature of the resistor as the bridge power was increased while at the same time the temperature of the CMN remained unchanged. No specific heat data for temperatures below .125°K were used in the final analysis. The resistor was calibrated against the CMN before the specific heat experiments were undertaken. The calibration was repeated again roughly six months later after the experiments were finished at which time there was no measurable change in the calibration constants.

PART II

A CALORIMETRIC MEASUREMENT OF THE NUCLEAR QUADRUPOLE COUPLING CONSTANT IN PURE, SINGLE CRYSTAL RHENIUM METAL

Chapter I

A. Introduction

In crystals having non-cubic symmetry there may exist large internal electric field gradients at the site of the nucleus. In the discussion to follow the sources of the electric field gradient will be outlined. This will be followed by a discussion of the quadrupole moment of the nucleus. The end result will be to derive the quantum mechanical Hamiltonian for the interaction between the electric field gradient and the nuclear quadrupole moment. In Section B the results are applied to rhenium and the expected effect upon the specific heat is calculated. This specific heat has been measured in the present work.

In pure, ordered metals electric field gradients arise from three principal sources: (1) the lattice contribution due to the positive ion cores at each of the lattic sites, (2) the contribution of the conduction electrons found within an atomic sphere centered on each lattice site, (3) contributions of the non-conduction, closed-shell core electrons which may either amplify or shield contributions (1) and (2) above. Theoretical calculations of the field gradients have not been very successful and little work has been done on the subject. One paper has been presented by Watson et al.,[37] for

V_3X (X = Si, Ge, Ga, etc.) in which an explanation is given for the dependence of the quantity $|e^2qQ|$ on the density of states at the Fermi surface. In the expression above e is the electronic charge, eq the z-z component of the electric field gradient tensor, and Q the nuclear quadrupole moment. Typically the electric field gradient in a metal is 5 to 20% of what a single valence electron could produce in the free parent ion. Thus the gradients in metals arise from rather severe cancellations among the three terms listed above. It is this fact which makes the theoretical calculations most difficult.

It is well known that nuclei with $I > 1/2$, where I represents the total nuclear angular momentum, may possess electric quadrupole moments which implies a non-spherical charge distribution. If this non-spherical charge distribution is located in an electric field gradient there will result an electrostatic energy which varies with the nuclear orientation. Following the notation of Slichter[41] the derivation of the mathematical form of this interaction proceeds as follows: consider first the classical interaction energy E of a charge distribution $\rho(\vec{x})$ with a potential V due to external sources.

$$E = \int \rho(\vec{x})\ V(x)\ d^3x \tag{58}$$

Expanding $V(\vec{x})$ in a Taylor's series about the origin and defining

$$V_\alpha = \frac{\partial V}{\partial x_\alpha}\bigg|_{\vec{x}\,=\,0} \qquad V_{\alpha\beta} = \frac{\partial^2 V}{\partial x_\alpha \partial x_\beta}\bigg|_{\vec{x}\,=\,0} \tag{59}$$

where x_α (α = 1, 2, 3) stands for the cartesian coordinates x, y and

z, respectively, then

$$E = V(0)\int \rho(\bar{x})d^3\bar{x} + \sum_{\alpha} V_{\alpha}\int x_{\alpha}\rho(\bar{x})d^3\bar{x} + \frac{1}{2!}\sum_{\alpha,\beta} V_{\alpha\beta}\int x_{\alpha}x_{\beta}\rho(x)d^3\bar{x} \quad (60)$$

$$+ \ldots$$

Choosing the origin at the center of mass of the nucleus, the first term is the electrostatic energy of the nucleus taken as a point charge. The second term involves the electric dipole moment of the nucleus. This term vanishes since the center of mass and the center of charge coincide; which in turn is due to the nuclear states possessing a definite parity. All experimental evidence supports the contention that nuclei do have definite parity. The third term is the electric quadrupole moment. It is possible to find principal axes of the potential V such that $V_{\alpha\beta} = 0$ if $\alpha \neq \beta$; moreover, if there is no net electronic charge at the nucleus V satisfies Laplace's equation. $\nabla^2 V = 0$. Evaluation at the origin gives

$$\Sigma_{\alpha} V_{\alpha\alpha} = 0 \quad (61)$$

Conventionally one considers for convenience the quantities $Q_{\alpha\beta}$ defined by

$$Q_{\alpha\beta} = \int [3x_{\alpha}x_{\beta} - \delta_{\alpha\beta} r^2] \rho(\bar{x})d^3\bar{x}, \quad (62)$$

where $\delta_{\alpha\beta}$ is the Kronecker delta. Then in terms of the $Q_{\alpha\beta}$'s the quadrupole interaction becomes

$$E^{(2)} = \frac{1}{6}\sum_{\alpha,\beta} [V_{\alpha\beta} Q_{\alpha\beta} + V_{\alpha\beta} \delta_{\alpha\beta}\int r^2 \rho(\bar{x})d^3\bar{x}] \quad (63)$$

Since V satisfies Laplace's equation the second term on the right vanishes, hence

$$E^{(2)} = \frac{1}{6} \sum_{\alpha,\beta} V_{\alpha\beta} \, Q_{\alpha\beta} \tag{64}$$

To obtain a quantum mechanical expression for the quadrupole coupling the classical charge density ρ is replaced by the quantum mechanical operator[41]

$$\rho^{(op)} (\bar{x}) = e \sum_{p} \delta(\bar{x} - \bar{x}_p) \tag{65}$$

where e is the electronic charge and the sum on p runs over all the protons in the nucleus. Substitution of this operator into Eq. (62) gives the quadrupole operator

$$Q_{\alpha\beta}^{(op)} = e \sum_{p} (3 \, x_{\alpha p} \, x_{\beta p} - \delta_{\alpha\beta} \, r_p^2) \tag{66}$$

The quadrupole term in the Hamiltonian is then

$$H_Q = \frac{1}{6} \sum_{\alpha,\beta} V_{\alpha\beta} \, Q_{\alpha\beta}^{(op)} \tag{67}$$

In resonance work one is generally concerned with eigenstates specified by the quantum numbers I and m, m being the z component of the total angular momentum I. Since we are interested only in the spatial reorientation of the nucleus for a given nuclear energy state, it is sufficient to consider matrix elements of the form

$$(I \; m \; n \mid Q_{\alpha\beta}^{(op)} \mid I \; m' \; n)$$

where n denotes any other quantum numbers characteristic of the nuclear energy state which need not be specified.

To evaluate the matrix elements of $Q_{\alpha\beta}^{(op)}$ it is convenient to employ the Wigner-Eckart theorem.[42] This theorem states that for a system of wave functions characterized by the quantum numbers J or J', for the total angular momentum, and M or M', for the z component of the angular momentum, matrix elements of the form $(J\ M\ n \mid T_q^k \mid J'\ M'\ n')$ are equal to the product of the Clebsch-Gordon coefficient $C(J'kJ;\ M'qM)$ and a quantity $(J\ n \parallel T^k \parallel J'\ n')$ which is independent of M and M'. The quantity $(J\ n \parallel T^k \parallel J'\ n')$ is called the reduced matrix element and T_q^k represents the q^{th} component of the k^{th} order irreducible tensor operator T^k. Stated mathematically this is

$$(J\ M\ n \mid T_q^k \mid J'M'n') = C(J'k\ J;\ M'\ q\ M)(J\ n \parallel T^k \parallel J'n') \quad (68)$$

Tensor operators are defined by their properties under rotations. They also obey specific commutation relations with the angular momentum operators. These relations assure that a T_q^k transforms under rotations of the coordinate axes into linear combinations $T_{q'}^k$ in the same way that the spherical harmonics Y_{LM} transform into linear combinations of $Y_{LM'}$'s.[43]

The expansion of the electric potential $V(\bar{x})$ (Eqs. (59),(60)) could have been done in terms of the spherical harmonics Y_{LM} in which case the quadrupole contribution would have been found to arise from combinations of the Y_{2M}'s.[40] Thus the quadrupole operator $Q_{\alpha\beta}^{(op)}$

of Eq. (66) can be expressed as a linear combination of T_q^2's.

Returning to Equation (68), consider two T_q^k's, one a function of variables s, and the other a function of variables t. Then Equation (68) states that

$$(JMn|T_q^k(s)|J'M'n') = (JMn|T_q^k(t)|J'M'n') \frac{(Jn\|T^k(s)\|J'n')}{(Jn\|T^k(t)\|J'n')} \tag{69}$$

This equation also applies in a more general form to functions that are linear combinations of T_q^k's, all of the same k, i.e., $F(s) = \sum_q a_q T_q^k(s)$. $Q_{\alpha\beta}^{(op)}$ is such a linear combination of T_q^2's as discussed above, hence, the desired matrix element is

$$\begin{aligned}(Imn|e \sum_p (3x_{\alpha p} x_{\beta p} - \delta_{\alpha\beta} r_p^2)|Im'n) \\ = (Imn| 3\frac{(I_\alpha I_\beta + I_\beta I_\alpha)}{2} - \delta_{\alpha\beta} I^2|Im'n)A\end{aligned} \tag{70}$$

where A is a constant, the same for all m, m', α and β. To determine A take the case $m = m' = I, \alpha = \beta = z$, then

$$\begin{aligned}(IIn|e \sum_p (3z_p^2 - r_p^2)|IIn) &= A(IIn|3I_z^2 - I^2|IIn) \\ &= A\, I(2I-1)\end{aligned} \tag{71}$$

where n has been dropped since it is assumed to commute with I^2 and I_z. One can define a symbol Q by

$$eQ = (IIn|e \sum_p (3z_p^2 - r_p^2)|IIn) \tag{72}$$

where Q is called the quadrupole moment of the nucleus. Then

combining Equations (71) and (72),

$$A = eQ/I(2I-1) \tag{73}$$

Using Equations (73) and (70) to replace $Q_{\alpha\beta}^{(op)}$ in Equation (67), all matrix elements diagonal in I and n are just what would be calculated by adding an effective quadrupole contribution to the Hamiltonian.

$$H_Q = \frac{eQ}{6I(2I-1)} \sum_{\alpha,\beta} V_{\alpha\beta} \left[\frac{3}{2} (I_\alpha I_\beta + I_\beta I_\alpha) - \delta_{\alpha\beta} I^2\right] \tag{74}$$

Notice at this point that in spite of the nine components of $Q_{\alpha\beta}$ only one constant is needed, eQ. This is true because the fact that the nucleus is in a state of definite parity is the same as the classical statement that the charge distribution ρ has cylindrical symmetry. If z is taken to be along the symmetry axis, then the energy of the charge reorientation depends only on the difference between the charge parallel and transvers to z, $\int z^2 \rho \, d^3x$ and $\int x^2 \rho \, d^3 x$. This gives the critical parameter

$$\int (z^2-x^2) \, \rho \, d^3 x = \frac{1}{2} \int (3z^2-r^2)\rho \, d^3 x$$

Notice that the last integral is just the classical definition eQ.

The quadrupole interaction of Equation (74) is valid for an arbitrary orientation of the coordinates α = x, y, z. It is customary to choose a set of principal axes relative to which $V_{\alpha\beta} = 0$, $\alpha \neq \beta$, and using the fact that V satisfies LaPlace's equation (or Eq. (61)), then H_Q may be rewritten as:

$$H_Q = \frac{eQ}{4I(2I-1)} [V_{zz} (3I_z^2-I^2) - (V_{xx}-V_{yy}) (I_x^2-I_y^2)] \quad (75)$$

It is conventional to define two parameters to characterize H_Q as given above. These are the asymmetry parameter η

$$\eta = (V_{xx}-V_{yy})/V_{zz} \quad (76a)$$

and the field gradient q.

$$eq = V_{zz} \quad (76b)$$

B. Applications to Metallic Rhenium

Rhenium metal has a hexagonal close-packed lattice structure and hence possesses cylindrical symmetry. This means that the asymmetry parameter $\eta = 0$. The Hamiltonian given by Equation (75) above gives rise to the energy levels

$$E = \frac{e^2qQ}{4I(2I-1)} [3m^2 - I(I + 1)] \quad (77)$$

in the absence of an applied magnetic field. The nuclear spin of Re is 5/2 hence there are three doubly degenerate levels. The separation between the lower two is $3e^2qQ/20$ and the separation between the upper two is $6e^2qQ/20$. For sufficiently high temperatures, it is possible to excite the nuclear spin system thermally among these energy levels. To estimate roughly what range of temperatures is relevant take $Q \approx 10^{-24}$ cm^2 and $eq \approx 10^{15}$ e.s.u. then $e^2qQ/k \approx 10^{-2}$ ^oK so that thermal excitations of these levels will contribute to the specific heat for $T \gtrsim .010^oK$. This contribution will become negligible when $T \gg .010^oK$ for then all levels

will be equally populated.

To calculate the contribution of these excitations to the specific heat let $a = 3e^2qQ/20$. The internal energy of the spin system is given by

$$U = N \frac{\sum_{i=1}^{3} E_i g_i e^{-E_i/kT}}{\sum_{i=1}^{3} g_i e^{-E_i/kT}} \tag{78}$$

where k is Boltzmann's constant, T is the temperature, N the total number of particles, E_i the energy of the i^{th} level, and g_i is the degeneracy of the i^{th} level. In this case there are three levels and $g_i = 2$ for each. Choosing $E_1 = 0$, then $E_2 = a$, and $E_3 = 3a$. Then

$$U = N\left[\frac{a\, e^{-x} + 3a\, e^{-3x}}{1 + e^{-x} + e^{-3x}}\right] \tag{79}$$

where $x = a/kT$.

The specific heat is given by

$$C = \frac{\partial U}{\partial T} = (Nk)\, x^2 \left[\frac{e^{-x} + 9e^{-3x}}{1 + e^{-x} + e^{-3x}} - \frac{(e^{-x} + 3e^{-3x})^2}{(1 + e^{-x} + e^{-3x})^2}\right] \tag{80}$$

In the extreme high temperature limit where $a \ll kT$ ($x \ll 1$), this reduces to

$$C = (14/9)\, R(a/kT)^2 \tag{81}$$

plus higher order terms $\sim T^{-3}$ etc. R is the gas constant. It is thus possible, by measuring the low temperature specific heat, to extract a term having a temperature dependence of T^{-2} and from the

coefficient of this term to measure the quadrupole coupling constant e^2qQ.

A term of this form was first noted in the specific heat of rhenium by Keesom.[44] His measurements were made on a polycrystalline, and somewhat impure sample. He was able to measure the specific heat for temperatures down to .37°K.

The specific heat of Re metal in the normal state is given by three terms

$$C_n = \gamma T + \alpha T^3 + A/T^2 \qquad (82a)$$

The term linear in T represents the contribution of the conduction electrons and gives a measure of the density of electron states at the Fermi surface.[45] For Re the constant γ = 2.35 millijoules/K^2-mole.[46] The second term is the contribution of the lattice. For Re, α = .026 millijoules/K^4-mole. The final term arises from the nuclear spin system and is the quantity of interest here. Keesom measured a value for A of .06 ± .01 millijoules-K/mole when the sample was in the normal state.[44]

Re is also a superconductor with a transition temperature of T_c = 1.699°K.[46] In the superconducting state the electronic term is replaced by a term of the form $C_{eS} = a\, e^{-bT_c/T}$ where the BCS theory predicts the constants a and b to be 8.5 and 1.5, respectively.[47] The specific heat of Re in the superconducting state is thus given by

$$C_S = a\, e^{-b\, T_c/T} + \alpha\, T^3 + A/T^2 \qquad (82b)$$

The constant α is essentially the same in both the superconducting and normal states.[49] It is possible, however, that A may not be the same in both states. Recall from the discussion at the beginning of this chapter that one source of the internal field gradients is the conduction electrons. Furthermore, Re is a transition metal and Watson et al., predicted the conduction electron contribution is dominant in the transition metals which have a high density of electron states at the Fermi surface. Since the conduction electrons are drastically affected by the superconducting transition it is possible that the internal field gradients may be also. This would result in a difference in the values of A_{sc} and A_{normal}.

Chapter II. Calorimetry

A. Calorimeter Construction

The calorimeter is shown in Figure 23. The frame is made from copper with gold plated threaded connections. A copper sleeve threads onto the upper cap as shown. The sample is located inside and is totally surrounded by a medium that is at the mixing chamber temperature, keeping the heat leaks to the sample at a minimum. Calculations show the heat leaks to be on the order of 10^{-8} watts. The bottom plate on which the sample is located is easily removed to facilitate the mounting of the sample. The sample is thermally isolated from the calorimeter in the following manner: two No. 2-56 nylon screws are attached to the copper base plate with nylon thread as shown in Figure 23. The bottom face of the sample rests on these two screws

with the area of contact being very small. (The sample has a cylindrical shape with polished end faces.) Above the sample is a strap spring made from .015" thick phosphor bronze. Through this spring passes a No. 0-80 stainless steel machine screw which has been fitted with a pointed nylon tip. This screw is tightened down against the sample causing a bowing of the spring and is then locked with a lock nut. The sample is now held rigidly between pieces of nylon with a very small area of contact. Also, due to the action of the phosphor bronze spring, the sample remains rigid in spite of the different thermal contractions of the materials.

A weak thermal link between the sample and the mixing chamber is made with one strand of No. 39 copper wire. ($A/l = 3 \times 10^{-6}$ cm.) This copper wire is soldered to a .005" thick copper foil which is wrapped around the sample and fastened in place with nylon threads. The area of contact between the foil and the sample is about 1 cm^2. The use of a conventional superconducting heat switch was not possible since measurements were to be made in a magnetic field.

The resistance thermometer placed on the sample is greased into a copper sleeve. The wall thickness of this sleeve is ~ .010". One side of the sleeve is cupped to fit smoothly onto the side of the sample. This copper sleeve is held in place with the same nylon threads that hold the foil heat link. The nylon thread is wrapped uniformly along the length of the foil and resistor sleeve with the hope of making very tight contact between these components and the

sample. The nylon is used because when cooled it will shrink much more than the metals and hence pull the pieces even more tightly together. Two other methods of attaching the resistor to the sample were tried but proved inferior to the method described above in making thermal contact. One of the methods was to epoxy the copper resistor sleeve to the sample. The other was to wrap the resistor in a thin copper foil (.005" thickness) and wrap a portion of this foil around the sample as done with the thermal link. The fact that this last method gave poorer thermal contact than the first indicates that the dominant thermal impedance is between the copper and the resistor; for surely the copper foil with its larger surface made better thermal contact with the sample than did the copper sleeve. With the foil however, it was difficult to make a tight fit around the resistor and this must have been the reason for the poor thermal contact.

The heaters attached to the sample were approximately 12" of No. 38 Evanohm wire. The wire was rolled into a small flat coil on a piece of masking tape. One of these heaters was then epoxied to either face of the sample with Sycast 2850 GT cement. The heaters were clamped tightly to the sample while the epoxy cured in order to keep the thickness of the epoxy at a minimum. The two heaters were then wired in series. The final arrangement of sample, heaters, thermometers and heat link is shown in Figure 23. With this arrangement all of the heat generated in the heaters must flow into the sample before it can begin "leaking" away to the mixing chamber

through the heat link.

About 1/2" to 3/4" of the Evanohm wire was left extending from each of the heaters for thermal insulation. This was then soft soldered to No. 42 copper wires ($A/l = 10^{-6}$ cm), which extended up through the top of the calorimeter and were thermally grounded to the mixing chamber. In calculating the specific heat half of the heat generated in these short lengths of Evanohm wire was assumed lost to the mixing chamber and the other half was assumed to flow into the sample. The heat assumed lost to the mixing chamber in this manner amounts to something on the order of 6% of the total heat generated in the heaters. From the mixing chamber up to the terminal board the electrical leads were tinned Evanohm as discussed previously.

B. Specific Heat Techniques

Two different techniques were used for measuring the specific heat. One was the conventional "heat pulse" method. A known amount of electrical current is allowed to flow for a measured time through coils of high resistance wire attached to the sample. The energy input to the sample is $Q = I^2R\Delta t$. The change in temperature of the sample is recorded on a strip chart recorder attached to the resistance measuring bridge described previously (Fig. 21). The specific heat is calculated from the expression $C(\bar{T}) = Q/\Delta T$ where $\bar{T}$ is the mean absolute temperature during the heating period. The amount of heat applied is kept small so that $\Delta T < .1\ T$. The difficulty with this method is in estimating the heat lost to the surrounding material during the heating period. Heating times are kept small

compared to the characteristic thermal time constants for the decay of the sample temperature back to its equilibrium value. This characteristic time is RC where R is the thermal impedance of the heat link between the sample and its surroundings and C is the specific heat of the sample. Since $R \sim T^{-1}$ and $C \sim T^{-2}$ the time constant becomes increasingly large at low temperatures and the problem of heat loss becomes much less severe. A typical specific heat point taken in this manner is shown in Figure 24a. To determine the appropriate ΔT for the case of zero heat loss a line is first extrapolated back along the cooling curve (line A, Fig. 24a). Assuming Newton's law of cooling then the appropriate ΔT is the one which makes area 1 equal to area 2 as shown. A consistent usage, which keeps these areas approximately equal is to take ΔT as the temperature change measured at the midpoint of the heating period (points a and b). To keep the error involved in this extrapolation small the heat pulses are adjusted to keep ΔT small and the chart speed is adjusted so that the decay appears linear.

The second method could be called a "continuous cooling" measurement. Consider the heat flow into and out of the sample. In general, this will obey the equation

$$\dot{Q}_o + \dot{Q}_{in} - C(T) \frac{\partial T}{\partial t} = \dot{Q}_{sw}(T) \qquad (83)$$

where $\dot{Q}_o$ is the background heat leak into the sample, $\dot{Q}_{in}$ is the heat being supplied to the sample electrically, C(T) is the specific heat of the sample, and $\dot{Q}_{sw}(T)$ is the amount of heat flowing away from the

sample through the heat switch. Under steady state conditions $\dot{Q}_{in}(T') = \dot{Q}_{sw}(T') - \dot{Q}_o$ where the sample has come to an equilibrium temperature of T'. Several different $\dot{Q}_{in}$'s can be applied and the respective T' recorded. The heater is then turned off and the temperature of the sample changes according to

$$\dot{Q}_o - C\frac{\partial T}{\partial t} = \dot{Q}_{sw} \text{ or } -C\left(\frac{\partial T}{\partial t}\right) = \dot{Q}_{sw} - \dot{Q}_o \tag{84}$$

But the quantity $\dot{Q}_{sw} - \dot{Q}_o$ has been measured for various temperatures and is just the $Q_{in}(T')$'s discussed above. Thus

$$C(T') = -\dot{Q}_{in}(T')\left(\frac{\partial T}{\partial t}\right)^{-1}_{T'} \tag{85}$$

A typical set of specific heat points taken in this manner is shown in Figure 24b. This method has an advantage over the first one in that the heat leak away from the sample does not enter. There is a difficulty however, in that the data recorded on the chart recorder is dR/dt. What is needed in Equation (85) is dT/dt, hence, once must approximate two slopes: dR/dt from the cooling curve taken on the chart recorder, and dT/dR taken from the resistor calibration curve, and then take their product. The slopes cannot be estimated with enough precision to avoid introducing errors into the specific heat calculated from Equation (85) which are larger than the errors involved in the first method. Therefore, in practice most of the data were taken using the "heat pulse" technique. However, on each experimental run some data were taken using method 2 to serve as a consistency check. Agreement between the two data sets was always

satisfactory but the continuous cooling data contained more scatter.

C. Auxiliary Equipment

The power supply and switching network for the heaters are shown in Figure 25. Heating voltages were continuously adjustable from 0 to 3.54 millivolts. This voltage was coupled to the sample heaters through a switching network as shown. When the sample is not being heated the input is grounded to reduce rf pick-up, and the battery circuit is switched to a load equivalent to the heaters. The current drain from the battery is thus kept constant at all times. All leads to the dewar were of shielded cable and the ground for this heating circuit was separate from all other grounds in the system.

Two types of timing were used. One form consisted of manually throwing the switch and at the same time starting a stop watch. Synchronization of the two events was checked prior to the experiment by triggering an electric clock and comparing its time with that of the stop watch. Agreement was always within .1 sec. Normal heating periods were on the order of 5 sec. The electric clock employed a 6 volt D.C. solenoid clutch and could not be used for actual data taking because of the electronic noise generated by the switching transients.

The second method of timing was more elaborate. It consisted essentially of a frequency counter. The device could be set to count a given number of rectified pulses derived from the 60 Hz line. During the time the counter was running a mercury wetted relay was kept closed. As soon as the designated count had been reached

the relay was opened with a delay time on the order of 30μ sec. The design was such as to keep switching transients at a minimum. Using this device one knew quite accurately the time for which power had been supplied to the heaters. Although this method of timing is far superior to the first the scatter of the data was not improved indicating that timing was not the major source of error.

The resistance of the heaters was measured at room temperature with a General Radio D.C. bridge with an accuracy of better than 1%. The change in the resistance of Evanohm wire between room temperature and liquid He^4 temperatures is negligibly small.(48) The power applied to the heaters, and at the same time the resistance of the circuit, were determined by measuring at room temperature the voltage across the heater and the voltage across a 10Ω, .1% resistor in series with the heater. The later measurement gives the current in the circuit. These voltages were on the order of millivolts and were measured with a potentiometer having a sensitivity of ± 1μ volt. The resistance of the heater circuit found by the measurement above was, in the absence of an applied magnetic field, typically 1 to 2Ω less than the resistance measured at room temperature This is attributed to superconducting soft solder shorting out portions of the Evanohm wire at the junction with the copper wires. Since the resistance of the No. 38 Evanohm is 81.4Ω/Ft., 1 or 2Ω corresponds to roughly .3" which is a quite reasonable number for the length of wire used in making the solder connections.

When specific heat measurements were being made in the presence of an external magnetic field, it was found that the resistance of the heater circuit had increased. This is due to portions of the tinned

Evanohm wire being driven normal by the applied magnetic field. Since the ends of the tinned Evanohm leads are thermally grounded to the mixing chamber, it is assumed that all the heat generated in these leads is dissipated without reaching the sample. The heat generated in the sample is calculated from the measured current and resistance of the heaters as measured at room temperature.

The change in temperature of the sample was recorded during the heating — cooling cycle on a chart recorder (Hewlett-Packard Model 7000A, Hewlett-Packard, Moseley Division, Palo Alto, Calif.). The input to the chart recorder was taken off the resistance bridge VTVM. The displacement on the chart recorder in terms of resistance was calibrated by attaching a decade resistance box to the second bridge input.

For small change of ΔR from a null condition on the bridge ($\Delta R/R \ll 1$) the displacement of the chart recorder is linear with respect to resistance. Since the end points of the resistance change have been calibrated by use of the decade resistor the resistance at any intermediate value can be calculated. The temperatures can then be determined directly from the resistance — temperature calibration curve.

D. The Specific Heat of Copper

To check the calorimetry techniques as well as the absolute temperature calibration of the thermometer the specific heat of a high purity, single crystal copper sample was measured. This sample contained 6.56×10^{-2} moles of copper. Copper was chosen for calibration

purposes because its specific heat has been carefully measured by several experimenters.[51, 52] The most recent results are[51]

$$C_{cu} = \gamma T + \alpha T^3 \tag{86}$$

where γ = .6959 millijoules/K^2 mole, α = .0478 millijoules/K^4 mole. For the temperature range under consideration here, .1K - .5K, only the linear term is measurable. Thus C/T as a function of T should be a constant equal to γ given above.

Specific heat data were taken over the same range of temperatures to be covered by the Re experiment and in magnetic fields up to 1000 Oe. The result of these experiments is shown in Figure 26a. There is agreement to within 3% between our measured specific heat and the values taken from the literature, if a constant value of 6 microjoules/K^2 is subtracted from each specific heat point. This "background" is attributed to the experimental addenda attached to the sample of which the only major component is the carbon resistor. This number of 6μ joules/K^2, if taken to be the linear term in the specific heat of a carbon resistor agrees quite well with the value of 6.4μ joules/K^2 given by White.[27] This background correction corresponds to 13% of the total signal for the copper sample. However, the situation in Re is much better for in this case C is increasing as T^{-2} and the background will correspond to less than 1% of the total signal at low temperatures.

The rise in C/T from its expected constant value for temperatures below .15°K is attributed to a lack of thermal equilibrium

between the sample and thermometer. The thermometer no longer follows accurately the temperature variations in the sample during a specific heat measurement. Notice also that the effect is independent of the applied field. In any case, even if it should represent a real rise in the specific heat due to some portion of the experimental addenda, for example, the Evanohm wire, it would amount to less than 1% of the expected effect in Re.

Chapter III.

Experimental Results, Conclusions, and Future Experiments

A. The Specific Heat of Rhenium

The specific heat of Re has been measured in the temperature range .1°K - .5°K for magnetic fields H, of 0,300,1000 0e and 12.5 k0e. In the superconducting state the expected nuclear contribution is not observable. In the normal state a term of the expected form A/T^2, is found where A = .061 ± .002 millijoules-K/mole for fields of 300 - 1000 0e; increasing to A = .077 ± .004 millijoules-K/mole at a field of 12.5 k0e.

The Re sample used was manufactured by Westinghouse Lamp Division (Bloomfield, New Jersey).* It has a resistivity ratio of > 20,000. This is the ratio of the electrical resistivity at room temperature to that at 4.2°K. Assuming the resistance at low temperatures is determined by impurity scattering, this ratio gives a measure of the sample purity. A resistivity ratio of > 20,000 corresponds to a very pure sample with very few metals of this purity having ever been prepared.

The experimental data are shown in Figures 27 and 28. In Figure 27 C/T is plotted as a function of $1/T^3$. This is the most convenient form for data reduction since the specific heat at low temperatures is give by $C_{Re} = \gamma T + A/T^2$. Therefore, a plot of C/T vs. $1/T^3$ should be a straight line with a slope equal to A and an intercept of γ. To compute the desired values of A and γ a least-squares fit was made to the data shown in Figure 27.

1. The Superconducting State

Consider first the results of measurements made while the Re sample was in the superconducting state. Recall that $T_c = 1.70^{\circ}K$, so that in zero magnetic field, the Re was superconducting throughout the temperature range studied. We found the expected nuclear contribution to be almost totally absent when the sample was superconducting This can be seen from the data shown in Figures 27 and 28. This suppression of the nuclear contribution is attributed to the very long spin-lattice relaxation times in superconductors and has been noted by other experimenters.(49)

The dominant relaxation mechanism of nuclei in normal metals is by a coupling of their magnetic moments to the spin magnetic moments of the conduction electrons. A simple analogy can be made between the role played by the conduction electrons in this case and the molecules in the case of a classical gas. Just as stationary objects suspended in a gas would be kept in thermal equilibrium with the walls of a container by the action of the gas molecules, the essentially stationary nuclei in a metal are brought into thermal equilibrium

by energy exchange with the conduction electrons.

The spin-lattice relaxation time, commonly called T_1, is related to the temperature through T_1T = constant, an expression known as the "Korringa relation".[53] The physical cause of this behavior may be understood qualitatively as follows: The interaction between the nuclei and the conduction electrons is a scattering process. An electron in a state specified by a wave vector k, and spin s, is scattered into a new state $|k', s'>$ through a magnetic dipole interaction of the form $\vec{\mu}_n \cdot \vec{\mu}_e$. $\vec{\mu}$ is the magnetic moment related to the angular momentum $\vec{J}$ by the definition $\vec{\mu} = \gamma \vec{J}$ where γ is called the "gyromagnetic ratio". The subscripts n and e refer to the nucleus and electron respectively. Since the electrons must obey Fermi-Dirac statistics, only those electrons within kT of the Fermi surface have available unoccupied states into which they may be scattered. It is in this way that the temperature dependence arises. From this discussion it is also possible to see that the important quantities in the constant of the Korringa relation are the density of states at the Fermi surface, the gyromagnetic ratios γ_n and γ_e, and the probability of finding the electron in the vicinity of the nucleus $|<U(0)>|^2$. The assumption is made that the electron wave function is a product of a spin function and a Bloch function $U_k(r)e^{i\vec{k}\cdot\vec{r}}$. In a superconductor of high purity and at temperatures well below T_c the number of normal electrons free to take part in the scattering process described above is greatly reduced. The result is a very long relaxation time.

In contrast to our null results in the superconducting states, Keesom reported a value of $A_{sc} = .052 \pm .002$ millijoules-K/mole. This is apparently due to an enhancement of the relaxation process by the impurities present in his sample. However, his reported value for A_{sc} is significantly less than the value of $A_{normal} = .061 \pm .002$ millijoules-K/mole measured in this work. This suggests that the impurities in his sample were less than perfectly efficient in bringing the nuclear spins into thermal equilibrium when the sample was in the superconducting state. The question posed earlier as to whether A would be different for the superconducting and normal states is not accessible to experimental observation due to the long spin-lattice relaxation time in the superconducting state. Under these conditions it will not be possible to observe the nuclear spin system either by NMR or calorimetric techniques. The addition of impurities such as in Keesom's sample will enhance the relaxation process but still do not guarantee a complete equilibrium of the nuclear spin system.

Having found that the nuclear contribution was absent in the superconducting state in our sample, the variation of the specific heat during the transition from the superconducting to the normal state was measured next. An externally applied magnetic field was used to quench the superconductivity. A series of specific heat points as a function of the applied field were taken while the sample was held at a constant temperature. These results are shown in Figure 26b. Data were taken with the field being increased and then decreased as shown. The critical magnetic field of Re is 198 Oe.[46]

The upper critical field shown in Figure 26b is in excellent agreement with this value. The magnetic field was applied perpendicular to the symmetry axis of the crystal. For this geometry it is possible to have an intermediate state in which the sample is partially normal. Since a magnetic field is totally expelled from a metal in the superconducting state the magnetic field lines must curve around the sample. For the case of a cylinder of radius R in a transverse uniform magnetic field it can be shown that $H(r = R, \varphi = 90^{o}) = 2H_{o}$, $H_{r}(r = R) = 0$, where H_{o} is the applied field and r and φ are the usual polar coordinates. The angle φ is measured from $\vec{H}_{o}$. Thus the field at the sample edge is equal to the critical field H_{c}, when the applied field is $H_{c}/2$. This is again in good agreement with the lower critical field of 100 Oe shown in Figure 26b. In the intermediate state the measured specific heat appears to come entirely from the portion of the sample which is normal.

The lack of hysteresis in the specific heat is an indication of the purity of the sample. Impurities would serve as sites on which magnetic flux could be trapped. This "trapped flux" would then keep portions of the sample normal even in the absence of the external field. The results would be a hysteresis in the specific heat.

To investigate the effects of flux exiting from the sample another experiment was performed. The sample was held at an approximately constant temperature while the magnetic field was swept slowly from 300 Oe to 0. The chart record of the sample temperature during this period is shown in Figure 29b. The very sharp spikes on this trace are electronic noise in the resistance bridge and do not represent temperature fluctuations. Initially the sample was cooling at a very

constant rate of about $1m^{o}K$ every 90 seconds. When the field reached 190 Oe the sample warmed by about $4m^{o}K$ quite suddenly. This marks the beginning of flux exiting from the sample as the transition to the superconducting state takes place. Notice that 190 Oe agrees nicely with the upper critical field found in the specific heat measurements (Figure 26b). Between 190 Oe and about 110 Oe the sample temperature remains quite constant indicating that the flux expulsion is taking place at a constant rate. Below the lower critical field of 100 Oe (Fig. 26b) the temperature becomes more irregular until at 70 Oe all the flux has apparently been expelled and the sample returns to a very regular cooling rate. Quite likely it is not the 70 Oe field which is significant in marking the end of flux expulsion but rather the time period. This time of about 45 seconds measured from the instant that the applied field has passed the lower critical field gives a measure of the decay time for flux exiting from the sample. Recall that in the specific heat measurements the sample appeared entirely superconducting below 100 Oe. However, the time between stopping the field and the measurement of the specific heat was several minutes. If the specific heat data could have been taken closer together in time, there would probably have been a greater hysteresis in Figure 26b.

The reverse of the demagnetization experiment (Fig. 29b) is shown in Figure 29a. In this case the field is being increased at the same rate as before starting from a value of 30 Oe. Since in the superconducting state the specific heat is less than it is in

the normal state one can anticipate that adiabatic magnetization of a superconductor will product cooling. This is analogous to cooling by conventional adiabatic demagnetization of paramagnetic salts.[27] The situation is complicated in superconductors however by the eddy current heating. It can be seen that there indeed was some cooling as the sample began the transition into the normal state. However, the change in temperature was only about $2m^{o}K$. It should be pointed out that Re is not a good specimen to try this method of cooling on because the nuclear term decreases the difference between the specific heats in the superconducting state and the normal state. Still there is about a 50% difference at .3K and the cooling observed above was only ~ 1%. Furthermore, upon recycling the specimen to the normal state the increase in temperature was twice the decrease produced by magnetization. Hence the net effect would be an overall warming of the sample during each cycle of the field.

2. The Normal State

To suppress the superconducting transition and to check for a possible magnetic field dependence the specific heat of Re was measured in fields of 300 Oe, 1000 Oe, and 12.5 kOe. The results of these experiments are shown in Figures 27 and 28. The deviation from linearity in Figure 27 is believed to be due to a lack of thermal equilibrium between the sample and the thermometer just as was observed with the copper. Notice also that the next higher order term in the specific heat of Equation (82) would be of order $1/T^3$ which would result in a decreasing of the slope instead of the increasing slope which is

observed. A least-squares fit to all the data in the linear region corresponding to the temperature region .126°K - .520°K yields a value of A = .061 ± .002 millijoules-K/mole in both the 300 0e and 1000 0e fields. For a field of 12.5 k0e the value of A had increased to .077 ± .004 millijoules-K/mole. The value of A in the normal state obtained from measurements in the 300 0e and 1000 0e fields is in good agreement with the results of Keesom's A_{normal} = .06 ± .01 millijoules-K/mole.

B. The Electric Field Gradient

Using the measured value for A of .061 millijoules-K/mole the electric field gradient is computed to be $|eq| = 1.48 \times 10^{15}$ e.s.u. Recall from the discussion in Chapter I of this part the three sources of electric field gradients in metals: (1) the contribution of the crystalline lattice considered as point charges. This will be denoted by q_{latt}. (2) The contribution of the local conduction electrons located within a sphere centered on each lattice site. This will be called q_{loc}. (3) The shielding or antishielding effect of the closed-shell core electrons about each lattice point. A calculation by De Wette predicts that the lattice contribution to the EFG in Re should be $eq_{latt} = .020 \times 10^{15}$ e.s.u.[54] From the work of Watson et al., the effect of the conduction electrons is predicted to be ~ 100 times larger than the lattice contribution and of the opposite sign.[37] Following their notation the total field gradient is given by

$$q = (1 - \gamma_\infty)\, q_{latt} + (1 - R_Q) q_{loc} \qquad (87)$$

γ_∞ and R_Q are the Sternheimer antishielding factors which correct for distortions of the closed-shell core electrons.[55] Watson et al., assumed $(1 - R_Q) = 1$ and $(1 - \gamma_\infty) \sim 10$. Using this and their results that $q_{loc}/q_{latt} \approx -100$ the EFG computed from Equation (87) is $eq \approx 1.8 \times 10^{15}$ e.s.u. This is in surprisingly good agreement with the experimental results. It would appear that their theory is quite applicable to transition metals.

The calculation of q_{latt} by De Wette has some very interesting implications in respect to Re metal. He finds that for a hexagonal close-packed structure q_{latt} passes through zero at $\alpha = 1.6345$. The parameter $\alpha = c/a$ where c and a are the usual lattice constants. Not only does q_{latt} pass through zero, but near zero the change in q_{latt} with respect to α is very large. For Re, $\alpha = 1.6248$[55] thus placing it in the region where $dq_{latt}/d\alpha$ is largest. The implication is that for Re, q_{latt} will be very sensitive to strains in the metal. For example, a change in ϵ of $\epsilon = \frac{\Delta\alpha}{\alpha} = 10^{-6}$ will produce a change $\Delta q/q \sim 10^{-4}$. It would be an interesting experiment to attempt to observe the changes in the EFG with respect to strain. There are technical details which would make such experiments difficult if one attempts to measure the EFG by calorimetric methods. However, NMR techniques appear quite suitable for they are inherently of greater sensitivity and do not require ultra low temperatures. For example, consider a frequency such that the resonant field is 20 kG. A change in q of 0.1% will shift the resonant field by 20G. Such a large shift in the resonance could easily be measured. If the theory of

Watson et al., is correct a change in q of 0.1% requires an $\epsilon \approx 10^{-5}$. This , in turn, would require the application of pressures to the sample of approximately 6×10^7 dynes/cm^2. Such pressures are relatively small and should not present experimental difficulties. Thus one should be able to readily check the dependence of q upon q_{latt} which was calculated in Reference 37.

C. Magnetic Field Dependence and Further Experiments

To consider the value obtained for A in the 12.5 kOe field and further, to predict possible NMR transitions that may be observed, it is necessary to study solutions of the combined Hamiltonian,

$$H = H_Q + H_{mag}, \tag{88}$$

where H_Q is the electric quadrupole interaction Hamiltonian given by Equation (76) and H_{mag} is the magnetic interaction Hamiltonian $H_{mag} = -\vec{\mu} \cdot \vec{H}$. Numerical solutions for the eigenvalues of the combined Hamiltonian in the general case of arbitrary field and crystalline symmetry have been done by Matthias et al.[38] The solution for the eigenvalues and eigenvectors is done by a computer. A copy of Matthias' program was obtained and converted to FORTRAN IVG for use on the IBM 360/75 system present here at Caltech.† From this program the energy levels as a function of the applied magnetic field and the angle β between $\vec{H}$ and the crystalline symmetry axis were obtained. The results are shown in Figure 30 for the case $\beta = 90^\circ$. This was the orientation of our sample during the specific heat measurements. The parameter representing the applied field is y, and is defined by

$y = \nu_H/\nu_E$ where $\nu_H = \mu (H_o/hI)$ and $\nu_E = e^2qQ/h\ 4I(2I-1)$. In the expressions for ν_H and ν_E, μ is the nuclear magnetic moment, H_o the applied field, I the nuclear spin, Q the nuclear quadrupole moment, eq the z-z component of the electric field gradient tensor, e the electronic charge, and h is Planck's constant. Notice that $\nu_E = (1/6)(a/h)$ where a was the splitting between the lower two levels as defined in Part II, Chapter I-B. Using the results A = .061 ± .002 millijoules-K/mole the zero field splitting a/h is computed to be 45.2 ± .7 Mhz. Thus one unit of energy in Figure 30 is equivalent to a frequency of 7.5 Mhz. ν_H is equal to 9.68 Mhz at 10 kG thus one unit of y is equal to 7.8 ± .3 kG. In terms of temperature this zero field splitting corresponds to .002 ^oK so the extreme high temperature limit assumed in going from Equation (81) to (82) is certainly valid for all temperatures studied.

From the energy levels of Figure 30 it is possible to compute the expected specific heat for any value of the applied field. In particular, for the case of H = 12.5 k0e the calculated specific heat yields A = .070 ± .002 millijoules-K/mole. This lies slightly below our measured value of A = .077 ± .004. A possible source of error is that the resistance thermometer calibration was not checked in the 12.5 k0e field. Changes on the order of 1%/1000 G in the resistance of these carbon resistors have been reported.[12] Since the energy levels are extremely dependent upon β (compare Fig. 30 and 31) one might expect that the specific heat would also show an angular dependence. However computations will show that this is not the case

in the extreme high temperature limit. The trace of the Hamiltonian (Eq. (87)) equals zero. This, along with the fact that all the levels are equally populated to at least a first order approximation, requires that the overall internal energy and specific heat remain constant despite changes in the internal energy level structure. A comparison of the results at 12.5 kOe serves as a reasonable check of the self-consistency of our data. However, the most direct method of measuring the quadrupole coupling is through magnetic resonance experiments.

A transverse magnetic field, $\beta = 90^{\circ}$ as in Figure 30, represents the best orientation for conventional NMR studies. One should be able to observe the $\Delta m = 1$ transition of $m = +1/2 \rightarrow -1/2$. However, to use this transition to obtain information about the zero field separation measurements will have to be made in magnetic fields large enough to produce deviations from linearity in the energy level splitting. There will be a 10% deviation from linearity in the level splitting when the applied field is 3.9 kG. Thus if the NMR signal can be observed for fields at or above this value the results given here for the quadrupole coupling may be checked.

It should be emphasized that these energy levels labeled a-f in Figure 30 can be specified by the magnetic quantum number $m_I = -5/2, +5/2 \ldots -1/2, +1/2$, respectively, only in the case of low fields, and the special case $\beta = 0^{\circ}$. As the field, or the angle β, is increased there is considerable mixing of the states. As an example the eigenvalues and eigenvectors for several values of the

magnetic field and the angle β are listed in Table 4. The result of this mixing will be that the amplitude of the NMR signal will be reduced from the value expected if it is assumed that, for example, states e and f of Figure 30 correspond to pure states of $m_I = -1/2$, $+ 1/2$, respectively. The actual amplitude can of course be computed knowing the eigenvectors.

A second method which may be successful in studying the energy levels is Acoustic Magnetic Resonance (AMR).[39] In this case $\Delta m = 2$ transitions are most favorable. To observe such a transition at a reasonably low frequency the best orientation will be for small angles $\beta \approx 0^{\circ}$. In this case the predominantly + 3/2 and -1/2 levels approach one another as the field is increased. A measurement of the transition between these two levels along with the known level splitting scheme would allow one to extrapolate back to H = 0 and determine the zero field splitting. A detailed plot of the + 3/2 and -1/2 levels for angles of $\beta = 0, 10^{\circ}, 20^{\circ}$ is given in Figure 31. These are the best experimental conditions for attempting AMR.

Another fact which makes Re a very promising candidate for AMR studies in the extreme dependence of q_{latt} upon strains as discussed previously. In AMR a time varying strain is purposely induced in the sample in order to excite the nuclear spin system through the EFG — nuclear quadrupole interaction. Typical strains for AMR work are on the order of $\epsilon = 10^{-6}$ which in Re will produce changes in the field gradient of $\Delta q/q \sim 10^{-4}$. This should lead to a very strong coupling mechanism and a correspondingly strong resonance signal.

In fact the work of De Wette[54] on tetragonal and hexagonal crystal can be used for judging just which metals are promising for AMR work with respect to having a strong dependence of q upon ϵ.

From a plot such as Figure 31 the angular dependence of the resonant field for a fixed frequency was calculated. These results are shown in Figure 30 for the case of the transition $\Delta m = + 3/2 \rightarrow -1/2$. A check of this angular dependence by AMR studies probably affords the best opportunity for unambiguously determining the zero field splitting.

In conclusion, with respect to metallic rhenium experimental verification and further refinements of the results obtained here regarding the quadrupole coupling and the internal field gradients will come most directly from magnetic resonance studies. The optimum experimental conditions for both NMR and AMR studies have been outlined in this chapter. Conventional NMR experiments on rhenium have only been done successfully on powders and the skin depth problem may prevent any studies on single crystalline samples. The most promising technique appears to be AMR. To date AMR signals have only been observed in metals which possess cubic symmetry. Rhenium is a potentially good candidate for the first non-cubic crystal and should represent an interesting system to study. Experiments along this line are currently being planned here at Caltech.

Regarding the dilution refrigerator; it has proven to be a very useful and dependable experimental tool. Its two major features of producing steady state low temperatures, and an independence of D.C. magnetic fields opens the possibilities for many new experiments.

It should be most useful in the fields of nuclear physics where polarized samples are needed, and solid state physics where a very low thermal noise is important, for example, tunneling experiments and magnetic resonance phenomena.

REFERENCES

*We wish to thank Dr. Levy of the Physics Department of the University of California at Los Angeles for the loan of this sample.

†I am grateful to Dr. Persson for the loan of his original copy of this program.

1. G. K. Walters, W. M. Fairbank, Phys. Rev. 103, 262 (1956).

2. H. London, G. R. Clarke, E. Mendoza, Phys. Rev. 128, 1992 (1962).

3. H. E. Hall, P. J. Ford, K. Thompson, Cryogenics 6, 80 (1966).

4. B. S. Neganov, N. Borisov, M. Liburg, Zh. Eksperism i Thor. Fiz. 50, 1445 (1966); (English translation: Soviet Physics JETP 23, 959 (1966)).

5. J. C. Wheatley, O. E. Vilches, W. R. Abel, Physics 4, 1 (1968).

6. O. E. Vilches, J. C. Wheatley, Phys. Letters 24A, 440 (1967), 25A, 344 (1967).

7. D. O. Edwards, D. F. Brewer, P. Seligman, M. Skertic, Yaqub, Phys. Rev. Letters 15, 773 (1965).

8. A. C. Anderson, D. O. Edwards, W. R. Roach, R. E. Sarwinski, J. C. Wheatley, Phys. Rev. Letters 17, 367 (1966).

9. J. Bardeen, G. Baym, D. Pines, Phys. Rev. 156, 207 (1967).

10. C. Ebner, Phys. Rev. 156, 222 (1967).

11. E. C. Stoner, Phil. Mag. 25, 899 (1938).

12. W. C. Black, W. R. Roach, J. C. Wheatley, RSI 35, 587 (1964).

13. E. M. Ifft, D. O. Edwards, R. J. Sarwinski, M. M. Skertic, Phys. Rev. Letters 19, 831 (1967).

14. J. C. Wheatley, Am. J. Phys. 36, 181 (1968).

15. R. Radebaugh Thermodynamic Properties of He^3-He^4 Solutions with Applications to the He^3-He^4 Dilution Refrigerator, National Bureau of Standards Tech. Note 362, Dec. 1967.

16. W. R. Abel, R. T. Johnson, J. C. Wheatley, W. Zimmerman, Phys. Rev. Letters 18, 737 (1967).

17. E. C. Kerr, Proceedings of Fifth International Conference on Low Temperature Physics and Chemistry, Madison, Wisconsin, ed. by J. R. Dillinger (University of Wisconsin Press, Madison, Wis., 1958), p. 158.

18. J. C. Wheatley, Phys. Rev. 165, 304 (1968).

19. J. C. Wheatley 'Quantum Fluids' ed. by D. F. Brewer (North Holland Publishing Co., Amsterdam, 1966), p. 183.

20. W. R. Roach, Ph.D. Thesis, University of Illinois (1966).

21. G. Baym, C. Ebner, Phys. Rev. 164, 235 (1967).

22. A. C. Anderson, J. I. Connolly, J. C. Wheatley, Phys. Rev. 135, A910 (1968).

23. E. Ambler, N. Kurti, Phil. Mag. 43, 260 (1952).

24. S. G. Sydoriak, T. R. Roberts, Phys. Rev. 118, 901 (1960).

25. D. S. Betts, D. W. Osborne, B. Welker, and J. Wilks, Phil. Mag. 8, 977 (1963).

26. S. Brunauer, P. H. Emmet, E. Teller, J. Am. Chem. Soc. 60, 309 (1938).

27. G. K. White 'Experimental Techniques in Low Temperature Physics, 2nd Edition' Oxford at the Clarendon Press, 1968.

28. F. J. Shore, V. L. Sailor, H. Marshak and C. A. Reynolds, RSI 31, 970 (1960).

29. D. O. Edwards, R. E. Sarwinski, P. Seligmann, J. T. Tough (preprint).

30. W. C. Black, E. C. Hirshkoff, A. C. Mota, J. C. Wheatley (preprint)

31. C. Boghosian, H. Meyer, J. E. Rives, Phys. Rev. 146, 110 (1966).

32. J. P. Harrison, RSI 39, 145 (1968).

33. G. J. Ehnholm, T. E. Katila, O. V. Lounsman, P. Reivari, Cryogenics June, 136 (1968).

34. D. L. Goodstein, Ph.D. Thesis, University of Washington (1965).

35. J. M. Daniels, F. N. H. Robins, Phil. Mag. 44, 630 (1953); R. P. Hudson, R. S. Kaeser, H. E. Radford, Proceedings of the Seventh International Conference on Low Temperature Physics. ed. by G. M. Graham and A. C. Hollis Hallett (University of Toronto Press, Toronto, Canada, 1961), p. 100.

36. W. R. Abel, A. C. Anderson, J. C. Wheatley, RSI 35, 444 (1964).

37. R. E. Watson, A. C. Gossard, Y. Yafet, Phys. Rev. 140, A375 (1965).

38. E. Matthias, W. Schneider, R. M. Steffen, Arkiv für Fysik 24, 97 (1963).

39. See, for example, 'Physical Acoustics' Vol. IV-A, ed. by W. P. Mason (Academic Press, New York, 1966), Chapter 3.

40. See, for example, J. D. Jackson 'Classical Electrodynamics' (John Wiley & Sons, Inc., New York 1965), Chapter 4.

41. See, for example, C. Slichter, 'Principles of Magnetic Resoance' ed. by F. Seitz, (Harper & Row, New York, 1963), Chapter VI.

42. A. Messiah 'Quantum Mechanics' Vol. II, (John Wiley & Sons, Inc., New York, 1962) p. 571-573.

43. M. E. Rose 'Elementary Theory of Angular Momentum' (John Wiley & Sons, Inc., New York, 1957), Chapter 5.

44. P. H. Keesom, C. A. Bryant, Phys. Rev. Letters 2, 260 (1966).

45. See, for example, C. Kittel 'Introduction to Solid State Physics' Third edition (John Wiley & Sons, Inc., New York), p. 212.

46. Handbook of Chemistry and Physics, 48th Edition, ed. by R. C. Weast, S. M. Selby (The Chemical Rubber Co., Cleveland, 1967-1968).

47. J. Bardeen, L. N. Cooper, and J. R. Schrieffer, Phys. Rev. 108, 1175 (1957).

48. E. Lerner, J. G. Daunt, RSI 35, 1069 (1964).

49. H. R. O'Neal, N. E. Phillips, Phys. Rev. 137, A748 (1965).

50. E. C. Kerr, R.D.Taylor, Proceedings of the Seventh International Conference on Low Temperature Physics, ed. by G. M. Graham A. C. Hollis Hallett (University of Toronto Press, Toronto, Canada, 1961), p. 605.

51. G. Ahlers, RSI 37, 477 (1966).

52. N. E. Phillips, Phys. Rev. 134, A385 (1964).

53. J. Korringa, Physica 16, 601 (1950).

54. F. W. De Wette, Phys. Rev. 123, 103 (1961).

55. R. M. Sternheimer, Phys. Rev. 130, 1423 (1963).

56. Lattice constants of Re taken from, R. W. G. Wyckoff, Crystal Structures (Interscience Publishers, Inc., New York, 1948).

TABLE 1

FLOW IMPEDANCE AND SURFACE AREA FOR COPPER SPONGES

Number	Reduced Density	Volume cc	Flow Impedance cm^{-3}	Volume Resistivity cm^{-2}	Conductance cm^{6}	Area m^2/cc
3f	.06	.186	$(7.05 \pm .07) \times 10^{8}$	1.20×10^{8}	2.66×10^{8}	
1f	.15	.191	$(3.13 \pm .02) \times 10^{9}$	5.21×10^{8}	6.14×10^{-11}	$1.25 \pm .2$
2f	.24	.230	$(4.5 \pm .3) \times 10^{9}$	6.22×10^{8}	5.09×10^{-11}	$1.52 \pm .3$
4f	.51	.217	$(4.8 \pm .2) \times 10^{10}$	7.06×10^{9}	4.48×10^{-12}	$4.0 \pm .8$
5f	.60	.203	$(1.13 \pm .08) \times 10^{11}$	1.75×10^{10}	1.79×10^{-12}	
1c	.26	.210	$(9.4 \pm .1) \times 10^{8}$	1.41×10^{8}	2.23×10^{-10}	
5c	.35	.230	$(8.28 \pm .08) \times 10^{8}$	1.39×10^{8}	2.28×10^{-10}	
2c	.36	.184	$(1.21 \pm .04) \times 10^{9}$	2.08×10^{8}	1.51×10^{-10}	
3c	.37	.207	$(1.37 \pm .02) \times 10^{9}$	2.10×10^{8}	1.51×10^{-10}	
4c	.48	.192	$(4.52 \pm .02) \times 10^{9}$	7.82×10^{8}	4.07×10^{-11}	
6c	.64	.185	$(2.12 \pm .05) \times 10^{10}$	3.65×10^{9}	8.73×10^{-12}	
reground 1r	.25	.192	$(8.6 \pm .2) \times 10^{7}$	1.44×10^{7}	2.22×10^{-9}	$1.2 \pm .2$

Sponges of 5μ powder are labeled (1f-5f)

Sponges of 40μ powder are labeled (1c-6c)

TABLE 1 (Cont'd.)

Reduced density = density of sponge/density of copper where ρ_{cu} = 8.9 gm/cc

Flow impedance = $(P_2^2 - P_1^2)/2\eta \dot{V} P_1$ P_2 = driving pressure, P_1 = terminal pressure,

$\dot{V}$ = volume rate of flow, η = viscosity.

Volume resistivity = (flow impedance) $\times$ $(\pi r^2/\ell)$

r = radius of sponge, ℓ = sponge length

Conductance = (sponge volume)/(flow impedance). Density and volume are accurate to ~ 1%, relative error in conductance will be same as that of flow impedance.

TABLE 2

DIMENSIONS OF INTERCONNECTING CUPRONICKEL TUBING

	Location	O.D. & Wall	Length	Comments
Condensed Side	Still exchanger to 1st heat exchanger	.013" O.D. × .003" wall	3-3/4"	A 1.7" piece of No. 31 manganin wire has been inserted in this section to form a vapor suppressing impedance.
	1st heat exchanger to 2nd heat exchanger	.013" O.D. × .003" wall	1-7/8"	
	2nd heat exchanger to mixing chamber	.013" O.D. × .003" wall	2-3/4"	
Dilute Side				
	Mixing chamber to 2nd heat exchanger	.031" O.D. × .003" wall	3"	The diameter of this section should possibly be increased as mentioned on P. 68
	1st exchanger to still	.031" O.D. × .003" wall	6"	This section is looped as shown in Fig. 14. Direct distance between still and No. 1 exchanger is 3-1/2"
	2nd heat exchanger to 1st exchanger	.031" O.D. × .003" wall	1-7/8"	

TABLE 3

REFRIGERATOR CHARACTERISTICS

Amount of He Used:	.51 moles, 37% He^3
Condenser:	4.2 gm, -325 mesh sintered Cu. Condenses 4×10^{-5} moles/sec with overpressure of 30 mm-Hg. Condenser temperature 1.1°K.
Main Flow Impedance:	$Z = 1.5 \times 10^{12}$ cm^{-3}. Made from 7.3" of .010" I.D. Cu-Ni tubing with 7.0" of .0089" (No. 31 BS gauge) manganin wire inside.
Still:	All copper. Top, including orifice, is single piece construction. Orifice diameter = .040", thickness of diaphram = .020". Orifice is electropolished. Heater in bottom of still.
Still Heat Exchanger:	2.4 gm, -325 mesh sintered Cu. Liquid volume .47 cc. Flow impedance $\sim 10^9$ cm^{-3}. Exchanger is "greased" into port on still bottom (see Fig. 14).
Vapor Suppressing Impedance in Line Between Still and First Exchanger:	1.7" piece of No. 31 manganin wire inserted into the .010" I.D. Cu-Ni tubing $Z \sim 10^{11}$ cm^{-3}.
Mechanical Supports:	1/2" O.D. × 1/4" I.D. pitch-bonded graphite between all components.
	Lengths: Still - No. 1 exchanger 3-1/2"
	No. 1 exchanger - No. 2 exch. 1-5/8"
	No. 2 exchanger - M.C. 2-3/4"

TABLE 3 (cont'd.)

Heat Exchangers:	Design shown in Figure 13. Made from re-sintered sponges originally constructed with 5μ powder. Each side contains 3-4 gm Cu powder. He liquid volume ~ 1.5 cc per exchanger. Copper volume essentially the same as He volume. Impedance of dilute side only, $Z_D = 1.2 \times 10^8$ cm^{-3}. Impedance of total system below still 2.3×10^9 cm^{-3}. (This does not include vapor suppressing impedance.)

TABLE 4

EIGENVECTORS AND EIGENVALUES OF COMBINED HAMILTONIAN $H = H_Q + H_{mag}$ AS GIVEN IN EQUATION (88)

$Y = 2.6 \quad \beta = 0^o$

Eigenvalues (E)	Eigenvector, basis states denoted by magnetic quantum number m_I					
	+ 5/2	+ 3/2	+ 1/2	- 1/2	- 3/2	- 5/2
3.50000	1.0	0.0	0.0	0.0	0.0	0.0
-5.89999	0.0	1.0	0.0	0.0	0.0	0.0
-9.29999	0.0	0.0	1.0	0.0	0.0	0.0
-6.70000	0.0	0.0	0.0	1.0	0.0	0.0
1.89999	0.0	0.0	0.0	0.0	1.0	0.0
16.49998	0.0	0.0	0.0	0.0	0.0	1.0
$Y = 2.6 \quad \beta = 20^o$						
3.99563	.88430	-.38018	.19724	.18591	-.00105	-.00006
-5.24117	.44306	.54854	-.63844	-.30822	.00852	-.00988
-10.13361	.14327	.52405	.73874	-.39322	.06617	-.00938
-6.58133	.03366	.50916	.08296	.79126	-.32030	.06356
1.78410	.00643	.14287	-.02850	.29670	.89244	-.30697
16.17624	.00084	.01668	-.00679	.03940	.31062	.94954

The parameter $Y = \nu_H/\nu_E$ as defined in the text and Figure 30. One unit of Y = 7.8 kOe. 1 unit of energy/h for the eigenvalues E = 7.53 Mhz. β is the angle between the principle symmetry axis and the applied magnetic field. The data given here are a portion of the data displayed in Figure 31. The numbers read horizontally after an eigenvalue are the coefficients of the basis states $|I,m_I\rangle$ comprising the eigenvector corresponding to that eigenvalue.

FIGURE CAPTIONS

Figure 1 Refrigerator schematic. All important components within cryostat are shown in block form.

Figure 2 Ratio of heat capacity per mole of solution to RT, where R is the gas constant and T is the temperature for dilute solutions of He^3 in He^4 at its saturated vapor pressure. Experimental data from Reference 5. Lines through experimental data are theoretical ones based on the heat capacity of an ideal Fermi-Dirac gas as calculated in Reference 11.

Figure 3 Phase separation curve for He^3-He^4 mixture as a function of temperatures and He^3 concentration. $x = n_3/(n_3 + n_4)$ where n_3 and n_4 are the number of He^3 and He^4 atoms respectively.

Figure 4 The effective mass of He^3 in He^4 solutions as a function of the He^3 concentration. Theoretical calculations are from Reference 15.

Figure 5 Fermi temperature and deviation of the chemical potential from ideal Fermi-Dirac value as a function of concentration.

Figure 6 He^3 concentration in the dilute phase as a function of temperature. Theoretical calculation from Reference 15.

Figure 7 Molar enthalpy of pure and dilute solutions, cooling capacity and internal energy as a function of temperature. $\dot{Q}(T,T)/\dot{n}_3 = H_3(x_d, T) - H_3^{o}(T)$.

Figure 8 Vapor pressure of liquid in still for various mixing chamber temperatures as a function of the still temperature. The lines A and B represent still temperature vs. mixing chamber temperature for the two refrigerators built during this work.

Figure 9 This gives an accurate picture of all the low temperature components of the refrigerator. Important dimensions are indicated on the drawing. All tubing in cryostat whose dimensions are indicated in this figure was thin walled stainless steel. The radiation baffles were made of brass or copper as described in the text. The isolation vacuum can is copper with a 1" I.D. brass tail. The center of the magnet pole pieces is 2-5/8" below the bottom of the mixing chamber.

Figure 10 Details of the He^4 pot and condenser. The He^4 pot is made of copper. The orifice is .040" diameter through a .012" thick diaphram and is chemically polished. The pumping line is stainless steel 5/8" I.D. × .010" wall. The fill line is .010" I.D. Cu-Ni. The condenser contains 4.2 gm of -325 mesh copper powder sintered into a OFHC copper body of .375" O.D. × .250" I.D. × 1" length. The condenser is coated with silicone vacuum grease and slipped into the receptacle in the He^4 pot. The He^3 inlet line is 1/16" I.D. stainless steel. The main impedance is 7.3" of .010" I.D. Cu-Ni tubing with a 7" piece of No. 31 manganin wire inside.

Figure 11 The flow conductance and surface area of copper sponges as a function of the sponge density. The data are given in Table I. Only surface area of 5μ sponges was measured. The conductance is defined by (sponge volume)/(flow impedance). The flow impedance is defined by $Z = (P_2^2 - P_1^2)/2\eta\dot{V}P_1$ where P_2 is driving pressure, P_1 the terminal pressure, $\dot{V}$ the volume rate of flow, and η the gas viscosity. The reduced density is (sponge density)/(density of copper) where ρ_{Cu} = 8.9 gm/cc. The circles and squares represent conductance data for sponges of 5μ and 40μ powder, respectively. The triangles are area data.

Figure 12 The ratio of 5μ sponge area per unit volume to 5μ sponge flow impedance per unit volume as a function of the reduced density. This ratio is the product of the area and conductance given in Figure 11. Line A comes from using the upper line of Figure 11 for the area and Line B from using the lower line of Figure 11 for the area.

Figure 13A Method for measuring the electrical resistance between the sponge and the copper body. Voltage measurements are made with a Hewlett-Packard microvoltmeter, Model 425A (Hewlett-Packard Electronics Co., Palo Alto, Calif.). The current is supplied by a Harrison power supply, Model 855c (Harrison Laboratories, Berkeley Heights, N.J.).

Figure 13B Details of heat exchanger construction. Both sides of exchanger are of equal volume. The copper sponge is of the resintered type. The reduced density is ~ 0.5. The free He liquid volume is about 1.5cc/sponge. The couplings are threaded into the copper body before being soft soldered in place. The end caps are brass. The graphite supports thread onto the 3/8" – 16 screw machined onto the end plate.

Figure 14 Details of the still construction. All material is ETP copper. The orifice is electropolished. The still pumping line is 3/8" I.D. × .010" wall stainless steel. The inner sleeve which forms part of the level sensing capacitor is made of brass, .010" thick, Outer surface is covered with a sheet of .001" mylar to prevent shorting to the copper still wall. The return line is Cu-Ni; dimensions given in Table 3. The return line enters through a copper coupling as was used on the heat exchangers. The electrical leads are sealed with Stycast 2850 GT cement (Emmerson-Cumming, Inc., Los Angeles, Calif.). The tunnel diode oscillator for the level sensor is mounted on the face of the still bottom as shown. Power supply for the oscillator uses a 1.4 volt standard mercury cell. This is mounted on a styrofoam box to insure temperature stability. The heat exchanger on the still contains 2.4 gm of -325 mesh copper powder in a 1/4" I.D. × 1.020" length space. Liquid volume

is .47 cc. The still heater is mounted on the nylon pedestal which attaches to the still bottom with a No. 2-56 screw as shown.

Figure 15 Details of the Mixing Chamber construction. Inlet and outlet tubes of Cu-Ni pass through couplings as used with heat exchangers. All material for M.C. is ETP copper. The copper fins are made as described in text and soft soldered to M.C. wall.

Figure 16 Room temperature gas handling system. In the He^3-He^4 system the mechanical pump is a Welch model 1402KGB (Welch Scientific Co., Skokie, Ill.) and the booster pump is a NRC model B-2 (NRC Equipment Co., Newton, Mass.). All lines except the still line are 3/8" I.D. Cu tubing. The still pumping line from the cryostat to the booster is 2-1/8" I.D. Cu tubing. Its length is 66". The manometer is a conventional U-tube mercury manometer. The molecular sieve trap is filled with Linde 13X molecular sieve pellets kept at liquid nitrogen temperatures (Union Carbide Corp., Linde Division). Valve No. 3 is a Vecco bellows sealed 1-1/2" port valve. All others are Hoke model 4151M2B (Hoke, Inc., Cresskill, N.J.). These valves are bellows sealed and close with a Kel-F tip. The isolation vacuum system uses a Vecco model EP2-5W vacuum pump (Vecco Instrument Co., Plainview,

N.Y.). Pumping lines are 1" I.D. Cu. The pump for the He^4 pot system is a Stokes' model 149-H mechanical pump (F. J. Stokes Corp., Philadelphia, Pa.).

Figure 17A Needle valve for filling He^4 pot from the outer He^4 bath. Barrel and base are of brass. The seat is monel alloy No. 400 (Pacific Metals Inc., Los Angeles, Calif.). The valve stem is made of stainless steel. The valve is opened by a piece of thin wall stainless tubing (1/8" I.D. × .010" wall) which is hard soldered and pinned to the valve stem. This tube goes to room temperature through an o-ring seal at the dewar cap as shown in Figure 9.

Figure 17B Crushed Indium Seal for attaching isolation vacuum can. Upper and lower faces are made of brass. They are clamped together using 8, No. 8-32 stainless steel bolts, nuts and spring loaded washers. The indium wire is obtained from A. D. MacKay, Inc., 198 Broadway, New York, New York.

Figure 18 Behavior of the refrigerator during startup. Time is measured from the end of gas condensation which is about one and one-half hours after the initial He^4 transfer and cool down from $77^{\circ}K$. Symbols s, 1, 2, m stand for the still, first and second heat exchangers and the mixing chamber, respectively.

Figure 19 Internal energy of concentrated He^3 and $T\Delta S(T)$ for He^3-He^4 solutions as a function of the temperature. $\Delta S(T)$ is the change in entropy between the condensed and dilute phase. Results calculated from data given in Reference 5.

Figure 20 Cooling capacity data. Power, in microwatts, applied to the mixing chamber as a function of the mixing chamber temperature. Circulation rates are: Neganov et al.,[4] 1.4×10^{-4} moles/sec; Wheatley et al.,[5] 2.0×10^{-5} moles/sec; Ehnholm et al.,[33] 3.0×10^{-5} moles/sec; this refrigerator 2.0×10^{-5} moles/sec.

Figure 21 Block diagram of components of low power resistance bridge. This is a fairly standard design. The 30 hz oscillator is synchronized to the line frequency to avoid beats with 60 cycle pick-up. There are two identical inputs to the bridge. The thermometer is attached to one and a standard decade resistance box to the other.

Figure 22A Mutual inductance measuring coils. Primary consists of six layers with 224 turns/layer. The secondaries are 38 layers each with 64 turns/layer. No. 42 Formvar coated copper wire was used. This coil set slips over the tail piece of the isolation vacuum chamber.

Figure 22B Adjustable mutual inductance for compensating measuring coils. Winding is done on Bakelite forms using No. 36 Formvar coated copper wire. Primary consists of one layer

with 440 turns. Secondaries are counterwound, six layers each with 260 turns/layer. The secondary slides inside the primary and is adjusted with a micrometer feed. Coil set is enclosed in a grounded copper box to reduce electronic noise pick-up.

Figure 23 Calorimeter. All material is ETP copper unless labeled otherwise. All threaded connections are gold plated to improve thermal contact. The thermal link is soft soldered to the top of the calorimeter. The No. 0-80 screw for clamping the sample is stainless steel with a nylon tip. Calorimeter base is bolted onto the four support rods using No. 2-56 nuts.

Figure 24A Representative specific heat data taken by "heat pulse" method. Shown is chart record of sample temperature for a point taken on Re with H = 12.5kOe. The noise seen on the tracing is due to currents generated in the resistance thermometer due to the sample vibrating in the magnetic field. The noise in tracings taken for low values of H is much less. Line A is the extrapolate cooling curve. Points a and b mark the end points of the interval ΔT as explained in the text. Voltage and time scales are indicated as well as the resistance of the thermometer at points a and b.

Figure 24B This indicates the manner in which specific heat data were taken using the continuous cooling method. For a given voltage applied to the heater an equilibrium temperature is reached as shown. The resistance (temperature) is recorded. This is done for several power settings. The heater power is then turned off and the temperature decay of the sample back to its original temperature is recorded. Notice the changed time scale on the chart recorder just prior to turning off the heater power. The slope of the cooling curve in ohms/sec is indicated at each data point. These data were taken with the Re sample in a 500 Oe field.

Figure 25 Power supply and switching network for calorimetery. The adjustable 500Ω resistance is a 10 turn helipot. The battery is a standard D-cell, 1.5 volt alkaline battery. The voltage is read using a Leeds & Northrop microvolt potentiometer. The relay of the electronic time clock may be inserted in series as shown. Otherwise switching is done manually with the DPDT switch.

Figure 26A Specific heat of copper sample divide by the temperature, T as a function of the temperature. The sample contained 6.64×10^{-2} moles Cu. The coefficient of the linear term in the specific heat, γ, should be 4.62×10^{-2} millijoules/$^{o}K^{2}$. Data are shown for magnetic fields H = 0 and 300 Oe. Also data are shown taken at lowest temperature using a lower power input to the thermometer from

the resistance measuring bridge.

Figure 26B Specific heat of rhenium sample as a function of the applied magnetic field. The sample is being taken from the superconducting state to the normal state and back again by the changing magnetic field. All data were taken at a constant temperature of .286°K. The sample contains 2.26×10^{-2} moles pure Re.

Figure 27 C/T for rhenium sample as a function of $1/T^3$, where C is the specific heat in millijoules/°K and T is the absolute temperature. The sample contains 2.26×10^{-2} moles. Data are shown for superconducting state (H = 0), the normal state with H = 300 0e, and high field case of 12.5 k0e. Data taken in 500 0e and 1000 0e fields are identical to the data taken in the 300 0e field and are not shown for clarity. A few values of the absolute temperature have been shown on the $1/T^3$ scale for reference purposes.

Figure 28 C/T for rhenium as a junction of T where C is now the molar specific heat in millijoules/$^oK^2$-mole and T is the absolute temperature. Our data in the superconducting state are shown along with some data of Reference 44 for comparison. The line labeled C_{es}/T is the theoretical electronic contribution to specific heat in the superconducting state. (Equation 82b, first term). The solid line drawn through our normal-state data is $C/T = 2.35 + (.061)/T^2$ millijoules/$^oK^2$-mole.

Figure 29A Chart record of the temperature of the Re sample as a function of the magnetic field as the field is swept slowly from 0 to 300 0e. Critical temperatures and fields have been shown.

Figure 29B Chart record of the temperature of the Re sample as the field is swept slowly from 300 0e to 0. As in Figure 29A important temperatures and fields are shown.

Figure 30 Energy levels for $\beta = 90^{o}$ and angular dependence of resonant magnetic field for a fixed frequency as a function of the applied field. One unit E = 7.53 Mhz., β = angle between applied field and principle axis, $y = \nu_H/\nu_E$ where $\nu_H = g\mu_N H/h$ with g = nuclear g-factor, H = applied field, μ_N = nuclear magneton, h = Planck's constant, and $\nu_E = (1/6)a/h$ where a is the zero field splitting as defined in the text. One unit y = 7.8k0e. Levels a-f correspond to m_I = -5/2, + 5/2, ... -1/2, + 1/2, respectively. Curves 1, 2, and 3 represent the transition $\Delta m_I = 3/2 \rightarrow -1/2$ for frequencies of 15.1 Mhz, 16.6 Mhz, and 18.7 Mhz, respectively.

Figure 31 Detailed plot of energy for levels d and e of Figure 30 for the cases $\beta = 0^{o}$, 10^{o}, and 20^{o} as a function of the applied field. As in Figure 30, one unit E = 7.53 Mhz and one unit y = 7.8k0e.

FIG. 1

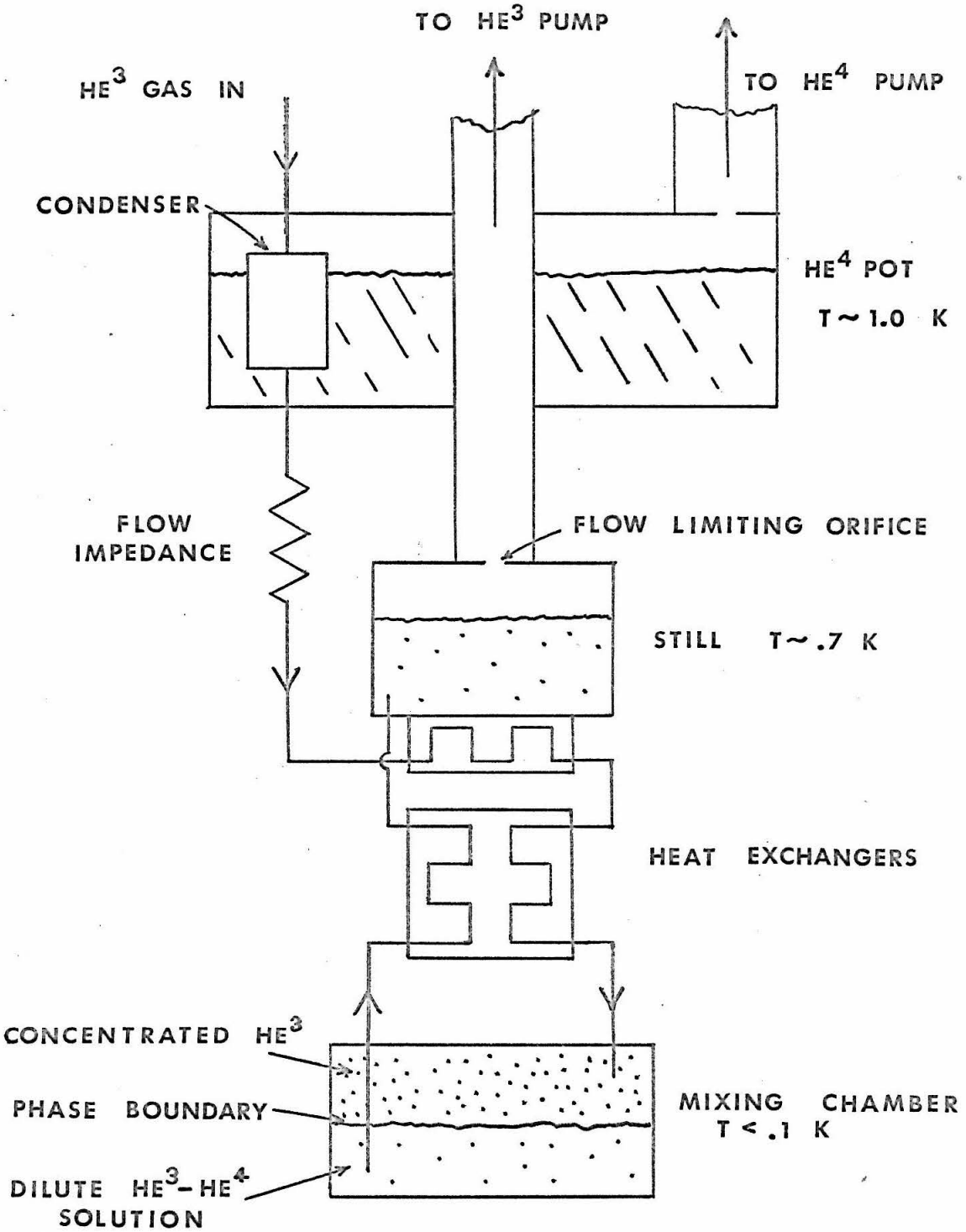
TO HE3 PUMP
HE3 GAS IN
TO HE4 PUMP
CONDENSER
HE4 POT
T ~ 1.0 K
FLOW IMPEDANCE
FLOW LIMITING ORIFICE
STILL T ~ .7 K
HEAT EXCHANGERS
CONCENTRATED HE3
PHASE BOUNDARY
DILUTE HE3 - HE4 SOLUTION
MIXING CHAMBER
T < .1 K

FIG. 2

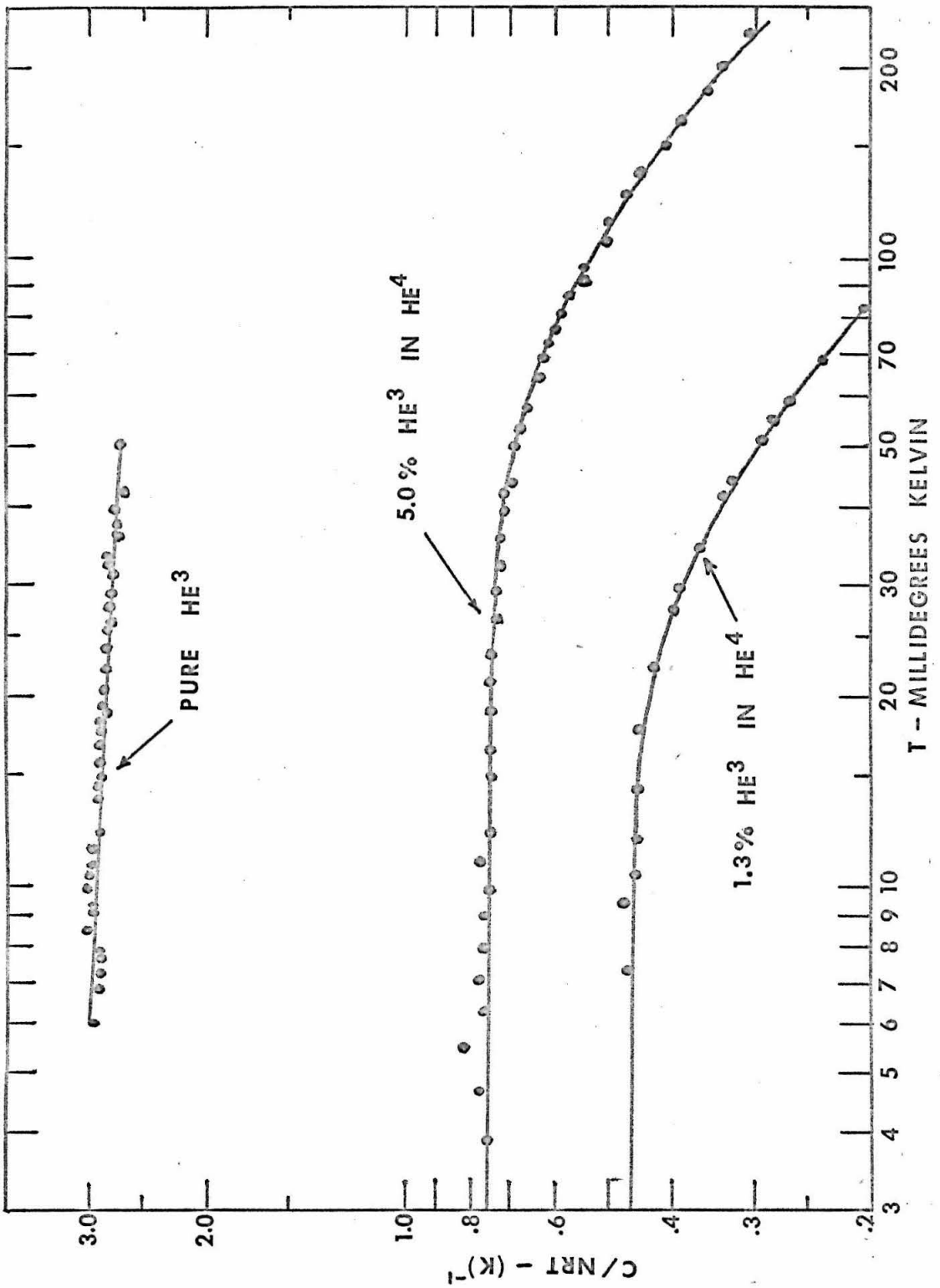
PURE HE3
5.0 % HE3 IN HE4
1.3% HE3 IN HE4
C/NRT - (K)-1
T - MILLIDEGREES KELVIN
3.0
2.0
1.0
.8
.6
.4
.3
.2
3
4
5
6
7
8
9
10
20
30
50
70
100
200

FIG. 3

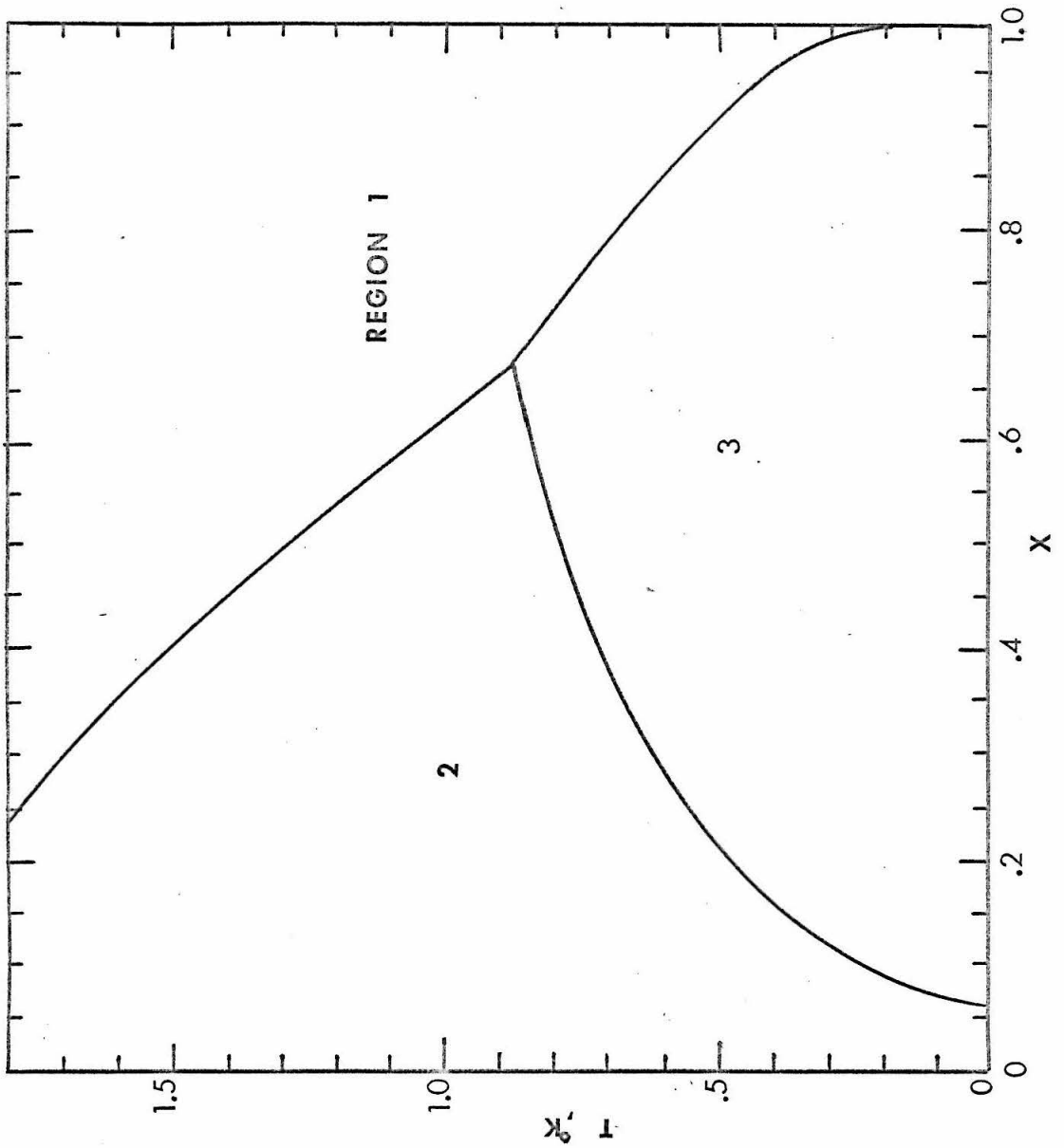

FIG. 4

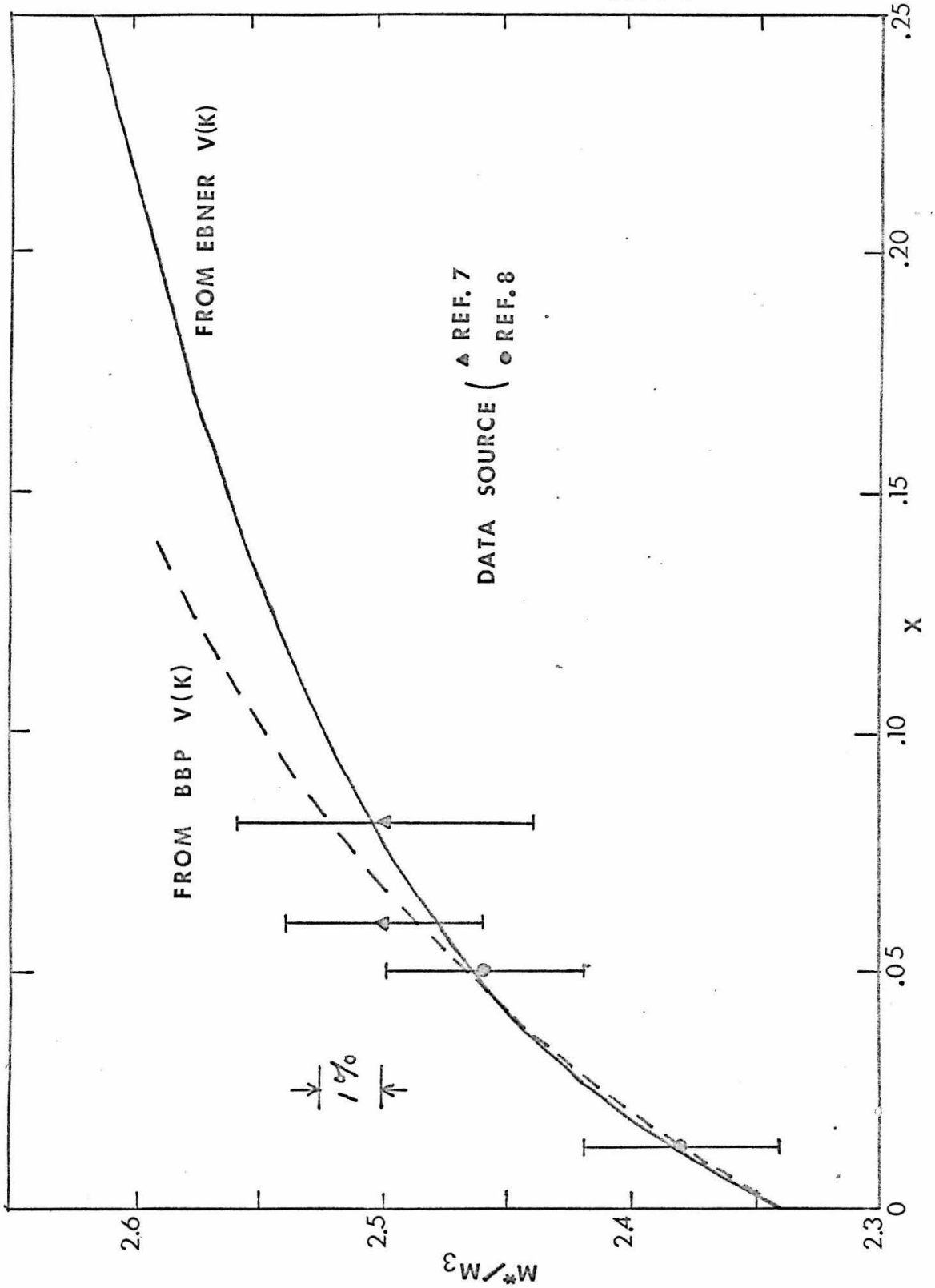
FROM EBNER V(K)
FROM BBP V(K)
DATA SOURCE (▲ REF. 7 ● REF. 8
1%
M*/M3
2.6
2.5
2.4
2.3
0
.05
.10
.15
.20
.25
X

FIG. 5

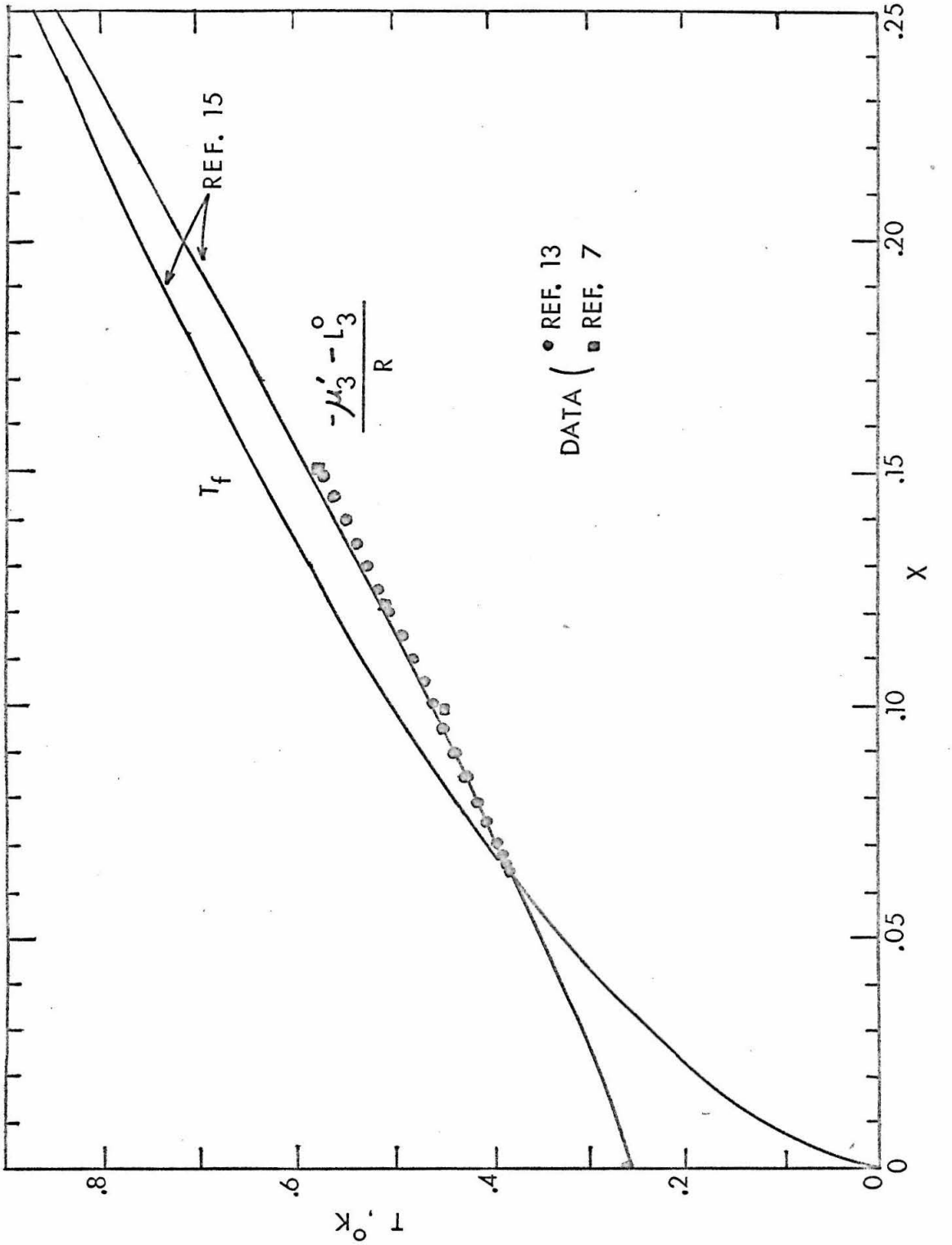

FIG. 6

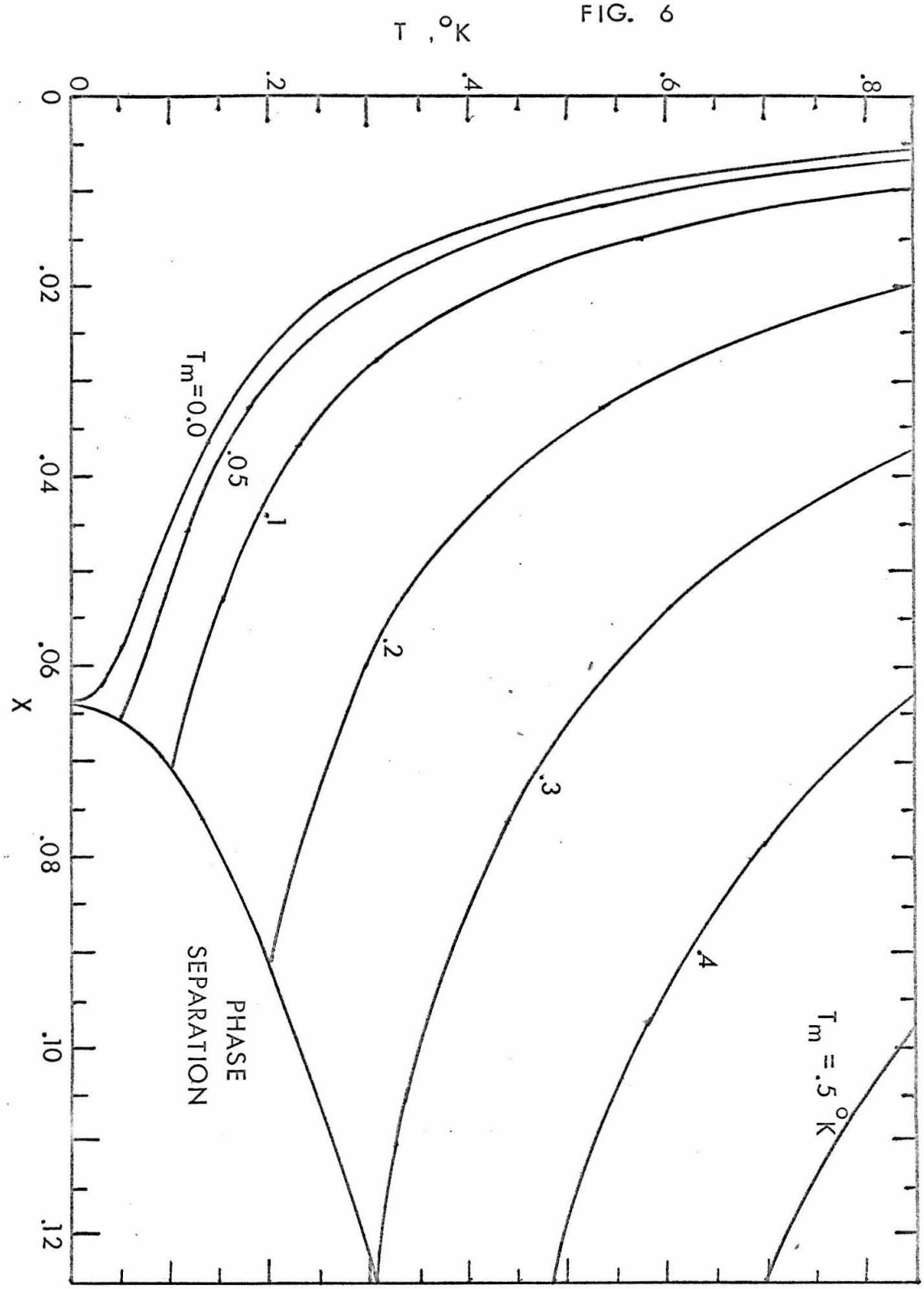
T , °K
0
.2
.4
.6
.8
X
0
.02
.04
.06
.08
.10
.12
T_m=0.0
.05
.1
.2
.3
.4
T_m = .5 °K
PHASE
SEPARATION

FIG. 7

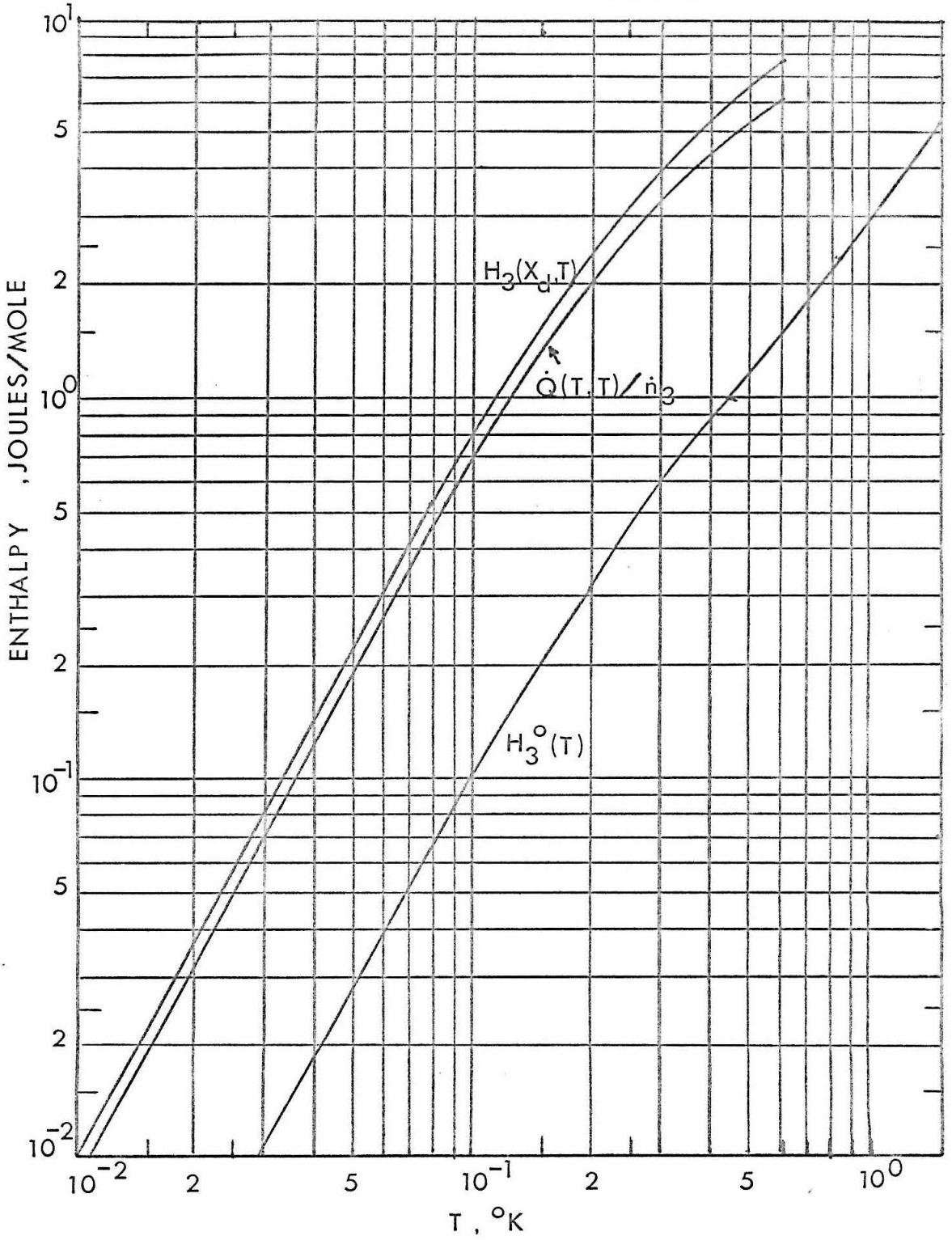
ENTHALPY , JOULES/MOLE
T , °K
$H_3(X_d,T)$
$\dot{Q}(T,T)/\dot{n}_3$
$H_3^o(T)$
10^1
5
2
10^0
5
2
10^{-1}
5
2
10^{-2}
10^{-2}
2
5
10^{-1}
2
5
10^0

FIG. 8

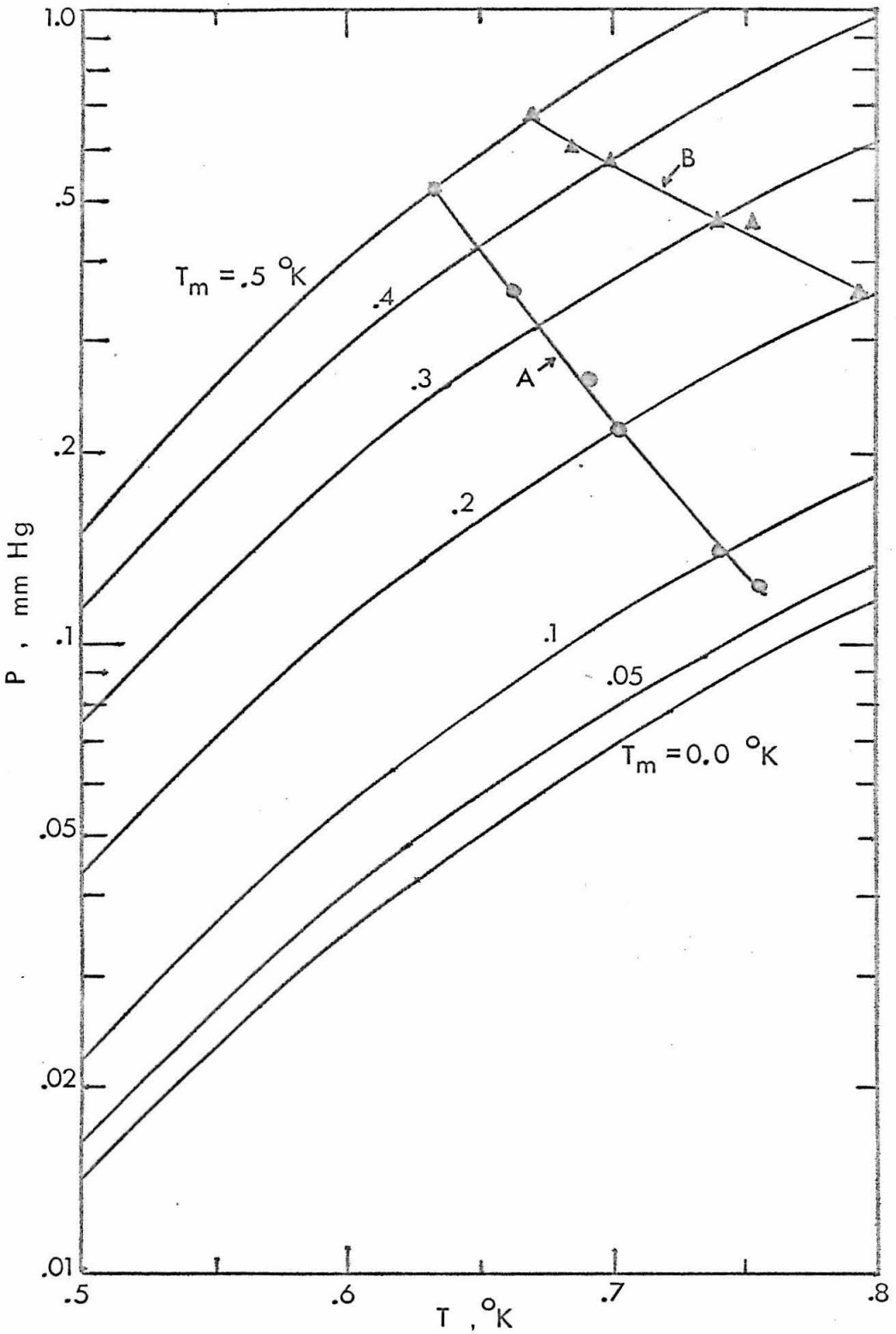

FIG. 9

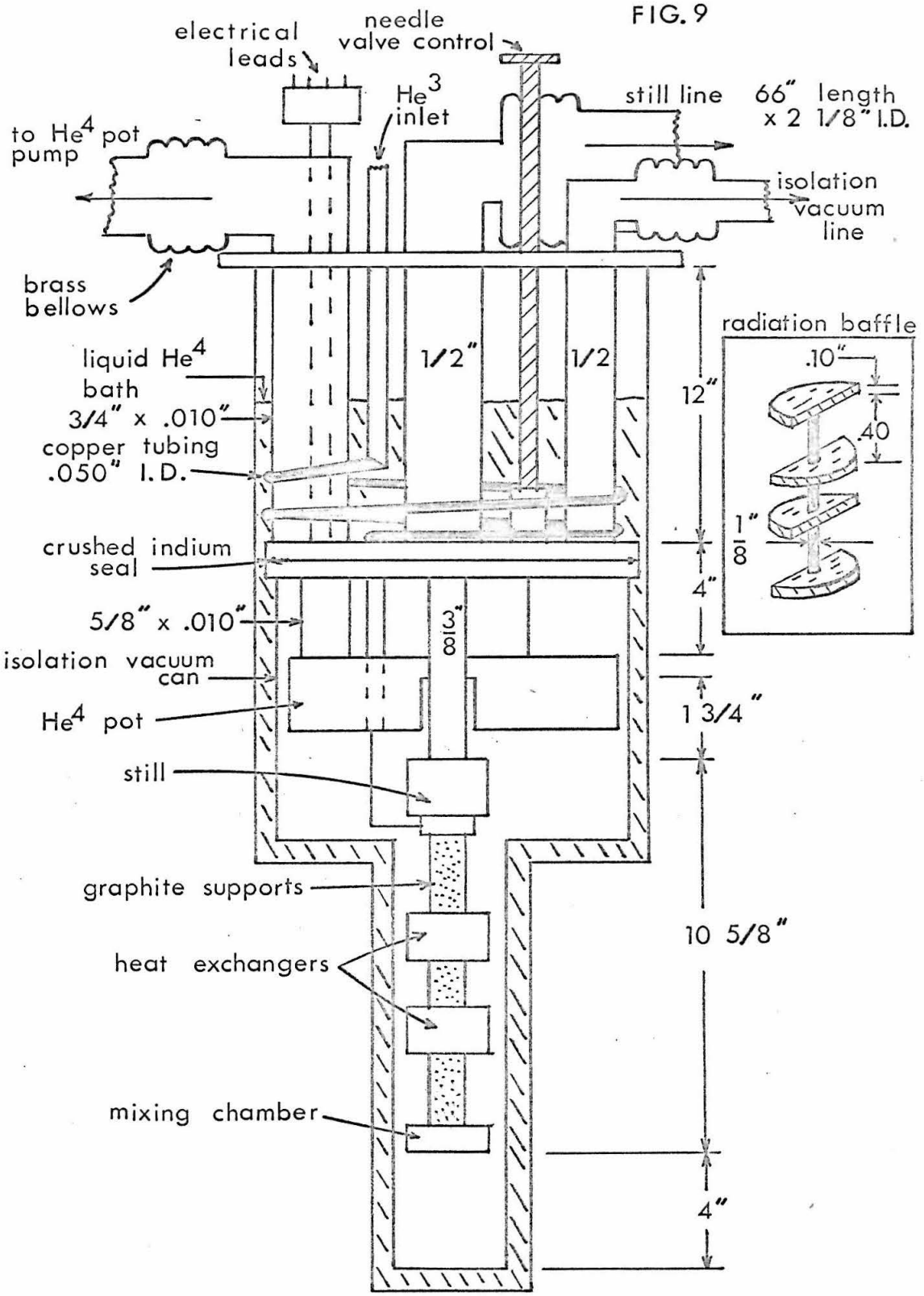
electrical leads
needle valve control
He^3 inlet
still line 66" length x 2 1/8" I.D.
to He^4 pot pump
isolation vacuum line
brass bellows
radiation baffle
.10"
.40
1/8"
liquid He^4 bath 3/4" x .010"
copper tubing .050" I.D.
1/2"
1/2
12"
crushed indium seal
4"
5/8" x .010"
3/8"
isolation vacuum can
He^4 pot
1 3/4"
still
graphite supports
10 5/8"
heat exchangers
mixing chamber
4"

FIG. 10

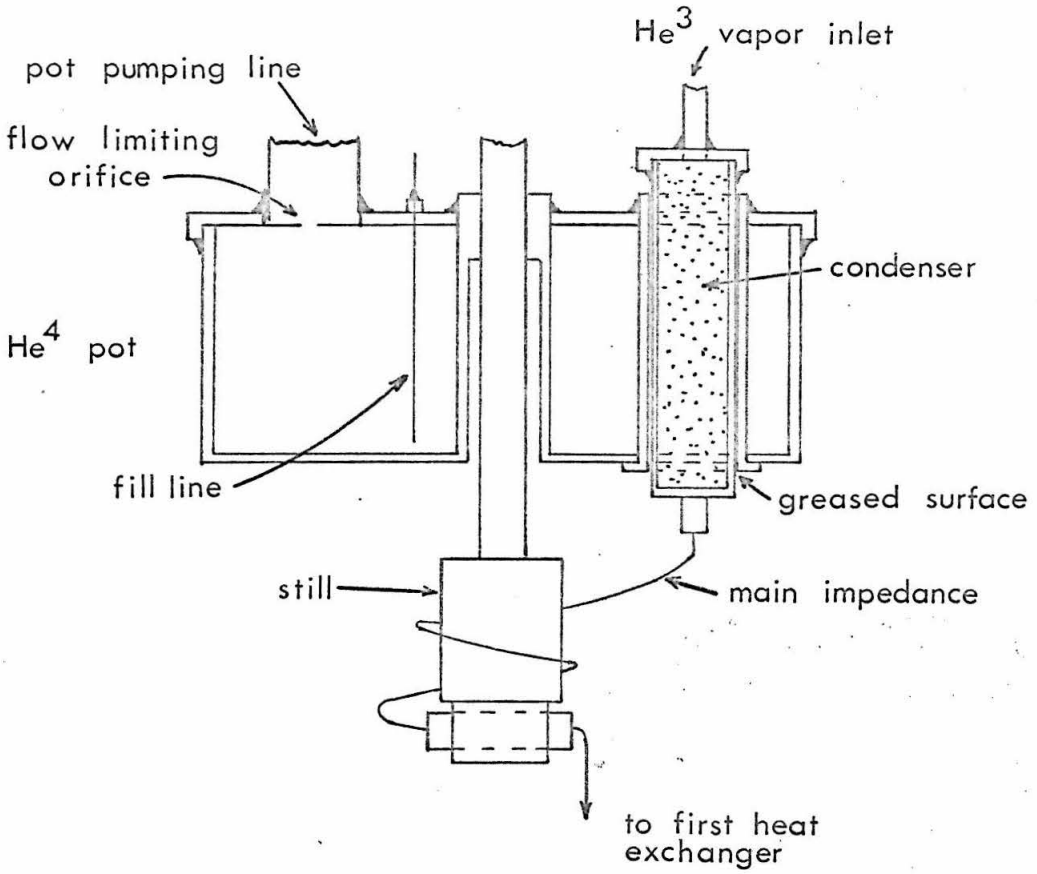
He^3 vapor inlet
pot pumping line
flow limiting orifice
condenser
He^4 pot
fill line
greased surface
still
main impedance
to first heat exchanger

FIG. 11

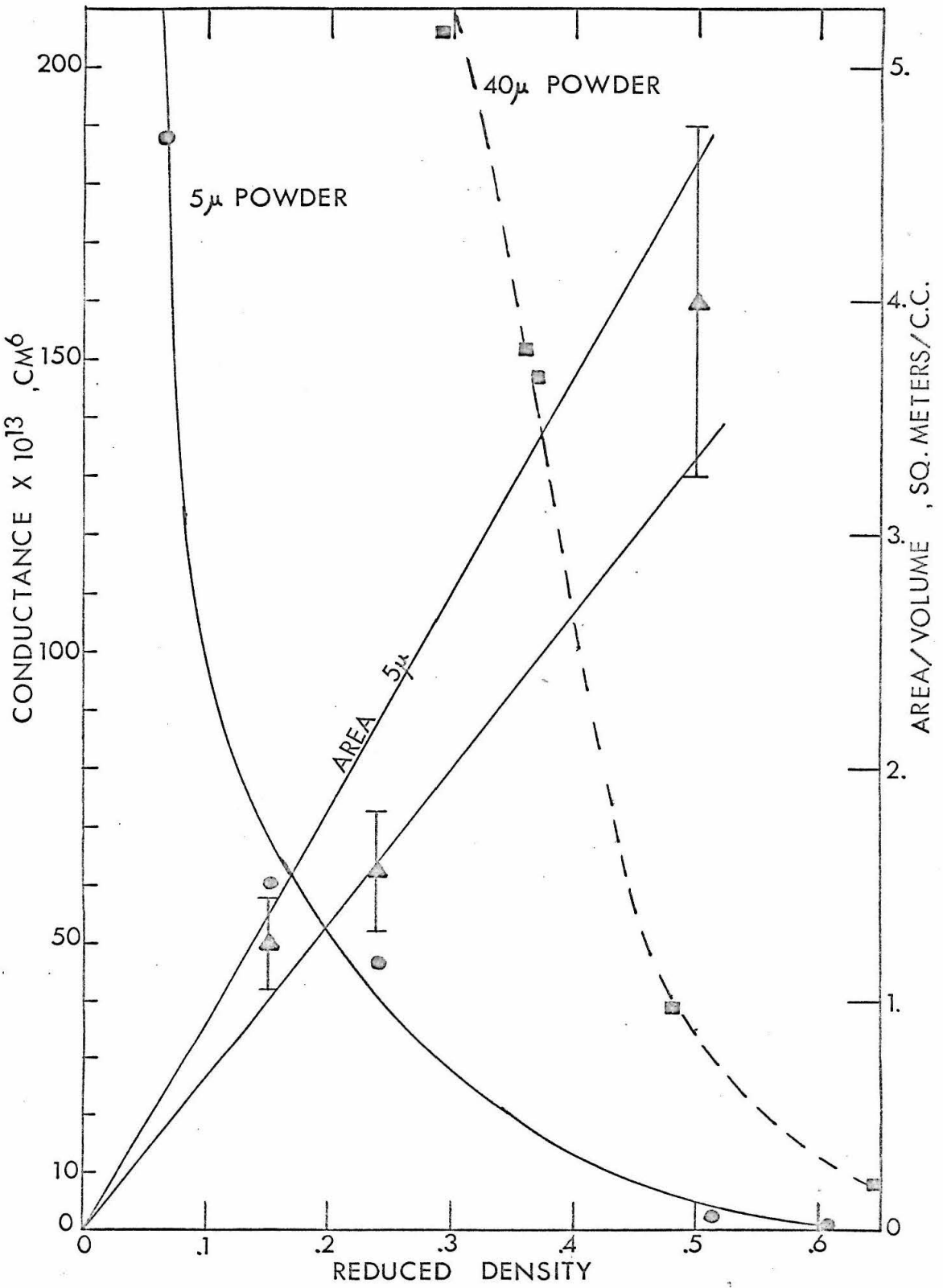
40μ POWDER
5μ POWDER
AREA 5μ
CONDUCTANCE X 10^13, CM^6
AREA/VOLUME, SQ. METERS/C.C.
REDUCED DENSITY
200
150
100
50
10
0
5.
4.
3.
2.
1.
0
.1
.2
.3
.4
.5
.6

FIG. 12

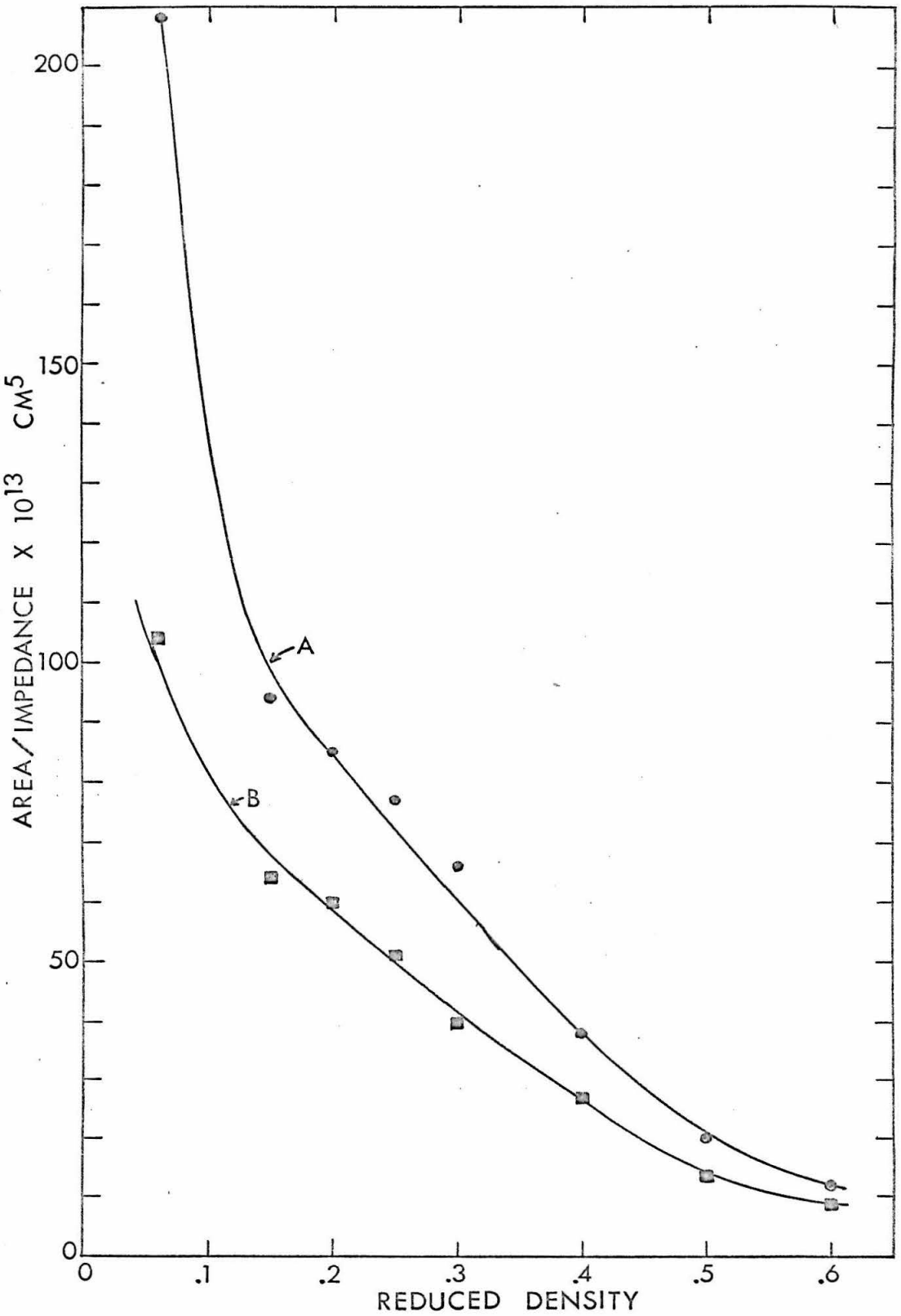
200
150
100
50
0
AREA / IMPEDANCE X 10^{13} CM^5
A
B
0
.1
.2
.3
.4
.5
.6
REDUCED DENSITY

FIG. 13

A.

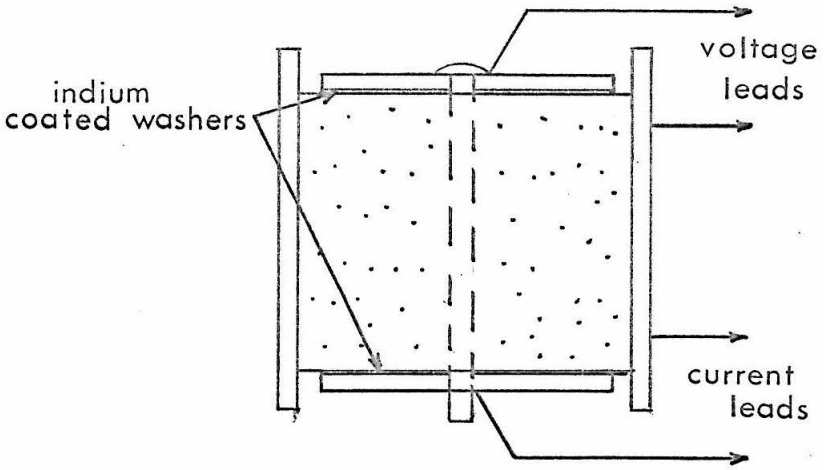
indium
coated washers
voltage
leads
current
leads

B.

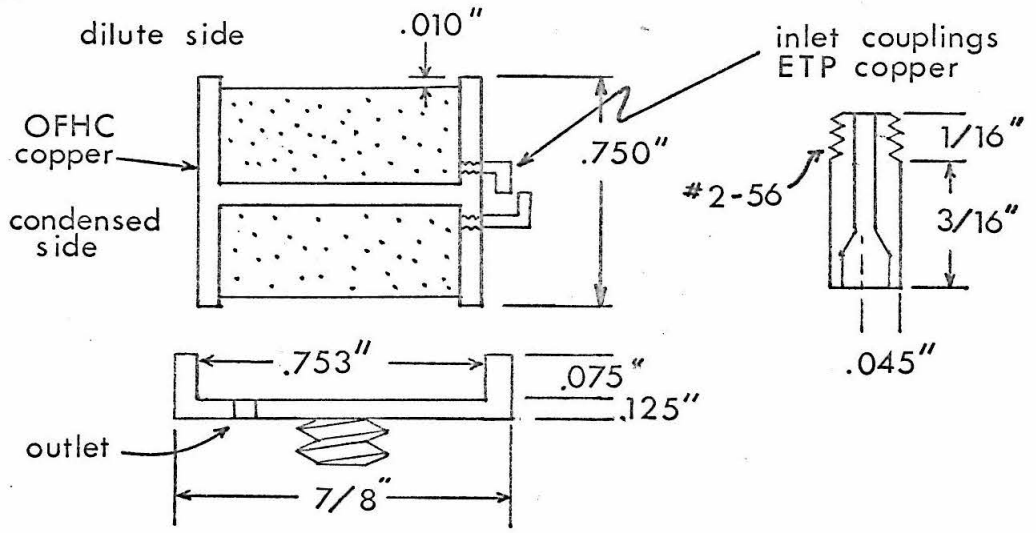
dilute side
.010"
inlet couplings
ETP copper
OFHC
copper
condensed
side
.750"
#2-56
1/16"
3/16"
.045"
.753"
.075"
.125"
outlet
7/8"

FIG. 14

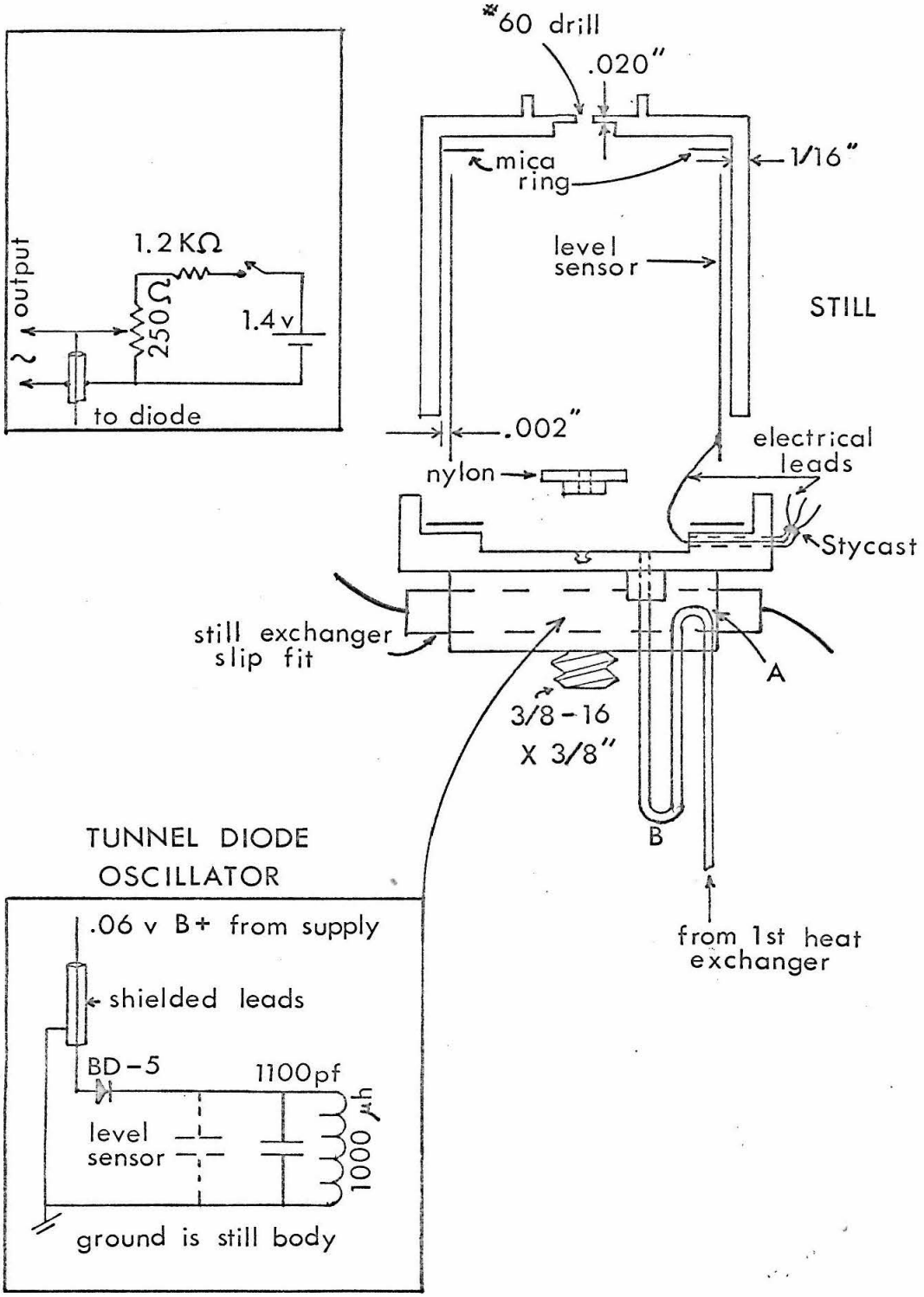
OSCILLATOR SUPPLY
1.2 KΩ
250Ω
1.4 v
output
to diode
#60 drill
.020"
mica ring
1/16"
level sensor
STILL
.002"
nylon
electrical leads
Stycast
still exchanger slip fit
3/8-16 X 3/8"
A
B
from 1st heat exchanger
TUNNEL DIODE OSCILLATOR
.06 v B+ from supply
shielded leads
BD-5
1100pf
level sensor
1000 μh
ground is still body

FIG. 15

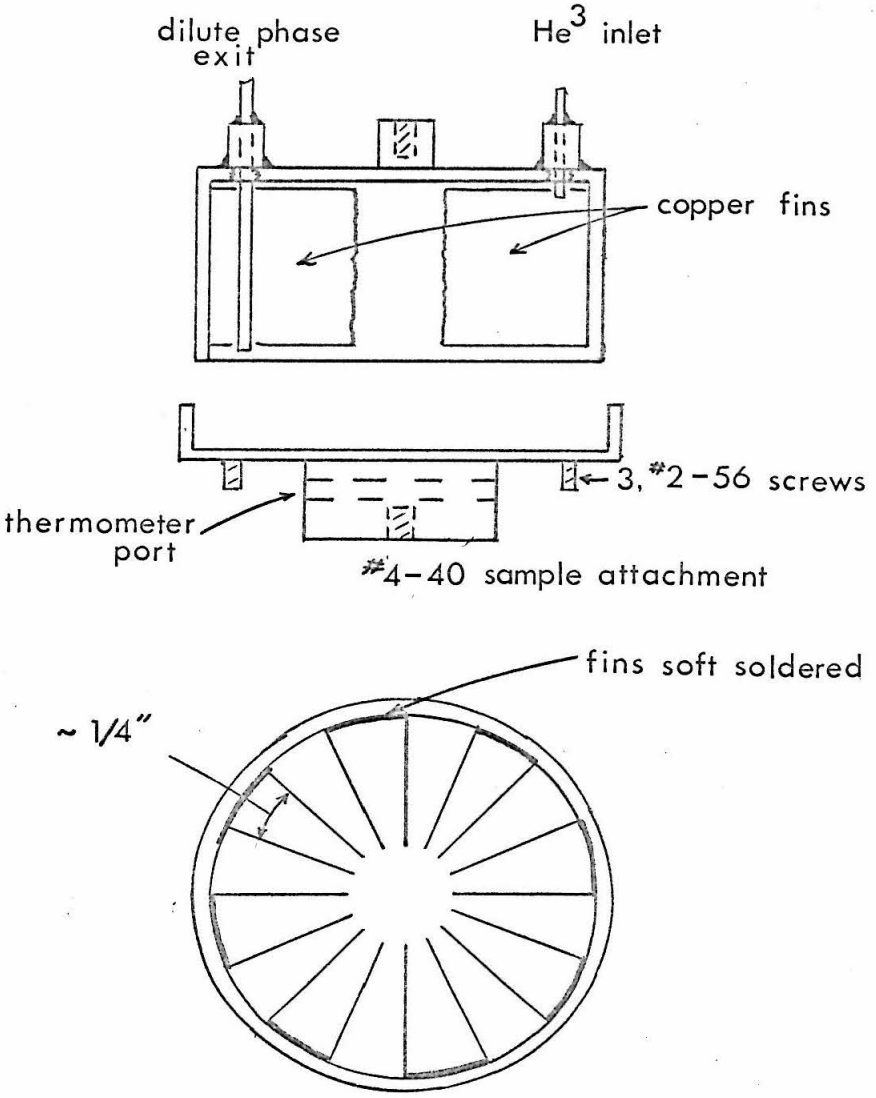
dilute phase exit
He^3 inlet
copper fins
3, #2-56 screws
thermometer port
#4-40 sample attachment
fins soft soldered
~ 1/4"

FIG. 16

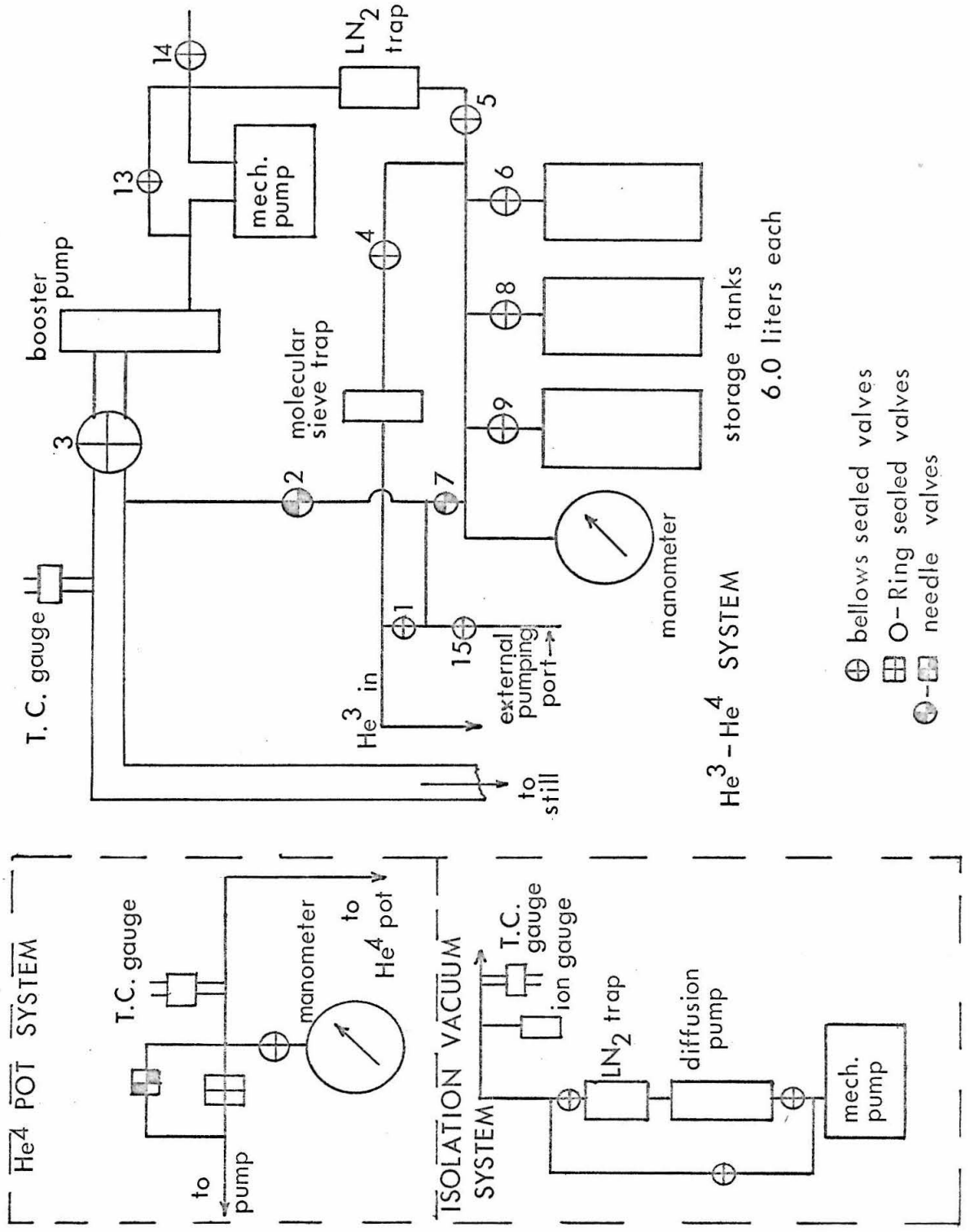
booster pump
mech. pump
molecular sieve trap
LN_2 trap
T. C. gauge
He^3 in
external pumping port
to still
manometer
storage tanks
6.0 liters each
He^3 - He^4 SYSTEM
bellows sealed valves
O-Ring sealed valves
needle valves
He^4 POT SYSTEM
T.C. gauge
manometer
to He^4 pot
to pump
ISOLATION VACUUM SYSTEM
T.C. gauge
ion gauge
LN_2 trap
diffusion pump
mech. pump

FIG. 17

A. NEEDLE VALVE

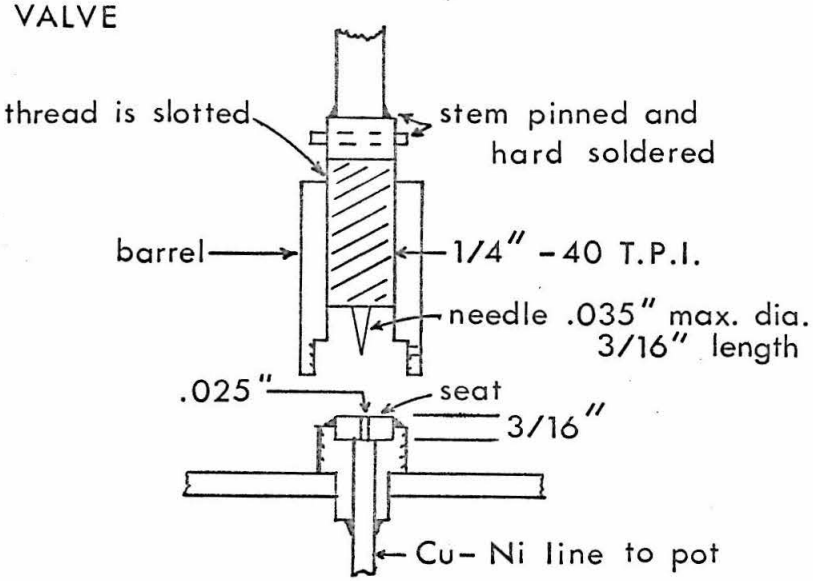

B. CRUSHED INDIUM SEAL

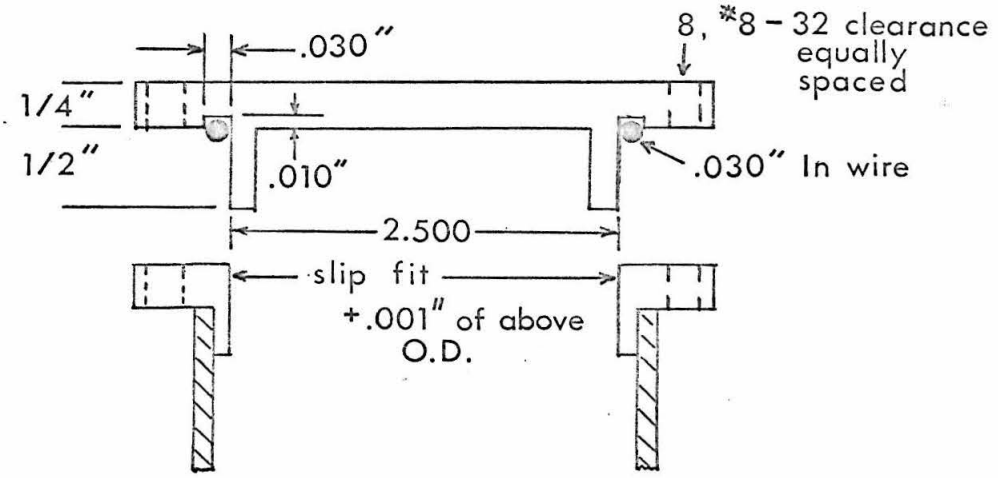

FIG. 18

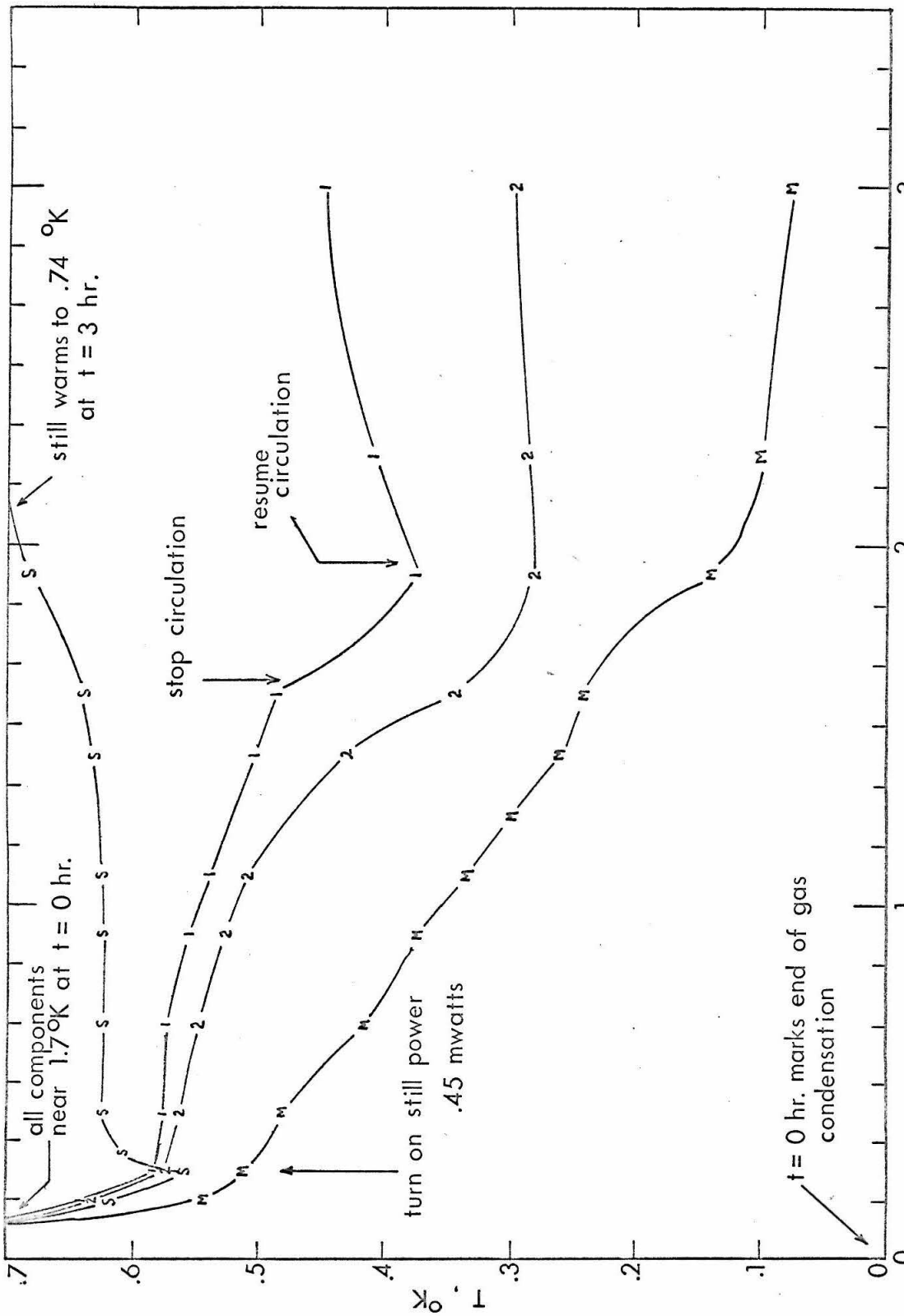
all components
near 1.7°K at t = 0 hr.
still warms to .74 °K
at t = 3 hr.
stop circulation
resume
circulation
turn on still power
.45 mwatts
t = 0 hr. marks end of gas
condensation
T, °K
time, hours
.7
.6
.5
.4
.3
.2
.1
0
1
2
3
S
1
2
M

FIG. 19

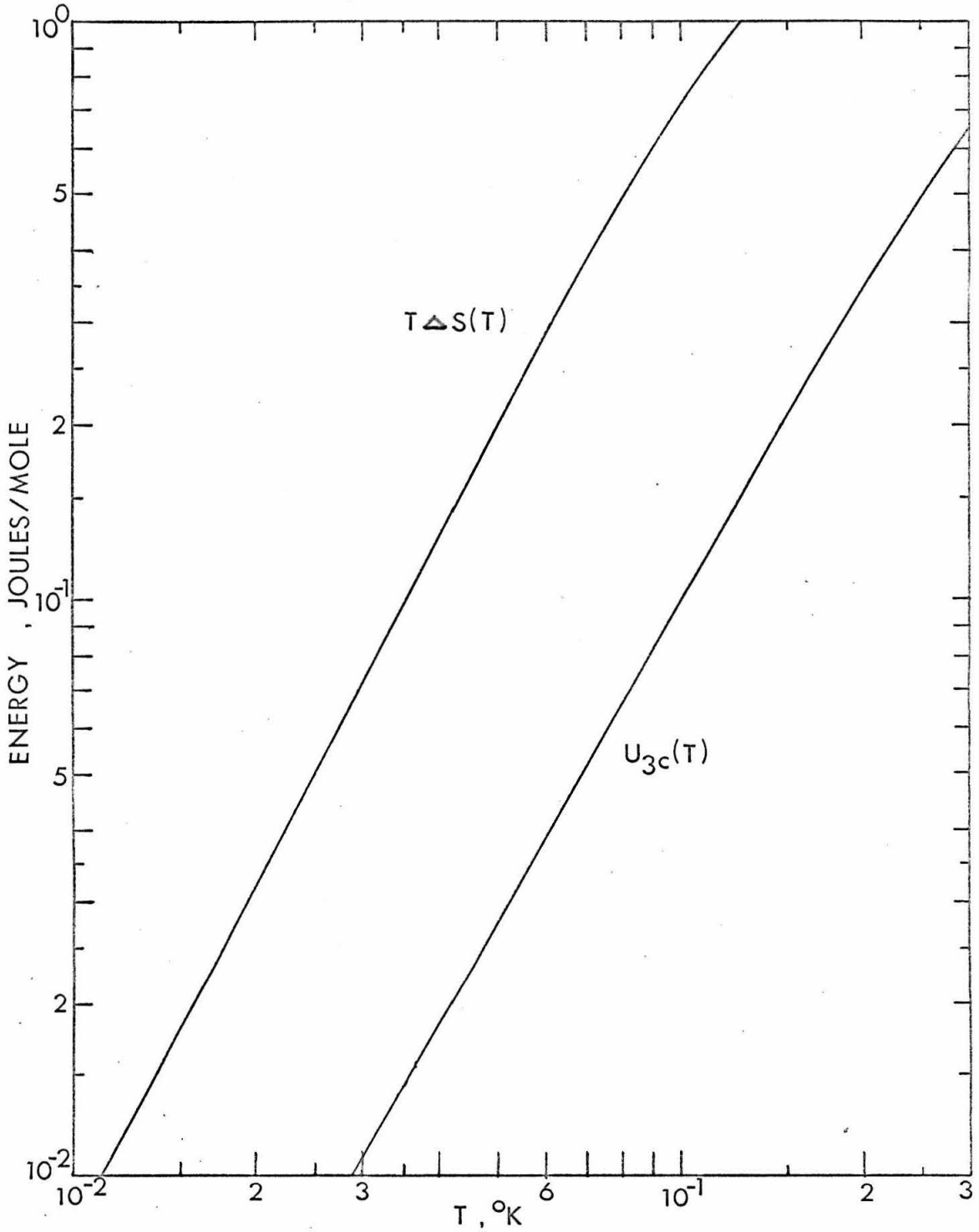
10^0
5
2
10^{-1}
5
2
10^{-2}
ENERGY , JOULES/MOLE
$T\triangle S(T)$
$U_{3c}(T)$
10^{-2}
2
3
6
10^{-1}
2
3
T , °K

FIG. 20

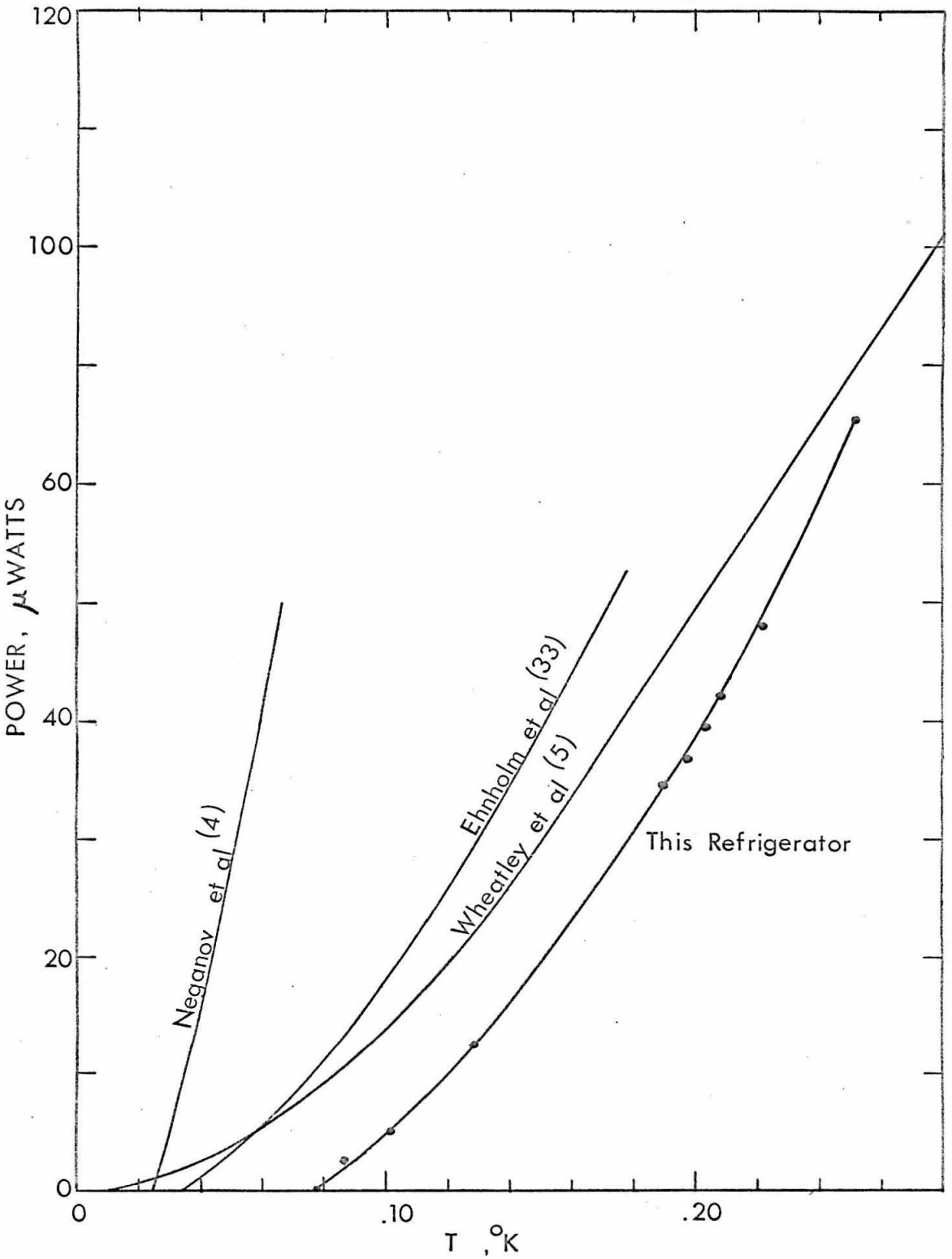
120
100
60
40
20
0
POWER, μWATTS
0
.10
.20
T , °K
Neganov et al (4)
Ehnholm et al (33)
Wheatley et al (5)
This Refrigerator

FIG. 21

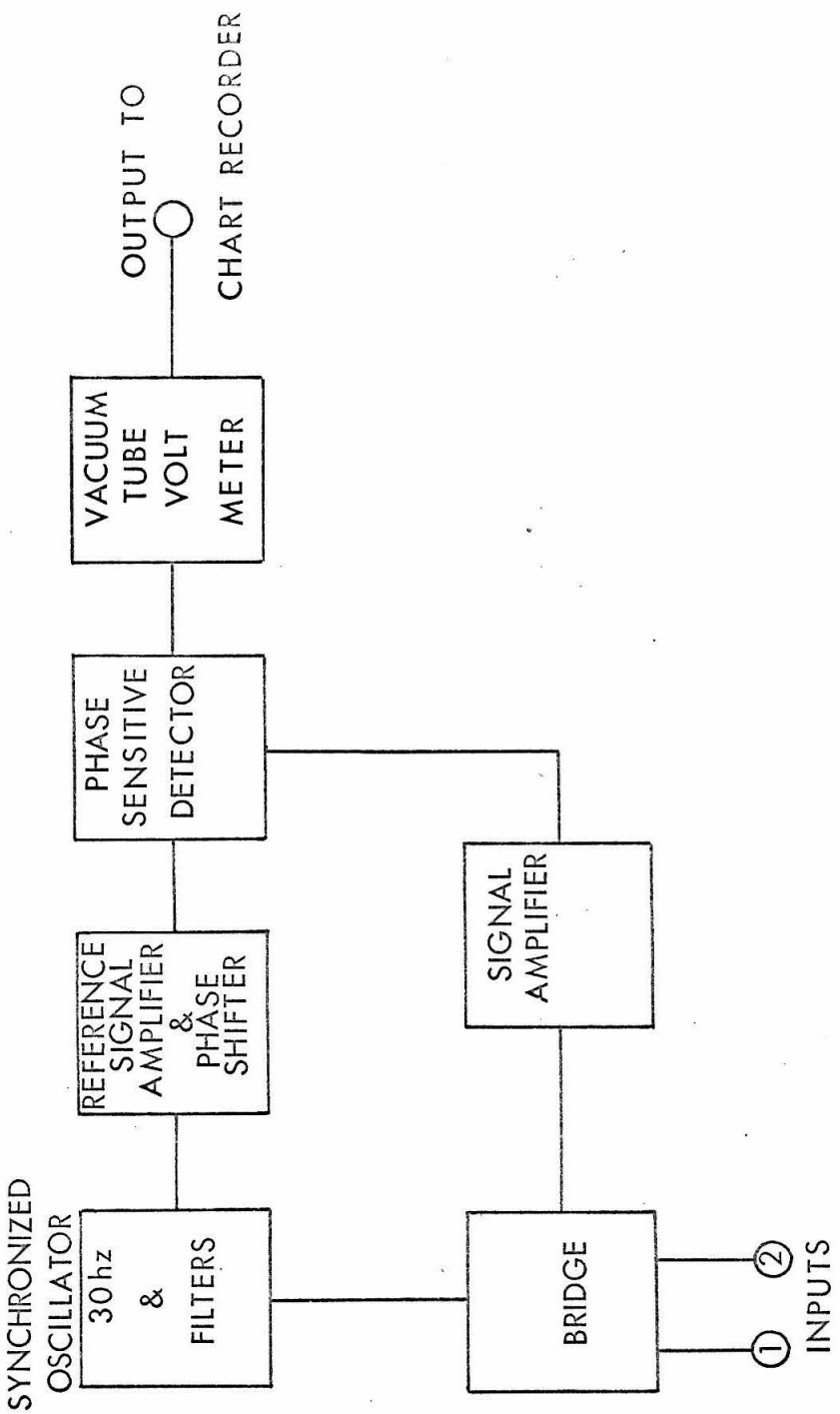
SYNCHRONIZED OSCILLATOR
30 hz & FILTERS
REFERENCE SIGNAL AMPLIFIER & PHASE SHIFTER
PHASE SENSITIVE DETECTOR
VACUUM TUBE VOLT METER
OUTPUT TO CHART RECORDER
BRIDGE
SIGNAL AMPLIFIER
1
2
INPUTS

FIG. 22

A. MEASURING SET

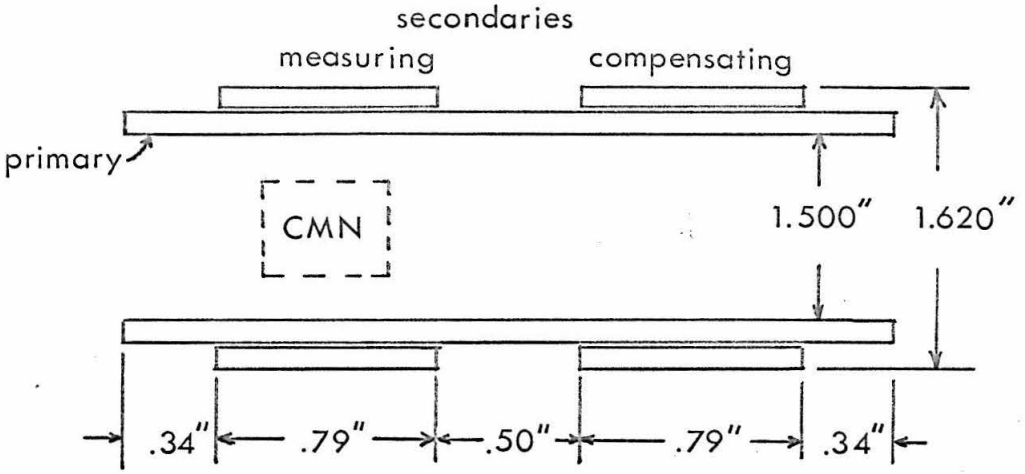

B. ADJUSTABLE COMPENSATORS

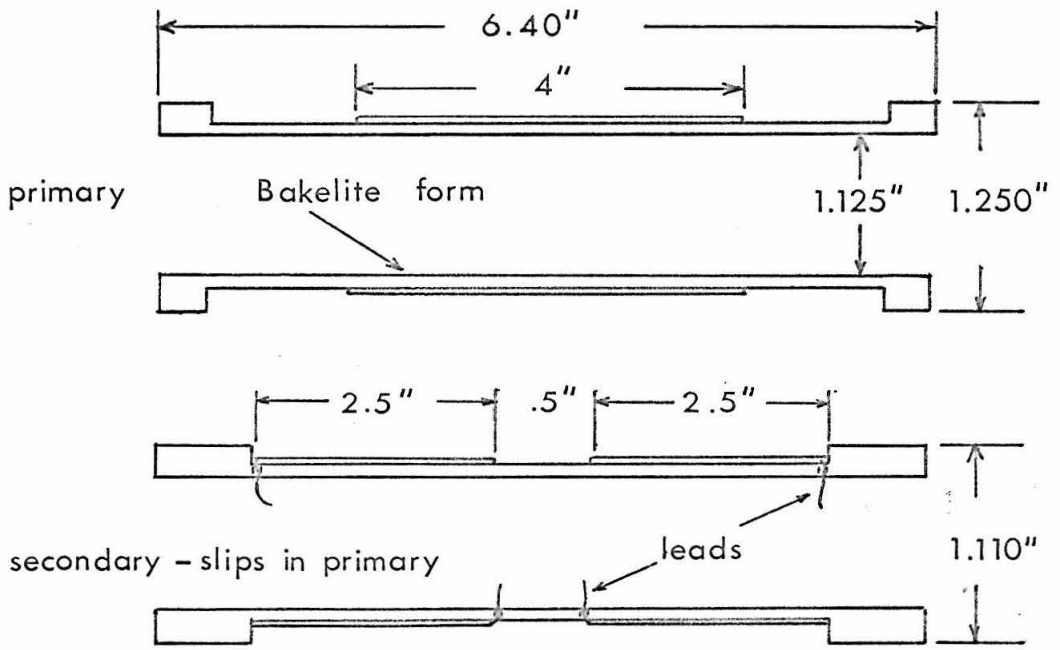

FIG. 23

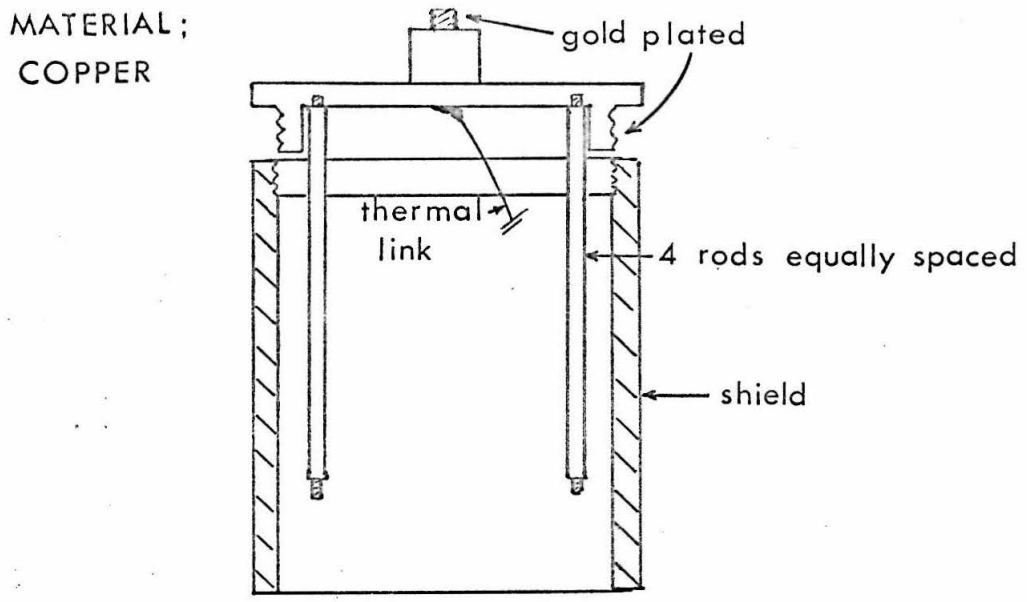
MATERIAL;
COPPER
gold plated
thermal
link
4 rods equally spaced
shield

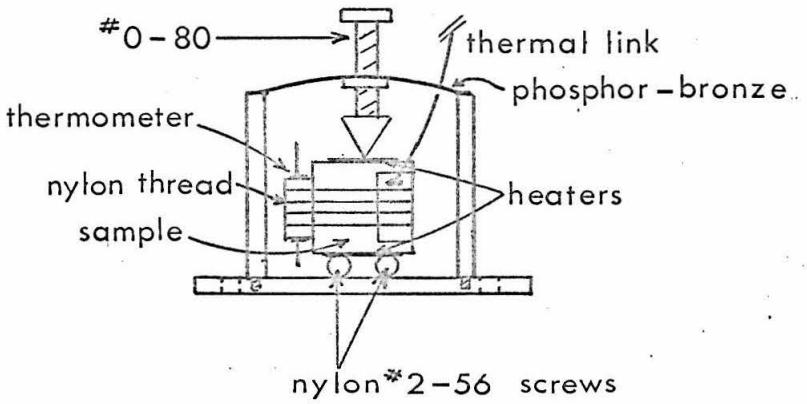
#0-80
thermal link
phosphor-bronze
thermometer
nylon thread
heaters
sample
nylon #2-56 screws

FIG. 24

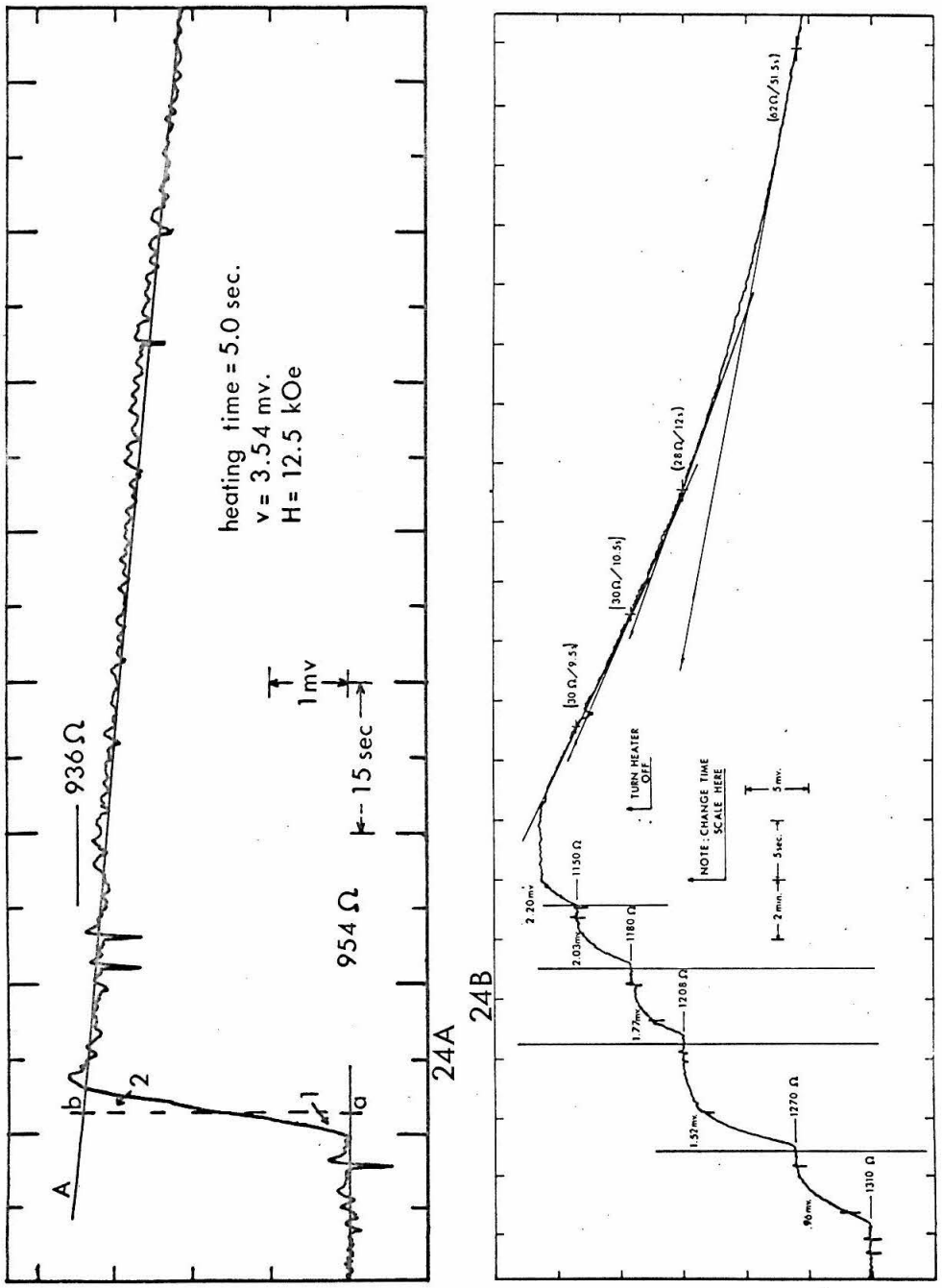
heating time = 5.0 sec.
v = 3.54 mv.
H = 12.5 kOe
936 Ω
954 Ω
1mv
15 sec
A
a
b
1
2
24A
24B
TURN HEATER OFF
NOTE: CHANGE TIME SCALE HERE
2 min
5 sec
5 mv.
1130 Ω
1180 Ω
1208 Ω
1270 Ω
1310 Ω
2.20mv
2.03mv
1.77mv
1.52mv
.90mv

FIG. 25

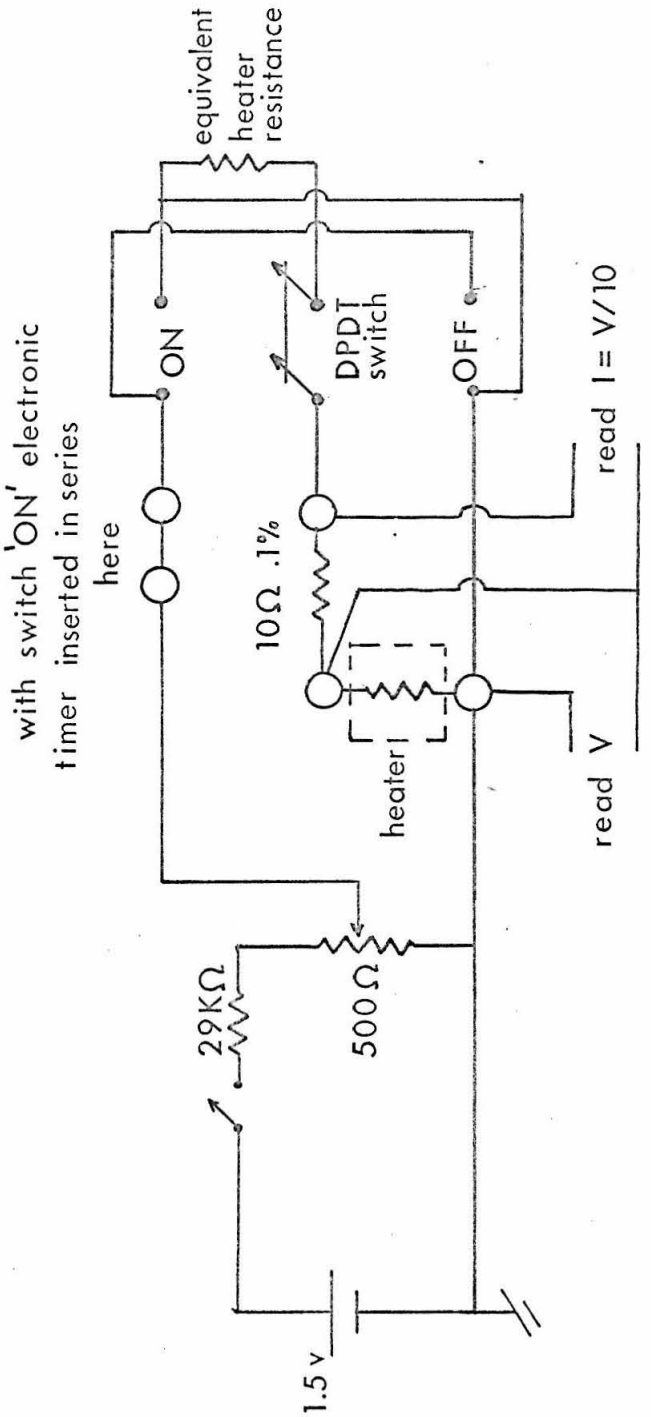
equivalent heater resistance
ON
DPDT switch
OFF
with switch 'ON' electronic timer inserted in series here
10Ω .1%
read I = V/10
heater I
read V
29KΩ
500Ω
1.5 v

FIG. 26

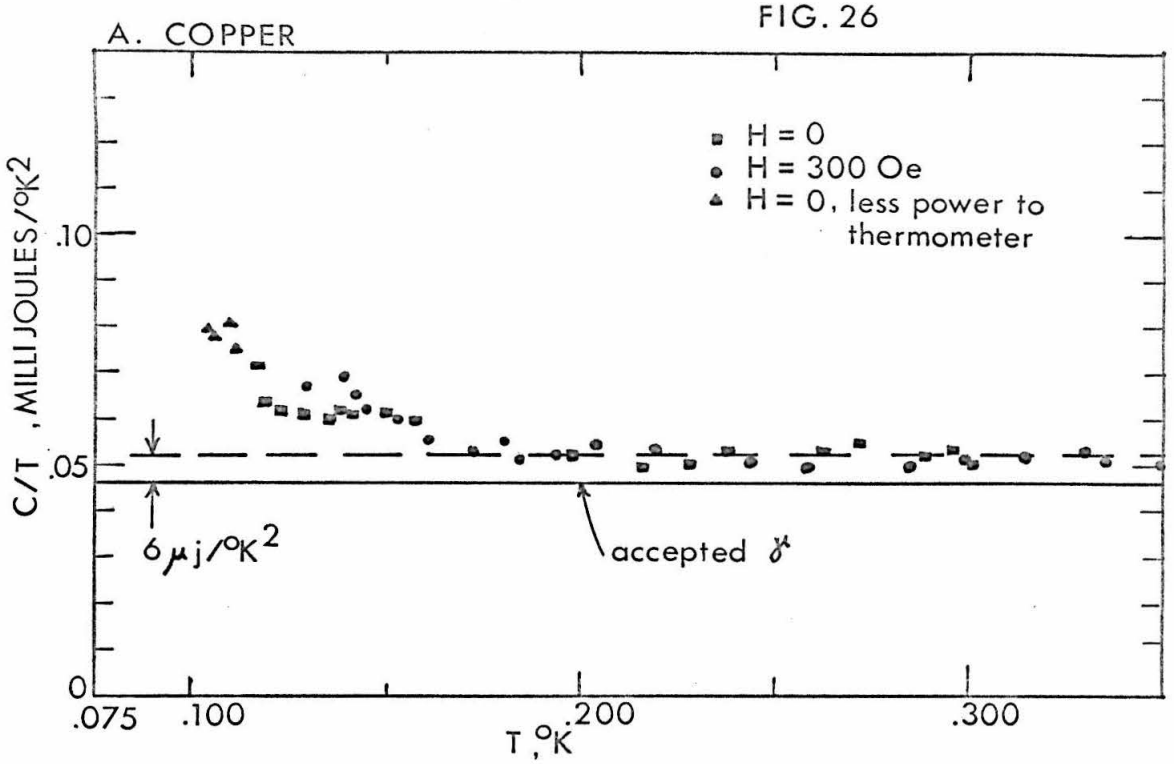
A. COPPER
H = 0
H = 300 Oe
H = 0, less power to thermometer
C/T , MILLIJOULES/°K²
.10
.05
0
6 μj/°K²
accepted γ
.075
.100
.200
.300
T, °K

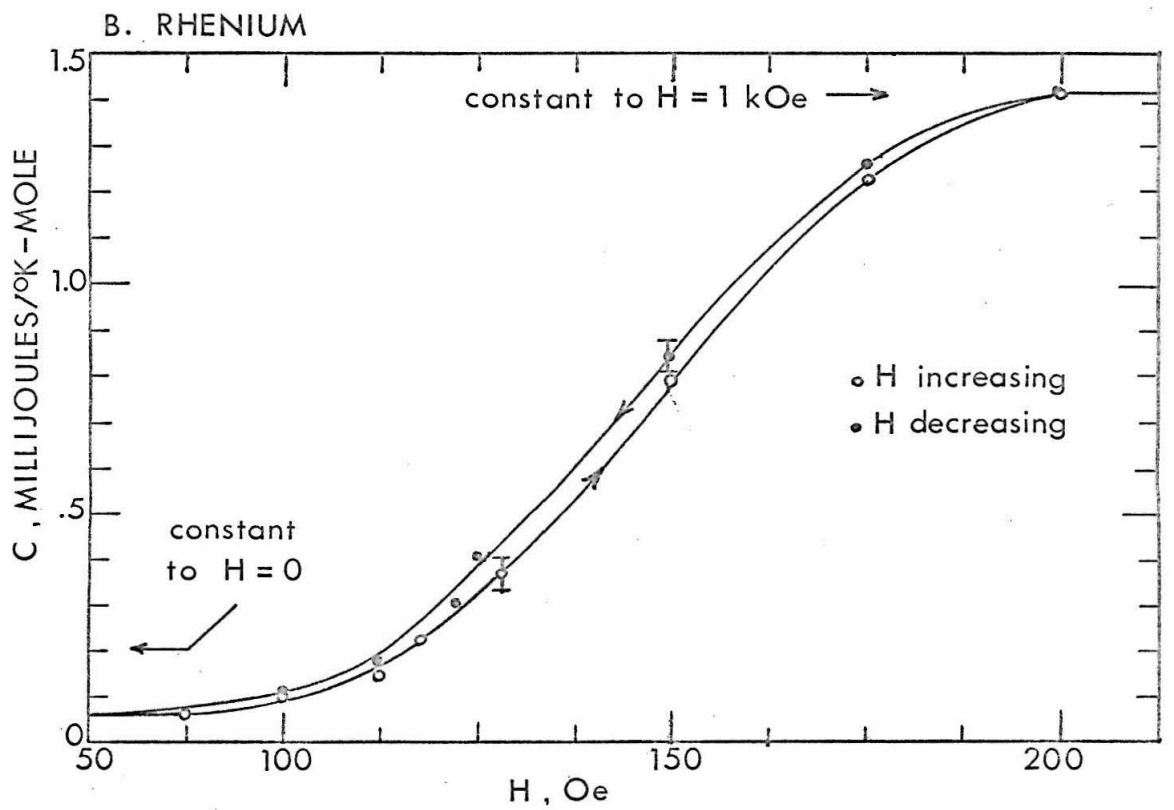
B. RHENIUM
1.5
1.0
.5
0
constant to H = 1 kOe
H increasing
H decreasing
constant to H = 0
C , MILLIJOULES/°K-MOLE
50
100
150
200
H , Oe

FIG. 27

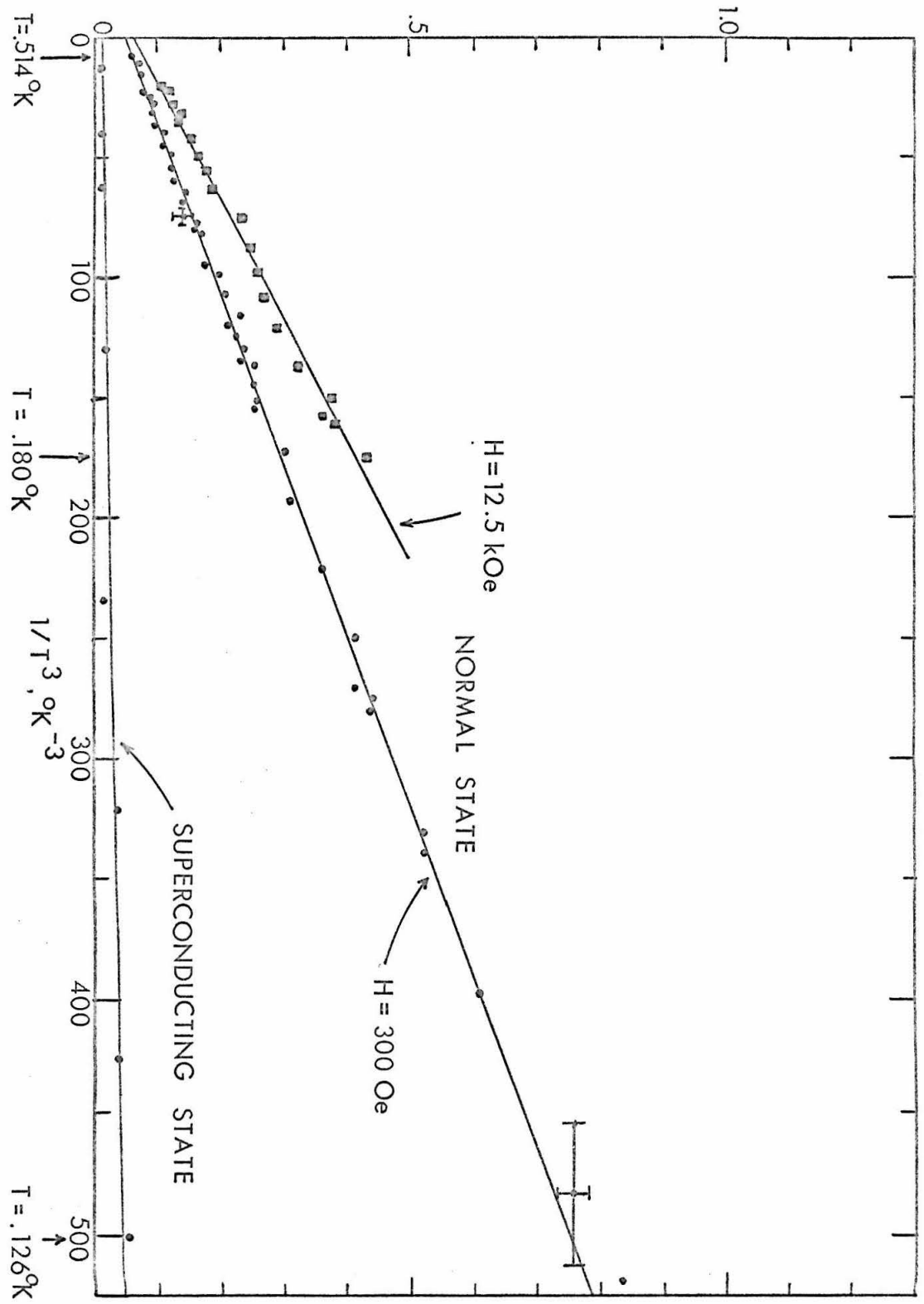
C/T, MILLIJOULES/°K²
0
.5
1.0
T=.514°K
T = .180°K
T = .126°K
100
200
300
400
500
1/T³, °K⁻³
H=12.5 kOe
H= 300 Oe
NORMAL STATE
SUPERCONDUCTING STATE

FIG. 28

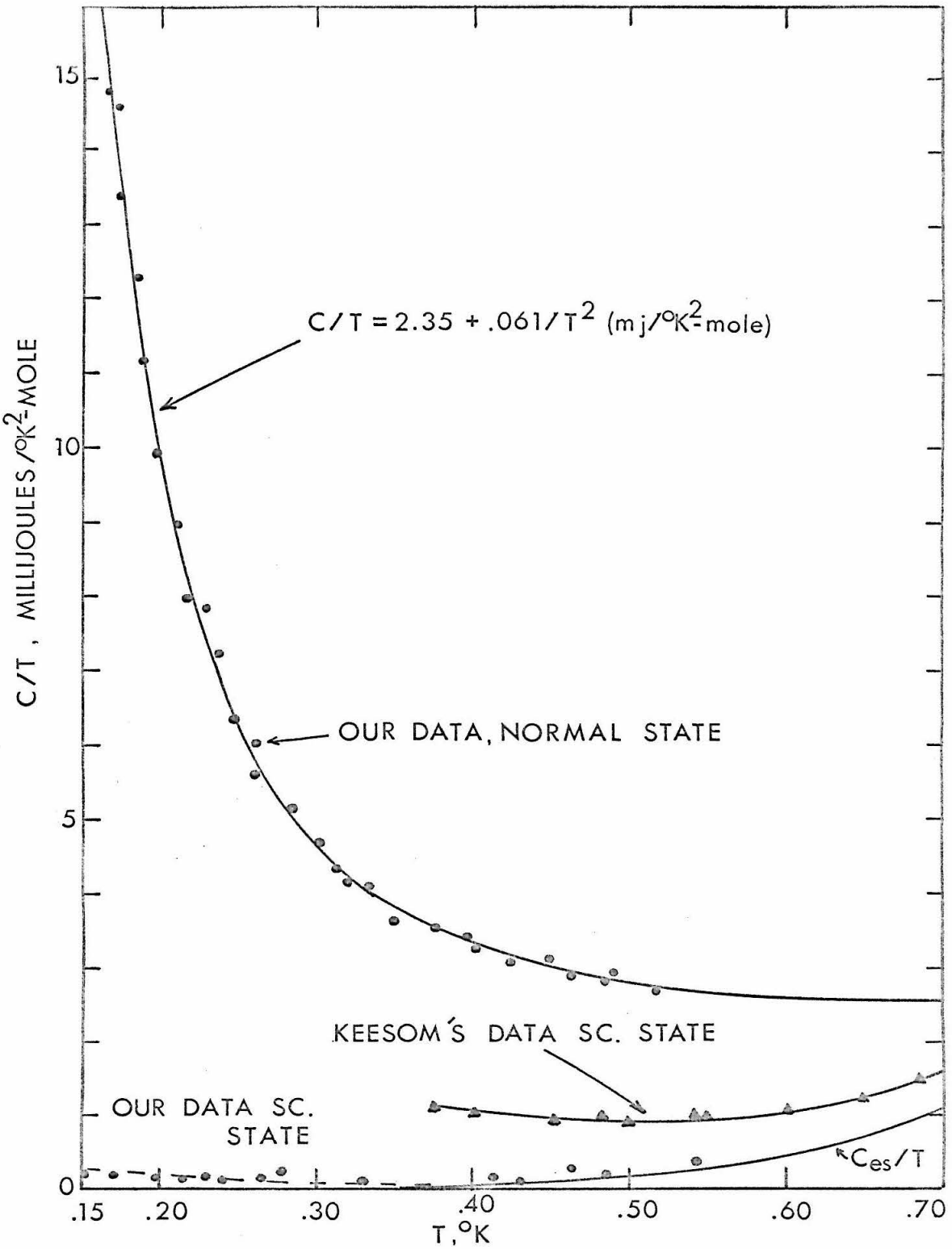
15
10
5
0
C/T , MILLIJOULES/°K²-MOLE
C/T = 2.35 + .061/T² (mj/°K²-mole)
OUR DATA, NORMAL STATE
KEESOM'S DATA SC. STATE
OUR DATA SC. STATE
Ces/T
.15
.20
.30
.40
.50
.60
.70
T, °K

FIG. 29

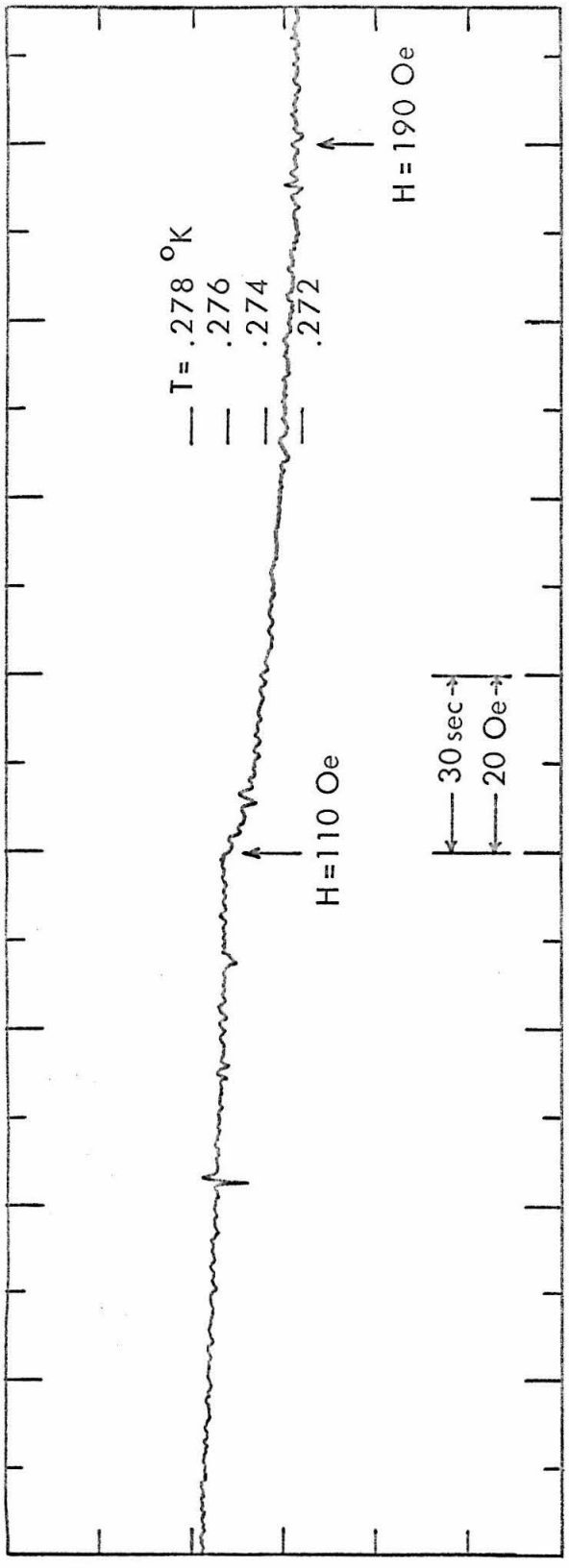

FIG. 29 a

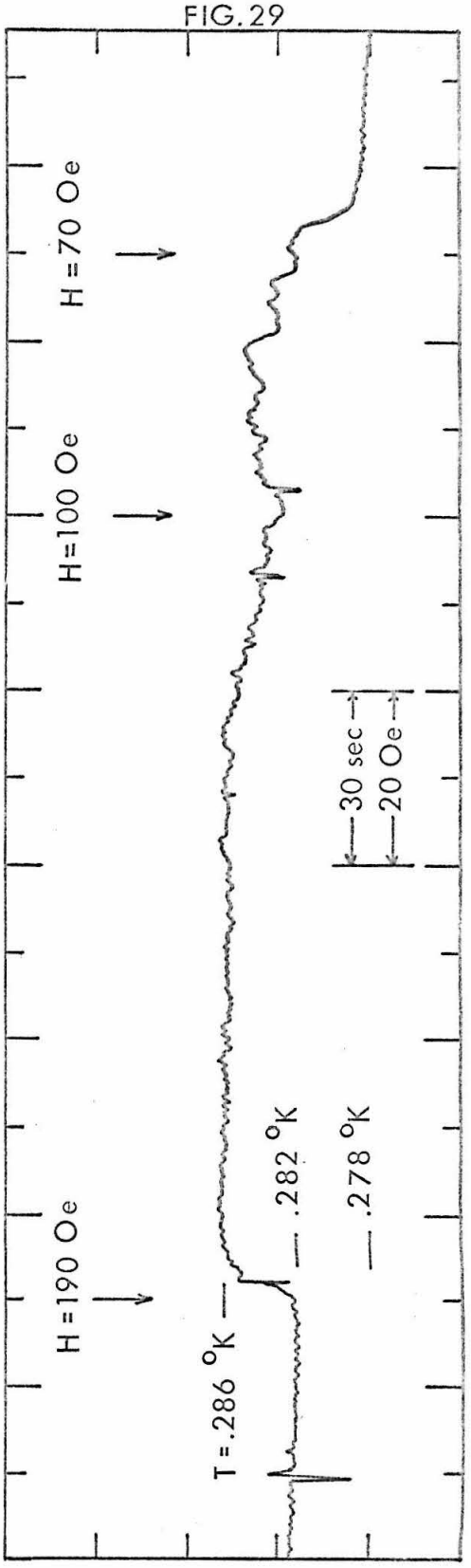

FIG. 29 b

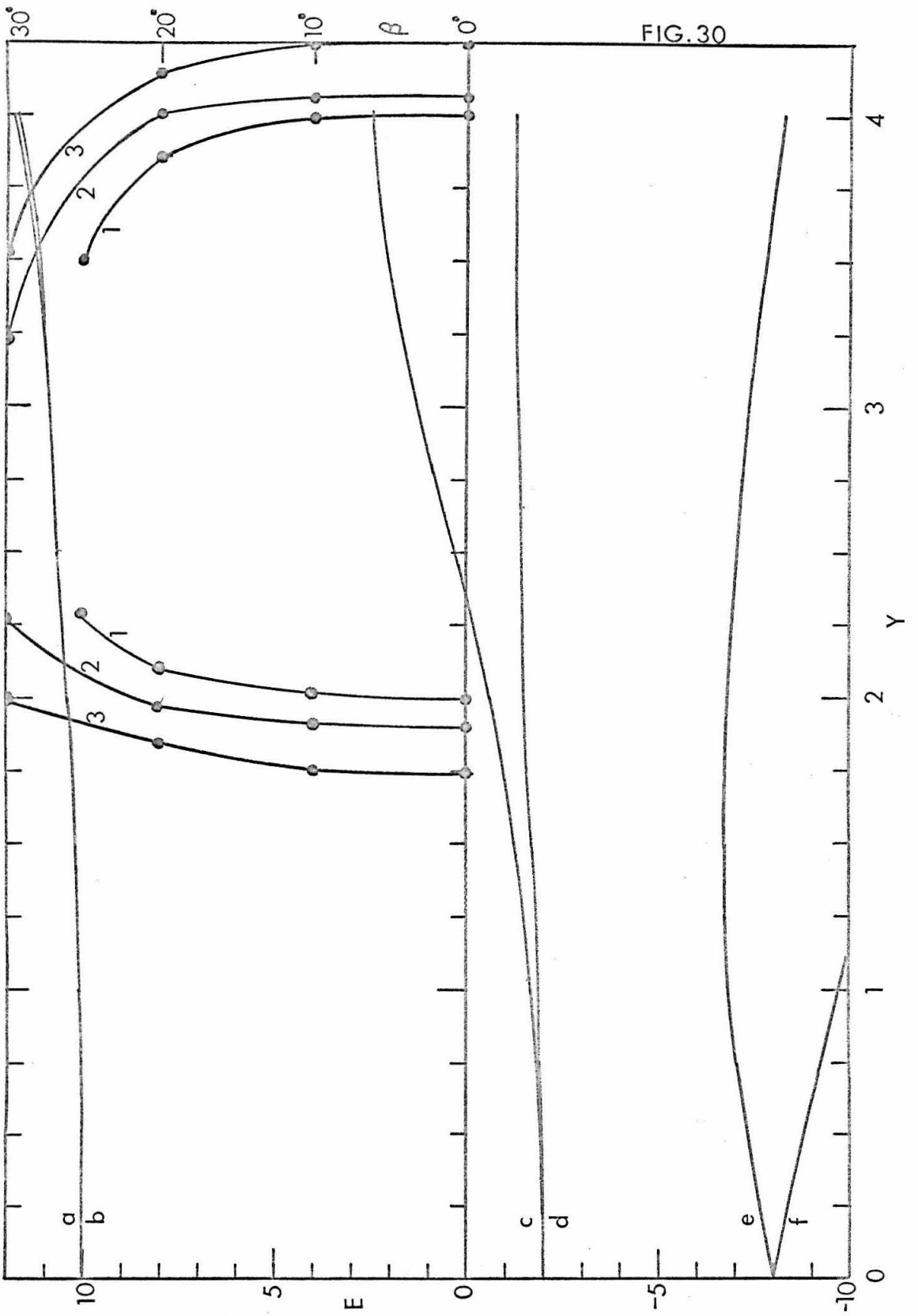

FIG. 30

FIG. 31